



University of Kentucky
UKnowledge

Theses and Dissertations--Chemical and
Materials Engineering

Chemical and Materials Engineering

2019

DEVELOPMENT OF MAGNETIC NANOCOMPOSITE MATERIALS AS REUSABLE ADSORBENTS FOR CHLORINATED ORGANICS IN CONTAMINATED WATER

Angela Gutierrez

University of Kentucky, amgu232@g.uky.edu

Digital Object Identifier: <https://doi.org/10.13023/etd.2019.407>

[Right click to open a feedback form in a new tab to let us know how this document benefits you.](#)

Recommended Citation

Gutierrez, Angela, "DEVELOPMENT OF MAGNETIC NANOCOMPOSITE MATERIALS AS REUSABLE ADSORBENTS FOR CHLORINATED ORGANICS IN CONTAMINATED WATER" (2019). *Theses and Dissertations--Chemical and Materials Engineering*. 107.

https://uknowledge.uky.edu/cme_etds/107

This Doctoral Dissertation is brought to you for free and open access by the Chemical and Materials Engineering at UKnowledge. It has been accepted for inclusion in Theses and Dissertations--Chemical and Materials Engineering by an authorized administrator of UKnowledge. For more information, please contact UKnowledge@lsv.uky.edu.

STUDENT AGREEMENT:

I represent that my thesis or dissertation and abstract are my original work. Proper attribution has been given to all outside sources. I understand that I am solely responsible for obtaining any needed copyright permissions. I have obtained needed written permission statement(s) from the owner(s) of each third-party copyrighted matter to be included in my work, allowing electronic distribution (if such use is not permitted by the fair use doctrine) which will be submitted to UKnowledge as Additional File.

I hereby grant to The University of Kentucky and its agents the irrevocable, non-exclusive, and royalty-free license to archive and make accessible my work in whole or in part in all forms of media, now or hereafter known. I agree that the document mentioned above may be made available immediately for worldwide access unless an embargo applies.

I retain all other ownership rights to the copyright of my work. I also retain the right to use in future works (such as articles or books) all or part of my work. I understand that I am free to register the copyright to my work.

REVIEW, APPROVAL AND ACCEPTANCE

The document mentioned above has been reviewed and accepted by the student's advisor, on behalf of the advisory committee, and by the Director of Graduate Studies (DGS), on behalf of the program; we verify that this is the final, approved version of the student's thesis including all changes required by the advisory committee. The undersigned agree to abide by the statements above.

Angela Gutierrez, Student

Dr. Thomas D. Dziubla, Major Professor

Dr. Stephen Rankin, Director of Graduate Studies

DEVELOPMENT OF MAGNETIC NANOCOMPOSITE MATERIALS AS
REUSABLE ADSORBENTS FOR CHLORINATED ORGANICS IN
CONTAMINATED WATER

THESIS

A thesis submitted in partial fulfillment of the
requirements for the degree of Doctor of Philosophy in the
College of Engineering
at the University of Kentucky

By

Angela Maria Gutierrez

Lexington, Kentucky

Co- Directors: Dr. Thomas D. Dziubla, Professor of Chemical Engineering

and Dr. J. Zach Hilt, Professor of Chemical Engineering

Lexington, Kentucky

2019

Copyright © Angela Maria Gutierrez 2019

ABSTRACT OF THESIS

DEVELOPMENT OF MAGNETIC NANOCOMPOSITE MATERIALS AS REUSABLE ADSORBENTS FOR CHLORINATED ORGANICS IN CONTAMINATED WATER

The constant growth in population worldwide over the past decades continues to put forward the need to provide access to safe, clean water to meet human needs. There is a need for cost-effective technologies for water and wastewater treatment that can meet the global demands and the rigorous water quality standards and at the same maximizing pollutant efficiency removal. Current remediation technologies have failed in keeping up with these factors without becoming cost-prohibitive. Nanotechnology has recently been sought as a promising option to achieve these goals. The use of iron oxide magnetic nanoparticles as nanoadsorbents has led to a new class of magnetic separation strategies for water treatment. We have developed magnetic nanocomposite systems able to capture polychlorinated biphenyls (PCBs), as model organic pollutants, in aqueous solution, providing a cost-effective water remediation technique. Two distinct methods were employed to develop these polyphenolic nanocomposite materials. The polyphenolic moieties were incorporated to create high affinity binding sites for organic pollutants within the nanocomposites. The first method utilized a surface initiated polymerization of polyphenolic-based crosslinkers and co-monomers on the surface of iron oxide magnetic nanoparticles to create a core-shell nanocomposite. The second method utilized a bulk polymerization method to create macroscale films composed of iron oxide nanoparticles incorporated into a polyphenolic-based polymer matrix, which were then processed into microparticles. Both methods produce nanocomposite materials that can bind chlorinated organics, can rapidly separate bound organics from contaminated water sources using magnetic decantation, and can use thermal destabilization of the polymer matrix for

contaminant release and material regeneration. The polyphenol functionalities used to bind organic pollutants were quercetin multiacrylate (QMA) and curcumin multiacrylate (CMA), which are acrylated forms of the nutrient polyphenols quercetin (found in berries) and curcumin (found in turmeric), both with expected affinity for chlorinated organics. The affinity of these novel materials for PCB 126 was evaluated at equilibrium conditions using a gas chromatography coupled to electron capture detection (GC-ECD) for quantification purposes, and the data was fitted to the nonlinear Langmuir model to determine binding affinity (K_D) and maximum binding capacity (B_{max}). The K_D values obtained demonstrated that the presence of the polyphenolic-based moieties, CMA and QMA, as crosslinkers enhanced the binding affinity for PCB 126, expected to be a result of their aromatic rich nature which provides sites for $\pi - \pi$ stacking interactions between the nanoparticle surface and the PCBs in solution. These values are lower than the reported affinity coefficients for activated carbon, which is the gold standard for capture/binding of organic contaminants in water and waste water treatment. Furthermore, upon exposure to an alternating magnetic field (AMF) for a period of 5 minutes, over 90% of the bound PCB on these materials was released, offering a low-cost regeneration method for the nanocomposites. Additionally, this novel regeneration strategy does not require the use of large volumes of harsh organic solvents that oftentimes become harmful byproducts. Overall, we have provided strong evidence that these novel nanocomposites have a promising application as nanoadsorbents for specific organic contaminants in contaminated water sources providing high binding affinities, a low-cost regeneration technique and are capable of withstanding use under environmental conditions offering a cost effective alternative to current remediation approaches.

KEYWORDS: Environmental remediation, nanoadsorbent, magnetic nanoparticles, nanocomposites, polychlorinated biphenyls

Angela Maria Gutiérrez

(Name of Student)

04/24/2019

Date

DEVELOPMENT OF MAGNETIC NANOCOMPOSITE MATERIALS AS
REUSABLE ADSORBENTS FOR CHLORINATED ORGANICS IN
CONTAMINATED WATER

By
Angela Maria Gutierrez

Thomas D. Dziubla

Co-Director of Thesis

J. Zach Hilt

Co-Director of Thesis

Stephen Rankin

Director of Graduate Studies

04/24/2019

Date

To my mom and dad, Angela Maria Echeverri and Alvaro Gutiérrez. Nada de esto sería posible sin el amor y apoyo incondicional que me han dado.

ACKNOWLEDGMENTS

This dissertation would not have been possible without the support, guidance and encouragement of multiple people in my life, and I am beyond grateful for those who have been part of my journey at the University of Kentucky. First, I would like to sincerely thank my advisor, Dr. J. Zach Hilt, for his support and guidance inside and outside the lab. Research is never a straight line, neither is life, and through all of it Dr Hilt has consistently encouraged me to ‘stay positive’, two words that have left a mark in me. His influence has reached beyond molding my scientific intellect; his character, integrity, professionalism and passion for his work and the people around him have shown me what it truly means to have a successful career. I would not be where I am today had it not been for Dr. Hilt’s invaluable teachings, mentoring, advising and unconditional support, especially when medical issues got the best of me.

I would also like to thank my co-advisor Dr. Thomas D. Dziubla, for his invaluable mentorship and insight during this process. Working with Dr. Dziubla in the Materials and Chemical Engineering (MACE) Graduate Student Association, I was able to see his dedication and a degree of passion for service as much as for science, an experience that has shaped my passions and scientific career goals. I would like to thank my committee member Dr. Dibakar Bhattacharyya, without whom I would literally not be here if we hadn’t met at a conference in 2012 where I learned about UK. Since day one DB has been a pillar of example in engineering and in life, and I am grateful for his support and the countless conversations we have shared were I have always felt like one of his students. Dr. Kelly Pennell, my committee member, quickly became more than a source of scientific advice and offered me her trust and support to pursue my interests

outside of lab work. Over the last 3 years she has been a constant source of encouragement and sagely advice, and the best of travel companions. I am also thankful for the input, collaboration and expert advice of Dr. Arnold Stromberg.

This research has been supported by the University of Kentucky Superfund Research Program, a truly interdisciplinary center that has been instrumental in the development of my scientific persona. I would like to specially thank Dr. Bernhard Henig, the UK-SRP center director, for his support throughout my career, enabling incredible opportunities for network, and always being a wonderful travel companion. The UK-SRP has been instrumental to expand my growth as an engineer beyond the lab experience.

I would like to extend a special thank you to all of my fellow graduate students, past and present: Dr. Robert Wydra, Dr. Nathanael Stocke, Dr. Anastasia Kruse-Hausser, Dr. Carolyn Jordan, Dr. Vinod Patil, Dr. Prachi Gupta, Dr. Shuo Tang, Dr. Mai Trang, Irfan Ahmad, Molly Frazar, Rishabh Shah. I would like to specifically thank Dr. Brad Newsome and Dr. Rohit Bhandari for being a great mentors and for the countless conversations we have shared. And Dustin Savage and Kelley Wiegman, thank you always being up to listen and make me laugh when I needed it most. I have also had the pleasure to work with incredibly talent undergraduate students: Phillip Jhonson, Benjamin Stacey, Francisco Leniz, Xinya Wang, Alexandra Miozza, Nicole Cordonnier, and Ronita Mathias. Mentoring students has always been a passion of mine and one of my favorite parts of graduate school, to all of you, thank you for your hard work. To all the UK-SRP students, thank you for the shared moments and company.

I must also extend my gratefulness to a group of physicians who have helped me make it to this point: Dr. Matthew J. Neltner, Christina D. McGlothlin-Boggs APRN, Dr. Ayman A. Al-Salaimh, Dr. Abdunnasser Alhajeri, and the staff at University of Kentucky Neuroscience Institute. And Dr. Ivan Ossma, Chief anterior segment surgeon at Fundacion Valle del Lili, I am forever thankful for, in your words, giving me my most essential tools back.

Lastly, I would like to thank my friends and family for their love and encouragement. To Lodz Pierre, Ramon Juanso, Mirranda Hubbs, Haley Wilson, Kate Kremers, Alicia Juncoz, Sandra Nava Nieto, Ben Ishmael, Chris Millisor, Jacob Lilly, Jason Absher, Rob Wensing, Alfred Cotton, Matt Wilson, David Nemer, along with many others, thank you for making my time in graduate school so much more memorable and enjoyable. A most special thank you to my parents, Alvaro Gutiérrez and Angela M. Echeverri, for their unconditional support. Even though my passions keep taking me further away from home, I am blessed to have your unwavering encouragement and trust in me, and for your willingness to come every year to Lexington to see me. To my sisters, Luisa and Vicky, for always being able to make me laugh, and being my number one fans. To my nieces Julieta and Gabriela, and my soon-to-be-born nephew Nicolas, for giving me one more reason to smile. I can only aspire to be worthy role model for all of you. Amidst all the knowledge I have gained in graduate school, the most important lesson has been to value each moment of the process and not focus just on the end goal, for there is more value in what you become than in the single moment of what you achieve.

TABLE OF CONTENTS

ACKNOWLEDGMENTS	III
LIST OF TABLES	XI
LIST OF FIGURES	XII
CHAPTER 1. INTRODUCTION	1
1.1 Objectives	3
CHAPTER 2. RECENT ADVANCES ON IRON OXIDE MAGNETIC NANOPARTICLES AS SORBENTS OF ORGANIC POLLUTANTS IN WATER AND WASTEWATER TREATMENT	6
2.1 Abstract	6
2.2 Introduction	7
2.2.1 Core-shell iron oxide magnetic nanoparticles	10
2.2.2 Magnetic Nanocomposites	17
2.3 Conclusions	23
CHAPTER 3. NOVEL MAGNETIC CORE –SHELL MAGNETIC NANOPARTICLES FOR THE REMOVAL OF POLYCHLORINATED BIPHENYLS FROM CONTAMINATED WATER	25
3.1 Abstract	25
3.2 Introduction	26
3.2.1 Experimental details	30
3.2.1.1 Materials	30

3.2.1.2	Curcumin multiacrylate synthesis and purification	30
3.2.1.3	Quercetin multiacrylate synthesis and purification	31
3.2.1.4	Iron oxide nanoparticle synthesis	31
3.2.1.5	Surface initiated polymerization	32
3.2.2	Particle Characterization	32
3.2.2.1	Fourier transform infrared (FTIR) spectra	32
3.2.2.2	Thermogravimetric analysis (TGA)	33
3.2.2.3	Transmission electron microscopy (TEM)	33
3.2.2.4	X-Ray Diffraction (XRD)	33
3.2.2.5	Dynamic light scattering (DLS)	34
3.2.2.6	Ultraviolet (UV)-visible spectroscopy	34
3.2.3	PCB 126 Binding Studies	34
3.3	Results and discussion	37
3.4	Conclusions	46
CHAPTER 4.	SYNTHESIS OF MAGNETIC NANOCOMPOSITE MICROPARTICLES FOR	
	BINDING OF CHLORINATED ORGANICS IN CONTAMINATED WATER SOURCES	47
4.1	Abstract	47
4.2	Introduction	47
4.3	Experimental	51
4.3.1	Materials	51
4.3.2	Iron oxide nanoparticle synthesis	51
4.3.3	Curcumin multiacrylate synthesis and purification	52
4.3.4	Quercetin multiacrylate synthesis and purification	52

4.3.5	Magnetic nanocomposite microparticle synthesis	53
4.3.6	Cryomilling	54
4.3.7	Microparticle characterization	54
4.3.7.1	Fourier transform infrared (FTIR) spectra	54
4.3.7.2	Thermogravimetric analysis (TGA)	55
4.3.7.3	Particle sizing using a micron sizer	55
4.3.7.4	Scanning electron microscopy (SEM)	55
4.3.7.5	Ultraviolet (UV)-visible spectroscopy	56
4.3.8	PCB 126 binding studies	56
4.4	Results and discussion	58
4.5	Conclusions	70
CHAPTER 5. ALTERNATING MAGNETIC FIELD MODULATED BINDING IN MAGNETIC NANOCOMPOSITES AS A LOW ENERGY REGENERATION STRATEGY IN ENVIRONMENTAL REMEDIATION 72		
5.1	Abstract	72
5.2	Introduction	72
5.3	Experimental	75
5.3.1	Materials	75
5.3.2	Magnetic nanocomposite microparticle synthesis	76
5.3.3	PCB 126 binding studies and AMF regeneration	77
5.4	Results and discussion	78
5.5	Conclusions	83

CHAPTER 6. THE IMPACT OF SOLUTION IONIC STRENGTH, HARDNESS AND PH IN THE ADSORPTION EFFICIENCY OF POLYCHLORINATED BIPHENYLS ON MAGNETIC NANOCOMPOSITE MATERIALS	85
6.1 Abstract	85
6.2 Introduction	86
6.3 Experimental	88
6.3.1 Materials	88
6.3.2 Magnetic nanocomposite microparticle synthesis	89
6.3.3 Particle characterization	89
6.3.4 PCB binding studies	89
6.4 Results and discussion	90
6.5 Conclusions	97
CHAPTER 7. EFFECT OF ATOM TRANSFER RADICAL POLYMERIZATION REACTION TIME ON PCB BINDING CAPACITIES OF STYRENE-CMA/QMA CORE-SHELL IRON OXIDE NANOPARTICLES	98
7.1 Abstract	98
7.2 Introduction	99
7.3 Experimental	102
7.3.1 Materials	102
7.3.2 Iron oxide nanoparticle synthesis	103
7.3.3 BMPA initiator addition	103

7.3.4	Surface initiated atom transfer radical polymerization	104
7.3.5	Particle characterization	104
7.3.5.1	Thermogravimetric analysis	105
7.3.5.2	X-ray diffraction	105
7.3.5.3	Dynamic light scattering	105
7.3.5.4	Ultraviolet (UV)-visible spectroscopy	106
7.3.5.5	Alternating magnetic field (AMF) heating	106
7.3.6	PCB 126 binding studies	107
7.4	Results and discussion	109
7.5	Conclusion	133
CHAPTER 8.	CONCLUSIONS	136
APPENDICES		140
REFERENCES		148
VITA		161

LIST OF TABLES

Table 3-1 T Size analysis from XRD diffractograms using the Scherrer equation and hydrodynamic size analysis via dynamic light scattering of the synthesized core-shell MNPs (mean \pm std dev. for three independent batches and three samples from each batch)	40
Table 3-2 Langmuir binding constants for the binding isotherms of PCB 126 for the four nanoparticle systems synthesized (n = 12, except for PEG MNPs where n = 15)	44
Table 4-1 Size analysis from SEM images and hydrodynamic size analysis via dynamic light scattering of the synthesized MNMs.....	62
Table 4-2 Langmuir binding constants for the binding isotherm of PCB 126 for the microparticle systems synthesized (n = 12 independent samples ^a n = 9 independent samples. ^b n = 15 independent samples. ^c values reproduced from [46] with permission from the authors.....	66
Table 7-1 Size analysis from XRD using the Scherrer equation; hydrodynamic size analysis of the synthesized core-shell MNPs (mean \pm std dev. for three independent batches and three samples from each batch); and SAR values from AMF heating)	118
Table 7-2 Langmuir binding constants for the binding isotherm of PCB 126 for the core-shell MNP systems synthesized (n = 9 independent samples). Confidence Intervals obtained from nonlinear regression using GraphPsd Prism	124
Table 7-3 Langmuir binding constants for the binding isotherm of PCB 126 for the core-shell MNP systems synthesized in terms of polymer mass (n = 9 independent samples). Confidence Intervals obtained from nonlinear regression using GraphPad Prism.....	128
Table 7-4 Langmuir binding constants for the binding isotherm of PCB 126 for the core-shell MNP systems synthesized (n = 9 independent samples), in terms of surface area. Confidence Intervals obtained from nonlinear regression using GraphPad Prism.....	132

LIST OF FIGURES

Figure 3-1 Schematic representation of the binding studies conducted with PCB 126 in a 99:1 DI water ethanol solvent	36
Figure 3-2 FTIR spectra of the synthesized core-shell magnetic nanoparticles	38
Figure 3-3 . Mass loss profile with increasing temperature of the synthesized core-shell magnetic nanoparticles	39
Figure 3-4 Suspended solution of CMA MNPs and capture of CMA MNPs in a static magnetic field (right).	40
Figure 3-5 XRD patterns of the synthesized core-shell magnetic nanoparticles	40
Figure 3-6 TEM images of (a) iron oxide magnetic nanoparticles, (b) PEG coated magnetic nanoparticles, (c) CMA coated nanoparticles and (d) QMA coated magnetic nanoparticles.	41
Figure 3-7 Normalized absorbance (at 540 nm) of the MNPs in DI water for 12 hours using UV-visible spectroscopy.	42
Figure 3-8 Adsorption isotherms for PCB 126 of the core-shell systems at room temperature. PCB 126 initial concentrations from 0.003 – 0.1 ppm fitted using the Langmuir model.	43
Figure 4-1 Schematic representation of the overall synthesis of magnetic nanocomposite polymers and their cryomilling to obtain magnetic nanocomposite microparticles (MNM).	54
Figure 4-2 Schematic representation of the binding studies conducted with PCB 126 in a 99:1 DI water ethanol solvent	58
Figure 4-3 FTIR spectra of the synthesized magnetic nanocomposite microparticles. A) CMA MNMs, B) QMA MNMs and C) PEG MNMs.	59
Figure 4-4 Mass loss profile with increasing temperature of the synthesized magnetic nanocomposite microparticles.	61
Figure 4-5 Suspended solution of CMA MNMs in water (left) and capture of CMA MNMs upon exposure to a static magnetic field (right).	61
Figure 4-6 SEM images of (a) CMA MNMs, (b) QMA MNMs and (c) PEG MNMs	62
Figure 4-7 Normalized absorbance (at 540 nm) of the MNMs in DI water for 12 hours using UV-visible spectroscopy.	63
Figure 4-8 Room temperature adsorption isotherms for PCB 126 of the A) MNM systems and B) MP systems. PCB 126 initial concentrations from 0.003 – 0.1 ppm fitted using the Langmuir model.	66
Figure 5-1 Schematic representation for the low energy regeneration strategy based on an alternating magnetic field for magnetic nanocomposites used in environmental remediation	78
Figure 5-2 Temperature variation data as a function of time for the MNMs upon exposure to an AMF operating at 55 kA m ⁻¹ and a frequency of 300 kHz. a) CMA MNMs, b) QMA MNMs, and c) PEG MNMs in isooctane. d) CMA MNMs, e) QMA MNMs, and f) PEG MNMs in 99:1 DI water to ethanol.	79
Figure 5-3 Percentage of PCB 126 released from the MNM systems upon exposure to different remediation strategies. a) 5 minute AMF exposure regeneration method and temperature release treatments b) 5 minute AMF exposure regeneration method and 30 minute temperature release treatments. (AMF operating at 55 kA m ⁻¹ and a frequency of 300 kHz)	81
Figure 6-1 Schematic representation of the crosslinked polymer matrix interaction with the iron oxide magnetic nanoparticles within the magnetic nanocomposite microparticles (MNM). Shown here is the CMA MNMs for representation purposes. Here, the squiggly line represents the continuation of the polymer chain.	91

Figure 6-2 Effect of ionic strength on the adsorption efficiency of PCB 126 on CMA MNMs, QMA MNMs and PEG MNMs. The ionic strength concentrations represent fresh water (0 mM), surface water (1.5 mM), and ground water (120 mM).	93
Figure 6-3 Effect of water hardness on the adsorption efficiency of PCB 126 on CMA MNMs, QMA MNMs and PEG MNMs. The water hardness concentrations represent soft (0 mM), moderately hard (0.8 mM), and hard (1.6 mM) waters.	94
Figure 6-4 Effect of pH on the adsorption efficiency of PCB 126 on CMA MNMs, QMA MNMs and PEG MNMs.	95
Figure 7-1 Schematic representation of the synthesis of the core-shell magnetic nanoparticles (MNPs): a) Co-precipitation synthesis of IO MNPs, shown inside the red rectangle b) Surface functionalization of the IO MNPs with BMPA to obtain BMPA MNPs, c) Atom transfer radical polymerization reaction with styrene (Sty) and curcumin multiacrylate (CMA) to obtain core-shell Sty-CMA MNPs.	110
Figure 7-2 FTIR spectra of the synthesized magnetic nanoparticles. A) Sty CMA MNPs, B) Sty QMA MNPs and C) Sty DVB MNPs.	112
Figure 7-3 Mass loss profile with increasing temperature of the synthesized core-shell magnetic nanoparticles at different ATRP reaction times, A) Sty CMA MNPs at 5% initial loading, B) Sty CMA MNPs at 10% initial loading, C) Sty QMA MNPs at 5% initial loading, D) Sty QMA MNPs at 10% initial loading, and E) Sty DVB MNPs at 5% initial loading.	116
Figure 7-4 XRD patterns of the synthesized core-shell magnetic nanoparticles. Iron oxide nanoparticle XRD pattern included for reference	117
Figure 7-5 Normalized absorbance (at 540 nm) of the core-shell MNPs in DI water for 12 hours using UV-visible spectroscopy.	120
Figure 7-6 Adsorption isotherms for PCB 126 of the core-shell MNP systems in terms of total mass at room temperature. A) Sty CMA MNP systems, b) Sty QMA MNPs systems and c) Sty DVB MNPs systems. PCB 126 initial concentrations from 0.005 – 0.1 ppm fitted using the Langmuir model.	122
Figure 7-7 Adsorption isotherms for PCB 126 of the core-shell MNP systems in terms of polymer mass at room temperature. A) Sty CMA MNP systems, b) Sty QMA MNPs systems and c) Sty DVB MNPs systems. PCB 126 initial concentrations from 0.005 – 0.1 ppm fitted using the Langmuir model.	128
Figure 7-8 Adsorption isotherms for PCB 126 of the core-shell MNP systems in terms of surface area at room temperature. A) Sty CMA MNP systems, b) Sty QMA MNPs systems and c) Sty DVB MNPs systems. PCB 126 initial concentrations from 0.005 – 0.1 ppm fitted using the Langmuir model.	131

CHAPTER 1. INTRODUCTION

Water pollution and water scarcity continues to be one of the most challenging problems facing mankind. The United Nations estimates 300 to 500 million tons of heavy metals, solvents, and other wastes generated as by-products of industrialization are discharged into the world's water supplies each year.^[1] As a result, around 1.7 million deaths a year, are caused by unsafe or inadequate access to water.^[2] Currently only 20% of global wastewater is properly treated, and current infrastructure for wastewater treatment, and production of safe water, cannot keep up with global demands and the rigorous water quality standards.^[3,4] There is an ever increasing need for the global community to develop efficient and affordable technologies to improve the quality of water to meet human and environmental needs.

Current water remediation technologies for organic pollutants still heavily depends on the use of activated carbon (AC) as a high capacity non-specific adsorbent.^[5,6] The porous structure of ACs provide high surface area for adsorption to occur, therefore providing high removal efficiencies.^[7] Additionally, the vast variety of low cost source materials enable it to be made with low production costs. Regeneration of AC is an important factor to restore its adsorption capacity for reuse without adversely affecting its porosity. In a traditional thermal regeneration process, the spent AC must first be dried to a desired moisture content, it heated to high temperatures (700 – 1000°C) and, near the end, injected with steam. In each cycle, it is common to have losses of 5 – 10% of the initial mass.^[8] During this process there are also concerns physical changes may on the AC may happen and result in loss of adsorption capacity. Therefore, it is necessary to find

alternative water treatment technologies, in the form of adsorbents that have high binding capacity for organic pollutants, and can be regenerated through alternate means.

In recent years, nanotechnology has become one of the fastest growing topics of interest given its potential to greatly improve areas in electronics, manufacturing, health, and environmental remediation. The advantages associated with nanocomposites in water remediation stems off their high specific surface area, compared to their bulkier counterparts. Additionally, physical properties like size, porosity, morphology and chemical composition can be readily tuned to target pollutants of interest. This combined with a rich surface chemistry modification capacity allows for significant advantages over conventional materials. Nanocomposites are generally composed by two or more materials, and combines the properties of the individual components into one composite systems, generally more efficient, stable or selective.^[9] A sub-class of these, magnetic nanocomposites, have attracted significant interest for application in environmental remediation due to their intrinsic magnetic properties, which allow for a simple separation method from solution by means of exposure to a static field. The most commonly used magnetic nanoparticle is iron oxide (IO MNPs), which is superparamagnetic, when small enough. More so, these magnetic nanoparticles can be produced with readily available materials through well-known methods, facilitating their scale up process.

This dissertation includes an investigation and discussion of a range of magnetic nanocomposite materials with the overall goal of developing sustainable nanoadsorbents for polychlorinated biphenyls in aqueous media, as model organic pollutant, that have high affinity, can be easily applied in the field, and can be regenerated using a low energy strategy, providing a cost-effective alternative to current water remediation technologies.

These nanocomposite materials consisted of iron oxide magnetic nanoparticles (IO MNPs), a polymer backbone (poly(ethylene glycol) 400 dimethacrylate (PEG400DMA), or styrene), and a functional monomer synthesized from plant derived polyphenols (curcumin multiacrylate (CMA) or quercetin multiacrylate (QMA)) in varying compositions. Iron magnetic nanoparticles were selected as the core of the magnetic nanocomposites developed, and Chapter 2 presents the most recent advances made on iron oxide magnetic nanoparticle sorbents in water and wastewater treatment.

1.1 Objectives

The overall objective of this dissertation was to develop magnetic nanocomposite materials as sorbents for organic pollutants in contaminated water and determine their binding capacity and affinity for polychlorinated biphenyls (PCBs), as model organic contaminants, to determine their use as water remediation technologies. This was accomplished through the following four projects:

1. 'Development of ' Novel' Magnetic Core-Shell Nanoparticles for the Removal of Polychlorinated Biphenyls from Contaminated Water Sources'
2. 'Synthesis of Magnetic Nanocomposite Microparticles for Binding of Chlorinated Organics in Contaminated Water Sources'
3. 'Alternating Magnetic Field Modulated Binding in Magnetic Nanocomposites as a Low Energy Regeneration Strategy in Environmental Remediation'
4. 'The Impact of Solution Ionic Strength, Hardness and pH in the Adsorption Efficiency of Polychlorinated Biphenyls on Magnetic Nanocomposite Materials'

This dissertation begins with the background on the relevant aspects of this research in Chapter 2. Recent advances on iron oxide magnetic nanoparticles as sorbents of organic pollutants in water and wastewater treatment are reviewed to determine the state of the art for water remediation technologies and determine existing pitfalls. Chapter 3, 'Development of novel magnetic core-shell nanoparticles for the removal of polychlorinated biphenyls from contaminated water sources' involves the development of core-shell magnetic nanoparticles (MNPs) and their potential as adsorbents in water treatment evaluated through equilibrium binding studies using PCB 126. In Chapter 4 titled 'Synthesis of magnetic nanocomposite microparticles for binding of chlorinated organics in contaminated water sources' homologous materials to those obtained in Chapter 2 are development of magnetic nanocomposite microparticles (MNM) and their potential as adsorbents in water treatment evaluated through equilibrium binding studies using PCB 126, and their binding affinities compared by virtue of particle size and composition. In Chapter 5, 'Alternating magnetic field modulated binding in magnetic nanocomposites as a low energy regeneration strategy in environmental remediation' the MNMs are used to develop a regeneration a low energy regenerating strategy for magnetic nanomaterials as a viable alternative to current regeneration techniques for spent adsorbents. In Chapter 6, 'The impact of solution ionic strength, hardness and pH in the adsorption efficiency of polychlorinated biphenyls on magnetic nanocomposite materials' the effect of environmental factors of fresh water, ionic strength, water hardness and pH are evaluated on the binding capacity of the MNMs.

Chapter 7, 'Effect of atom transfer radical polymerization reaction time on PCB Binding capacities of styrene-CMA/QMA core-shell Iron oxide nanoparticles' involves the development of core-shell nanoparticles and their potential as adsorbents in water treatment evaluated through equilibrium binding studies using PCB 126 and the effect reaction time has on the polymer shell growth and the binding constants. The results obtained here are also compared to those of the other MNP and MNM systems to evaluate the effect of the polymer component on the binding capacity of the systems. Finally, Chapter 8 reports the conclusions of the dissertation and potential future directions for iron oxide nanoparticle based adsorbents in water remediation.

CHAPTER 2. RECENT ADVANCES ON IRON OXIDE MAGNETIC NANOPARTICLES AS SORBENTS OF ORGANIC POLLUTANTS IN WATER AND WASTEWATER TREATMENT

Part of this chapter is taken directly or adapted from work **published in Gutierrez, Dziubla, Hilt (2017)** Copyright2017 De Gruyter. Used with permission from Angela M. Gutierrez, Thomas D. Dziubla, J. Zach Hilt, “Recent advances on iron oxide magnetic nanoparticles as sorbents of organic pollutants in water and wastewater treatment”, *Reviews on Environmental Health and De Gruyter*.

2.1 Abstract

The constant growth in population worldwide over the past decades continues to put forward the need to provide access to safe, clean water to meet human needs. There is a need for cost-effective technologies for water and wastewater treatment that can meet the global demands and the rigorous water quality standards and at the same maximizing pollutant removal efficiency. Current remediation technologies have failed in keeping up with these factors without becoming cost-prohibitive. Recently, nanotechnology has been sought as the best alternative to increase access to clean water supplies. The use of iron oxide magnetic nanoparticles as nanoadsorbents has led the way to a new class of magnetic separation strategies for water treatment. This review focuses on some of the most recent advances in core-shell iron oxide magnetic nanoparticles (IO MNPs) and nanocomposites containing iron oxide nanoparticles currently being developed for water and wastewater treatment of organic pollutants. We discuss the novelty of these materials and the insight gained from their advances that can help develop cost-effective reusable technologies for scale-up and commercial use.

2.2 Introduction

Water contamination continues to be a major environmental problem worldwide. The United Nations estimates around 3.1% of deaths worldwide, which translates to over 1.7 million deaths a year, are caused by unsafe or inadequate access to water.^[1] Access to safe drinking water is not only a human right but a necessary factor for economic productivity and technological development. There is an ever increasing need for the global community to develop efficient and affordable technologies to improve the quality of water to meet human and environmental needs.

In recent years, nanomaterial-based technologies have emerged as promising alternatives to current water treatment techniques, providing solutions able to remove pollutants from water with high affinity and efficiency, at lower operational costs and that can, at the same time, meet the increasingly stringent water quality standards.^[2-4] One of the main advantages associated with the use of nanomaterials for water remediation is associated with their high specific surface area. Because of this, nanomaterials are often times used as adsorbents for a variety of molecules in water and waste water treatment. Conventional adsorbents face challenges related to low capacity and selectivity, and/or short usable lifespan due to ineffective adsorption-regeneration cycles that reduce the adsorption capacity of the adsorbent thus making it less cost-effective.^[5,6]

Of particular interest among nanomaterials used as adsorbents in water remediation are iron oxide magnetic nanoparticles (IO MNPs). In addition to having high surface area to volume ratio, fast kinetics, strong adsorption capacities and high reactivity, IO MNPs possess magnetic properties. When an external magnetic field is applied to IO MNPs, they

rapidly aggregate together and then once the magnetic field is removed, the nanoparticles lose their magnetic moment and can easily be redispersed, if they are superparamagnetic.^[7-9] If small enough, IO MNPs, such as magnetite (Fe_3O_4) or its oxidation counterpart maghemite ($\gamma\text{-Fe}_2\text{O}_3$), will exhibit superparamagnetic properties. IO MNPs also have the ability to respond to exposure to an alternating magnetic field (AMF) and convert magnetic work into internal energy through magnetic relaxation processes and dissipating it as heat.^[10,11] Additionally, the purification process to regenerate these materials does not generate secondary or harmful waste and allows for their reuse in environmental remediation.^[12-16] Most importantly, IO MNPs can be easily synthesized with readily available materials and low cost methods, making them ideal for large-scale operations.

These IO MNPs can be directly used as nanoadsorbents or as the core component of core-shell structures, where the IO MNPs function as magnetic separation, granting operational simplicity to the treatment technology, and the shell provides the desired functionality for pollutant adsorption. Another strategy is to incorporate the IO MNPs into multiphase materials or nanocomposites.^[17] Magnetic nanocomposite materials are generally composed of a magnetic nanoparticle embedded within a non-magnetic matrix, commonly made up of polymers, surfactants, or different carbonaceous forms. These materials combine the properties of the organic matrix with the intrinsic magnetic properties of the nanoparticles, giving rise to unique materials with a variety of applications.

Contamination due to organic pollutants continues to pose a health risk to aquatic environments and humans. Persistent organic pollutants (POPs), such as polycyclic aromatic hydrocarbons (PAHs), polychlorinated biphenyls (PCBs), pesticides, various

industrial additives and pharmaceutical and personal care products (PPCPs) are ubiquitous in nature.^[18,19] POPs have consistently been found in seawater, groundwater, drinking water, sewage effluents and sludge, and they can enter the food chain and bioaccumulate to detrimental levels for human health.^[20, 21] A recent study conducted on orcas and other dolphins in European waters has shown the persistence of PCBs at dangerously high levels in cetaceans, even exceeding the levels found in the Arctic where PCBs are thought to accumulate more.^[22] Additional studies have demonstrated the accumulation of atmospheric POPs over Central and Eastern Europe specifically during the summer time, increasing the chances for direct exposure through inhalation, which can have adverse effects on human health.^[23] Slovakia and Poland are of particular concern, with multiple PCB contaminated sites.^[24] Studies in these regions have shown high levels of bioaccumulation of PCBs in fish up to 25 mg kg⁻¹, in bird's eggs up to 500 mg kg⁻¹, and in the human up to 10 mg kg⁻¹.^[24,25] The National Health and Nutrition Examination Survey (NHANES) in the United States has obtained serum samples from a representative group of people throughout the country. From an analysis of these samples, it was determined that 91 POPs, including 38 PCB congeners, are present in the serum all participants, and more than one tenth of the US population may have over 10 POPs circulating in their body at a concentration in the upper decile.^[26] The body concentrations for individuals living near contaminant accumulation sites, such as an old PCB production site, can be higher by as much as 16.7 pg g⁻¹ lipid compared to the average US population, especially for non-ortho and mono-ortho PCBs.^[27]

Despite their widespread distribution, most POPs are found at very low concentrations and in complex environmental matrixes making their enrichment, capture,

and degradation a strenuous task. Conventional treatment techniques currently applied in water and wastewater treatment are limited to site excavation, *in situ* bacterial remediation, degradation with highly reactive nanoparticles (zero valent iron, bimetallic Fe⁰/Pd or Au/Pd) to less harmful species, and adsorption onto activated carbon (AC), or other carbonaceous materials, as *in situ* or *ex situ* treatments.^[16,28-33] Among these techniques, adsorption is presented as the most favorable technology in terms of environmental friendliness, high affinities for pollutants at trace concentrations, high removal efficiencies, and low economical costs.^[34]

In this chapter review, we focus on highlighting some of the most recent developments in the application of IO MNPs containing materials as magnetic nanoadsorbents of organic contaminants for water and wastewater treatment. The design of these materials and their current applications are discussed, placing special emphasis on core-shell structures and nanocomposite materials. The environmental behavior, stability and other implications of IO MNPs use for environmental remediation fall out of the scope of this review and therefore will not be addressed here.

2.2.1 Core-shell iron oxide magnetic nanoparticles

Adsorption is the most commonly used technique to remove a vast majority of organic and inorganic contaminants in water and wastewater treatment.^[35-38] Conventional adsorbents like activated carbon (AC) are used to adsorb contaminants within its pores through a variety of hydrophobic interactions. Because of the nature of the adsorption mechanisms, AC is non-selective so it can remove a variety organic contaminants from

water, such as pesticides, dyes, PAHs, among others.^[33, 35,39-41] Nonetheless, despite the inexpensiveness of the raw materials needed, the high energy requirements to obtain high quality AC and regenerate it after its use, as well as the detrimental environmental effects traditional regeneration methods have (heating to temperatures above 800°C or using organic solvents to extract adsorbed molecules), have overall made its use less economically feasible for extensive use in environmental remediation.^[42,43] Moreover, the efficacy of such adsorbents is often limited by available surface area or active sites, lack of selectivity and their adsorption kinetics. IO MNPs, due to their very small size, offer significant improvements in terms of higher surface area and sorption sites, and the ability to tune their surface chemistry for enhanced selectivity.

Core shell IO MNPs consist on an iron oxide magnetic core and a shell material (outer layer) that surrounds the core. The core provides the system with unique magnetic properties inherent from IO MNPs, granting the nanoparticles with a significant advantage over other remediation technologies: a fast and easy way to recover the sorbent material from raw environmental samples, without the need of more sophisticated methods like centrifugation or membrane filtration steps.^[14,44,44a-b] The shell of these nanoparticles can be organic, inorganic or a combination of both, and the material selected strongly depends upon the end applications and use. The shell can also improve the stability of the MNPs in solution and help prevent their aggregation. The versatility shell material, allows for the tailoring of the core-shell nanoparticles and, thus, the development of nanocomposite materials that have high affinity for specific contaminants and can be readily used in the environment.

Surfactants are commonly used as surface modifiers to help control bare IO MNP aggregation and interactions.^[47,48] Surfactants can be non-ionic, amphoteric, cationic or anionic, the selection of which to use depends on the end application. Surfactants are oftentimes employed as the first step on the synthesis of a core-shell nanoparticle so as to stabilize the shell coating and the nanoparticle itself in solution.^[49,50] Other times, surfactants are used in conjunction with the shell in order to provide a desired functionality, such as obtaining monodispersed particles upon the incorporation of a surfactant, or enhance the application of the system as a sorbent by aiding in the creation of a porous structure favorable for adsorption.^[51,52] An example of the latter are magnetic permanently confined micelle arrays (Mag-PCMAs), which have been proven to be effective in removing organic contaminants from aqueous solutions.^[52,53] Here, a silica porous layer is used to confine the cationic surfactant micelles into the mesopores in order to prevent their loss during subsequent use. Huang et al.^[53] demonstrated a high adsorption rate and capacity for three different pharmaceuticals and personal care products (PPCPs) and industrial effluents (methyl orange, sulfamethoxazole and gemfibrozil, as well as two different PAHs (acenaphthene and phenanthrene). By adding a micelle swelling agent (the surfactant: 3-(trimethoxysilyl)propyl-octadecyldimethyl-ammonium chloride (TPODAC)), during synthesis in three different weight ratios (0, 30, and 60) and then removing it, Huang et al. were able to increase the pore volume and surface area of the Mag-PCMAs, thus increasing their sorption capacity and diffusion rate. The methyl orange removal efficiency based on visual color change, from dark a dark orange solution to a completely transparent one after 120 minutes of treatment time is shown. These results are then quantified, demonstrating 98% removal of methyl orange after just 30 minutes by all

the Mag-PCMA.s.. Further studies showed that pollutant sorption formed a mono layer dominated by hydrophobic interactions between the surfactants and the molecule in question. Core-shell structured Mag-PCMA.s have also been synthesized for the simultaneous removal of PAHs and metal contaminants in water treatment.^[54-55] This adsorbent presented high adsorption capacities for and Cd⁺ and acenaphthene, removing over 85% of the latter in under 30 minutes. The simultaneous adsorption of these contaminants was not significantly affected by changes in water hardness, increased slightly with increasing pH, and continued to perform, without adsorption losses after 5 regeneration cycles with ethanol extraction.^[54] Overall, Mag-PCMA.s show promise as high efficiency sorbents for organic pollutants having large pore sizes and high degree of porosity, hence providing a sustainable fast and reusable water treatment technique that can be extended and scaled-up to continuous batch reactors.

β -cyclodextrin (β -CD) is a 7 glucose cyclic oligosaccharide that is well-known for its capacity to form host-guest complexes with a variety of molecules due to the formation of cavities with an external hydrophilic surface, an internal hydrophobic pocket and a specific diameter.^[56,57] Due to these specific host-guest interactions, β -CD has been widely used as a surface modifier of IONPs specifically for the capture of some hydrophobic organic contaminants, such as PCBs, and has gained interests in environmental remediation.^[58-60] In 2016, Wang et al.^[61] developed a core-shell magnetic nanoparticle consisting of a magnetite core and a silica bonded β -cyclodextrin layer (Fe₃O₄@ β -CD) capable of adsorbing PCB-28 and PCB-52 in aqueous solutions,. The adsorption capacities of Fe₃O₄@ β -CD for the PCB congeners were studied in water and incubated for 24h, after which the nanoparticles were isolated with a magnet and UV

absorbance measurements were used to determine the concentration of the residual solution. It was demonstrated that the β -CD can increase the binding capacity almost threefold when compared to the magnetite core. The PCB inclusion within the Fe₃O₄@ β -CD cavity was 1:1, and due to the specific diameter of the cavity, the specific adsorption for PCB-28 was a little higher than that for PCB-52. The Langmuir isotherm for PCB-28 and PCB-52 are seen, where the absorptive capacities of 40.01 and 30.32 mmol kg⁻¹ respectively can be seen. The functionalized core-shell nanoparticle developed by Wang et al. can effectively be used to concentrate organic contaminants from water, easily separated from the contamination source and readily extended and applied for environmental remediation.

Recently our group has described a novel and versatile one step co-precipitation synthesis methodology of curcumin stabilized iron oxide magnetic nanoparticles (C-IO MNPs) that can potentially be used in environmental remediation, biomedical and catalysis applications.^[62] Curcumin is a naturally occurring antioxidant and polyphenol found in the Indian spice turmeric, with a high content of aromatic groups in its molecular structure.^[63,64] The presence of these groups allow for the possibility of interaction through π - π stacking with aromatic rich molecules, such as PCBs, in a variety of environments. Bhandari et al.^[62] demonstrated successful incorporation of the curcumin onto the surface of the IO MNPs, representing around 10-12% of the total mass of the nanoparticle's weight. The C-IO MNPs showed a ten-fold increase in safe administration limits compared to uncoated IO MNPs when incubated for 24 hours with human umbilical vein endothelial cells (HUVECs), factor attributed to the antioxidant response of curcumin. Additionally, when these cells were exposed to PCB 126 in the presence of C-IO MNPs a protective

effect against this inflammatory agent was seen. The % viability of HUVECs preincubated with $10 \mu\text{g mL}^{-1}$ of C-IO MNPs for 0, 12 and 24 hours followed by a 24 hour exposure to $50 \mu\text{M}$ PCB 126. It is seen that the antioxidant effect of curcumin protects the cells against PCB 126 showing a greater cell viability between treated and non-treated cells. This protection can be attributed to the interactions between PCB 126 and curcumin, most likely through π - π stacking, which reduced the bioavailability of this stressor, and in the cell burden in general. The results from this study can be further extended to environmental burden and reduced bioavailability of organic contaminants, like PCBs or other dioxin like pollutant, in contaminated water sources due to the aforementioned π - π stacking interactions that can be employed to capture/adsorb and sense these pollutants.

Conventional silica is a synthetic micropowder with a nanoporous structure made up of SiO_2 . Silica gel has traditionally been used during sample pre-concentration and clean up steps in the analysis of PAHs.^[65-67] Given that silica has shown to be effective in isolating PAHs from media, mesoporous silica nanoparticles have been developed for application in water remediation beyond post clean-up.^[68-72] One strategy involves the coating of the IO MNPs with SiO_2 and alkyl moieties to increase the lipophilicity of the nanoparticles.^[68,69] Fan et al.^[68] prepared a hexadecyl-silane magnetic nanoparticles ($\text{Fe}_3\text{O}_4@ \text{SiO}_2\text{-C}_{16}$) through a solvo-thermal method for the adsorption of PCBs in water. The $\text{Fe}_3\text{O}_4@ \text{SiO}_2\text{-C}_{16}$ were capable of removing PCBs from environmental water with absolute recoveries the range of 75.17–101.20%. Silica coated magnetic nanoparticles have also been applied in the removal of organic dyes from water. In this case, the IO MNPs can directly be functionalized with SiO_2 . Wang et al.^[70] synthesized $\text{Fe}_3\text{O}_4@ \text{SiO}_2$ nanoparticles and applied them for the removal of Congo red (CR) from wastewater. The adsorption of

CR onto the core-shell nanoparticles proved to be dependent upon solution pH and only slightly dependent on the ionic strength. The magnetic Fe₃O₄@SiO₂ were efficient in adsorbing CR from water and have the potential to be easily regenerated using ethanol.

Organic polymers have a highly branched structure with a large number of reactive organic functional groups, giving rise to unique 3D molecular networks with large external and internal surfaces, making them great sorbent materials for a variety of analytes.^[73-75] The selection of the monomer used in the core-shell nanoparticles is tightly linked with the ultimate application of the system and the target analyte. It is well known that the most common chemical moiety found in PAHs are aromatic rings, this indicates that the most favorable adsorption interactions with this type of molecule will occur via π - π interactions and other hydrophobic effects. Amiri et al.^[76] developed IO MNPs modified with polyfuran (PFu/Fe₃O₄) for their use as adsorbents of the naphthalene, fluorene and anthracene from water and urine samples. Polyfuran is a conductive polymer consisting of multiple furanyl rings, with multifunctional properties.^[77] The PFu/Fe₃O₄ were effective in binding the PAHs studied obtaining recovery ranges from 93.2% - 99.2% in environmental water samples, and 87.3% - 97.8% in urine samples. The high adsorption ability of the core-shell nanoparticles is a result of the π - π interactions occurring between the PAH molecules and the PFu shell.^[76] Fard et al.^[78] Synthesized polyvinylpyrrolidone (PVP)-coated magnetic nanoparticles to adsorb six emerging contaminants for aqueous environment: Tonalide, Bisphenol A, Triclosan, Metolachlor, Ketoprofen and Estriol. The PVP-coated MNPs were effective at adsorbing the contaminants, showing higher removal percentages for Bisphenol-A and Ketoprofen of 98 % and 95% respectively. The regeneration and recyclability of the nanoparticles using methanol showed no significant

loss in adsorption capacity after 5 cycles. Poly(acrylic acid) chains have been ‘grafted to’ IO MNP surfaces to obtain core-shell nanoparticles, obtaining an efficient nanoparticle system with high adsorption affinity and capacity (870 mg g^{-1}) for methylene blue.^[79]

2.2.2 Magnetic Nanocomposites

Another approach to developing high affinity magnetic nanomaterials for treatment of POPs in water consists on the immobilization of the IO MNPs in a confined micro- or macro-scale support. This immobilization helps prevent the aggregation of the IO MNPs, provides an easy and economic recovery process of the material, and can prevent any release of the nanoparticles into the environment during remediation treatment. The magnetic particles within the nanocomposites can still exhibit their inherent magnetic properties.^[80-83] The non-magnetic component/s have high surface areas, large nanoscale channels for adsorption to occur, and can provide ways to increase affinity or selective for specific contaminants by incorporation of functional chemical groups akin to those of the analyte.^[17,83-86] One such material is chitosan (CS). CS is the second most abundant natural biopolymer, is hydrophilic and contains active sites along its polymeric chain due to the presence of $-\text{NH}_2$ groups. Because of these properties, CS has recently been regarded as one of the most promising biosorbents for water and wastewater treatment for negatively charged contaminants.^[83,87-90] A very successful nanocomposite fabricated using CS, lignocellulose fibers (LCF) and IO MNPs has been developed by Zhou et al.^[91] for biosorptive removal of acidic azo dyes. First, the CS decorated LCF was prepared via surface deposition crosslinking and then magnetized through blending in an aqueous solution containing IO MNPs allowing for spontaneous adherence. The magnetic CS/LCF (mCS/LCF) was used to adsorb acid red 18 (AR 18) as model azo dye from water at

different pH, ionic strength, and temperature. As expected, the adsorption of azo dyes onto mCS/LCF is highly pH dependent due to the protonation of the amino groups ($-\text{NH}_3^+$) in CS at lower pH, which increases electrostatic interactions between the negatively charged AR 18 anions and the positively charged adsorption sites. Additionally, the adsorption isotherms of mCS/LCF indicate a homogeneous surface where the adsorption process is governed by intraparticle diffusion. As the AR 18 molecule is adsorbed onto the exterior surface of mCS/LCF, the available sites diminish until saturation is reached. From this point on, the AR 18 molecules need to overcome the diffusion resistance of the saturated surface to diffuse into the pores, resulting in a longer time needed to reach equilibrium. Hence, the two distinct slopes observed for the Weber-Morris diffusion model. Furthermore, Zhou et al. demonstrated that the removal of AR 18 remained at around 99.68% throughout ten consecutive cycles. Overall, the newly developed mCS/LCF nanocomposite offers a facile and reusable biosorbent that can be easily separated from the adsorption medium by means of applying a magnetic field, all while obtaining remarkably high adsorption capacities, 1181 mg g^{-1} compared to 828.1 mg g^{-1} for pure nanochitosan. Lately, significant focus has been placed on regeneration technologies of spent chitosan-based adsorbents used in water treatment due to concerns regarding its disposal.^[92-94] Several desorption agents have been proposed, such as salts, acids, bases, and organic solvents, however, there is not one strategy that can apply to all so selection of the best one will depend on the nature of the adsorbed contaminant.

Clay is a natural occurring adsorbent known for its hydrophilic nature. Advances in drug delivery have found that clay is capable of intercalating pharmaceuticals into its layered structure, suggesting this same mechanism could be employed to remove pharmaceutical from the environment.^[95-97] The use of unmodified clay proved efficient for removal of cationic pollutants, indicating the need of another component to target pharmaceuticals.^[99-102] Arya and Phillip^[103] have recently designed a nanocomposite containing clay, activated carbon, chitosan and IO MNPs for the adsorption of pharmaceuticals in water. Although activated carbon itself has long been considered one of the best available control technologies for a wide range of pollutants, the removal efficiencies reported for hydrophilic pollutants tends to be smaller.^[103,104] Therefore, with this new magnetic clay composite, the ability to remove cationic or anionic, and hydrophilic or hydrophobic contaminants was achieved. The selected pharmaceuticals for the adsorption studies utilized by Arya and Phillip were atenolol (beta blocker), ciprofloxacin (antibiotic) and gemfibrozil (lipid regulator), of which the first two are hydrophilic. A high removal for atenolol and ciprofloxacin was observed, 85% and 95% respectively. This was attributed to the hydrophilic nature of these compounds and of the chitosan-clay composite, as well as to cation exchange between the cationic form of the pharmaceuticals and the magnetic composite. Correspondingly, a high removal of gemfibrozil, 90%, was seen and attributed to the hydrophobic nature of the pharmaceutical and the activated carbon, as well as surface interactions with CS. The equilibrium sorption of the pharmaceuticals to the nanocomposite at different initial concentrations is fitted using the Langmuir model, allowing for determination of the maximum adsorption capacity of each system was determined. It was seen that this maximum adsorption

capacity was higher for ciprofloxacin (39.1 mg g^{-1}) than for gemfibrozil (24.8 mg g^{-1}) and atenolol (15.7 mg g^{-1}). Additionally, the equilibrium data shed insight into the highly heterogeneous nature of the nanocomposite which favored the adsorption of the pharmaceuticals used. The adsorption process was discovered to be occurring through ion exchange rather than physisorption. This discovery was corroborated by running pH dependent binding study with the three molecules of interest, where it was seen that adsorption of these pollutants was also highly pH-dependent. These results were similar to the findings from Zhou et al., where the pH determines the ionization of the pharmaceuticals.. At lower pH, the adsorption of anionic pollutants, like gemfibrozil, will be favored because of the presence of protonated amine groups on the surface of the clay and chitosan, as well as the presence of the IO MNPs, which contribute to an overall positive charge on the nanocomposite.

More recently, Arya et al.^[105] packed a fixed bed column using the Fe_3O_4 polymer coated clay composite adsorbent to simultaneously adsorb hydrophobic and hydrophilic pharmaceuticals. Complete saturation was achieved after 25h for atenolol where 75 g of the adsorbent had been used to treated volume of 1.5 L. For ciprofloxacin complete saturation was achieved after 45h for atenolol where 75 g of the adsorbent had been used to treated volume of 2.7 L. And for gemfibrozil, complete saturation was achieved after 20h for atenolol where 75 g of the adsorbent had been used to treated volume of 1.5 L. Even though adsorption was the dominating mechanisms for contaminate removal, a slight improvement in adsorption performance was observed when there was biofilm formation on the adsorbent. In general, the nanocomposite developed by Arya and Phillip proves to be a promising adsorbent for pharmaceuticals in water and waste water treatment

that is reusable and easy to use. Furthermore, the nanocomposite can be modified into a biologically active adsorbent giving rise to a scalable technology that already has shown promising results.

Polymers nanocomposites have attracted significant attention for their versatility in polymer functionality. Because of this, these materials have properties such as high specific surface area, tunable morphology and porosity that make them excellent adsorbents. The wide variety of monomer/ligand selection grant polymer nanocomposites with an endless strategy for targeting the analyte of interest. They have been used in the adsorptive removal of various toxic metal ion, dyes, POPs, pesticides, pharmaceuticals, personal care products, emerging contaminants, and microorganisms in water bodies.^[106-111] Polymer nanocomposites can give rise to structure increasingly complicated structures that aim to maximize the surface area for pollutant-sorbent interactions. One such case is the newly synthesized magnetic bouquet-shaped COF (TpPa-1), fabricated by a simple and facile room temperature solution-phase approach, and employed as a sorbent for magnetic solid phase extraction (MSPE) of environmental samples.^[113] The TpPa-1 is made up of clusters of core-shell magnetic nanoparticles and interconnected porous TpPa-1 nanofibers. In this bouquet-like structure, there is a large π - π framework as well as a high percentage of N and O atoms, for pollutant-sorbent interaction to occur. The synthesized nanocomposite has large specific surface area, high porosity, supermagnetism, making it an ideal sorbent for enrichment of trace analytes like fluoranthene (FluA), pyrene (Pyr), benzo(a)anthracene (BaA), benzo[b]fluoranthene (BbF), for benzo(a)pyrene (BaP), and benzo[g,h,i]perylene (BghiP). He et al.^[113] demonstrated the effectiveness of the nanocomposite at analyzing the selected set of PAHs from environmental samples with satisfactory accuracy. Because of

the unique three dimensional structure of the TpPa-1 nanocomposite and the reported affinities, it is believed the nanocomposite would also be effective at binding other contaminants.

There is a constant quest to find an alternative adsorbent to activated carbon and its carbonaceous counterparts that addresses the shortcoming of activated carbon while maintaining high capacity and affinity for organic pollutants. This has led to development in different ways. First, the integration of activated carbon, graphene oxide, carbon black, among others, into the nanocomposites to increase pollutant binding. Mahpishanian et al.^[114] developed a nanocomposite consisting of silica-coated magnetite and phenyl-functionalized graphene oxide for the extraction and pre-concentration of PAHs. The structure of this material provided a very large surface area, high adsorption capacity, high chemical stability and excellent analytical performance.^[114] Here the adsorption of PAHs occurred via π - π stacking interactions, while the hydrophilic oxygen-containing functional groups on the GO surface were stabilizing the system in the aqueous media to obtain a stable dispersion. Likewise, Wan et al.^[115] have core@double-shell structured magnetic halloysite nanotube nano-hybrid adsorbent with target micro-structure and high efficiency removal capacities for dyes. The HNTs skeleton consisted of Fe_3O_4 nanoparticles as inner shell, and poly(DA +KH550) as outside shell. This unique structure integrated the advantages of both components and contributed to a high adsorption capacity of methylene blue of up to 714.29 mg g^{-1} , and excellent cycling stability. Other groups have also worked on developing composites with carbonaceous materials, magnetic particles and a number of other components that can, synergistically, maximize pollutant binding and affinity,

composite efficiency, recyclability, and maintain production and operation costs low.^[116-120]

2.3 Conclusions

This chapter has examined the most recent developments of iron based nanoparticle technologies used for water and wastewater treatment. The unique properties of iron nanoparticles, specifically its magnetic characteristics, have proven to be advantageous for a variety of adsorbents and present great opportunities to keep revolutionizing the available techniques for organic pollutant remediation. Although many of the technologies being developed are still in the laboratory research stage, they have shown success in adsorbing pollutants from water under different pH, temperature, ionic strength, and organic matter conditions with high adsorption capacities and good reusability, showing progress towards pilot testing, up-scaling, and even commercialization.

The challenges faced by water and wastewater treatment IO MNP technologies rely mainly on the potential for human and environmental risk associated with their use, life cycle and disposal. The implications of these nanomaterials, however, can prove to be only temporary as more research is conducted in the area. Another important factor is the cost of making and applying these technologies, which has recently seen a decrease due to the use of readily available and low cost precursor materials such as iron, clay, silica, and chitosan, to name a few. In addition, there is a need for comparative testing to be adopted by the research community that allows comparison between different adsorbent materials and performance so that developments in the area can move forward at a faster pace.

Developing successful iron oxide nanoadsorbents that meet the stringent environmental regulations requires high surface areas nanocomposite with increased affinity that does not sacrifice the magnetic properties of its components, while minimizing the costs of the entire production process. The future for nanoadsorbents based on iron oxide nanoparticles looks very promising not only for removal of organic pollutants from water and wastewater but for other contaminants and from other contaminated media.

CHAPTER 3. NOVEL MAGNETIC CORE –SHELL MAGNETIC NANOPARTICLES FOR THE REMOVAL OF POLYCHLORINATED BIPHENYLS FROM CONTAMINATED WATER

The core-shell magnetic nanoparticle systems were synthesized through surface initiated atom transfer radical polymerization (SI-ATRP). The physicochemical properties of the nanoparticles were then characterized, and equilibrium binding studies with PCB 126 were conducted. The goal of this work was to evaluate ability of the synthesized nanoparticles to bind PCB 126, and obtain their binding coefficient constants. The chapter is taken directly or adapted from work **published in Gutierrez, Bhandari, et al (2019)** Copyright2019 Elsevier B.V. Used with permissions from Angela M. Gutierrez. Rohit Bhandari, Jiaying Weng, Arnold Stromberg, Thomas D. Dziubla and J. Zach Hilt. “Development of novel magnetic core-shell nanoparticles for the removal of polychlorinated biphenyls from contaminated water sources”, Materials Chemistry and Physics and Elsevier B.V.

3.1 Abstract

Nanotechnology has been sought as promising field to develop cost-effective technologies for water treatment to meet the global demands and the rigorous water quality standards. The use of iron oxide magnetic nanoparticles (IO MNPs) as nanoadsorbents has led to a new class of magnetic separation strategies for water treatment. In this work, we developed core-shell nanoparticle systems, via atom transfer radical polymerization, with magnetic core and polymer shell, and characterized them for the capture of polychlorinated biphenyls (PCBs), as model organic pollutants. Polyphenolic-based moieties, curcumin multiacrylate (CMA) and quercetin multiacrylate (QMA), were incorporated onto the polymeric shell to create high affinity binding sites for PCBs. The affinity of these novel

materials for PCB 126 was evaluated and fitted to the nonlinear Langmuir model to determine binding affinities (KD). The KD values obtained were: PEG MNPs (8.42 nM) < IO MNPs (8.23 nM) < QMA MNPs (5.88 nM) < CMA MNPs (2.72 nM), demonstrating that the presence of polyphenolic-based moieties enhanced PCB 126 binding affinity, likely as a result of $\pi - \pi$ stacking interactions. These values are lower than KDs for activated carbon, providing strong evidence that these novel core-shell nanoparticles have a promising application as nanoadsorbents for specific organic contaminants.

3.2 Introduction

Water is the most essential natural resource for human life, yet only 0.03% of the total available water on earth can be utilized for human consumption, and over 1 billion people lack access to safe drinking water.^[131, 132] The spread of a wide range of environmental contaminants in surface water has become a worldwide problem, affecting human health and the ecological environment.^[30, 133]

Polychlorinated biphenyls (PCBs) are some of the most persistent, ubiquitous, and bio-accumulated pollutants in the environment, despite the fact that their production was banned in 1979 in the United States and in 2001 by the Stockholm Convention on Persistent Organic Pollutants.^[135 - 137] PCBs have poor aqueous solubility and low volatility, which makes their extraction from the environment especially challenging. Because of environmental cycling, PCBs have been distributed worldwide.^[135] Current remediation techniques for persistent organic pollutants, such as PCBs, involve dredging and subsequent deposition in landfills, or complete degradation through incineration or chemical dehalogenation techniques^[138]. However, it has been shown that these techniques could result in harmful byproducts when insufficient temperatures are reached during

incineration, can require organic solvents that are often times more toxic than the pollutants being remediated, and could contribute to the pollutant's ubiquitous nature through air, water and slurry transport processes in the landfill's surrounding environment. [139 - 141]

Significant advances have been made in wastewater treatment and water remediation. Oxidation, photocatalytic degradation, membrane filtration, ion exchange, adsorption/separation processes and bioremediation all show promising results. [37,142,143] Nevertheless, their application has been limited due to a number of factors, of which the most important are efficiency, energy requirements and economic cost [37,133, 144, 145]. In contrast, adsorption is a useful strategy because of its ease of application, low cost and rich sorbent variety. The unique properties of sorbent materials such as porosity, large surface area, mechanical strength, tunable shapes and morphologies and a variety of functional groups present on their surface are being exploited for a range of industrial applications (e.g., heavy metal separation from water) [145-147]. Furthermore, nanoadsorbents have a very high specific surface area and associated sorption sites, provide very short diffusion paths, and allow tunable surface chemistry [148] and have been successfully used in environmental applications with promising performance in pollutant mitigation and/or removal.

Among nanoadsorbents, magnetic nanoparticles (MNPs) have gained interest as promising alternatives to current water treatment techniques that can meet the stringent water quality standards at lower costs and higher efficiencies. [11-12] Iron oxide magnetic nanoparticles (IO MNPs), such as magnetite (Fe_3O_4) or maghemite ($\text{Y-Fe}_2\text{O}_3$), possess superparamagnetic properties, when small enough. Because of this feature, an external magnetic field will rapidly aggregate the IO MNPs together, and once the magnetic field is removed, their magnetization decreases to zero, resulting in them being redispersed.

[13,16,149] Therefore, IO MNPs in combination with an external magnetic field can be used as a separation tool for organic contaminants from aqueous or slurry matrices, without requiring centrifugation or filtration steps even when dealing with raw environmental samples. IO MNPs also have the ability to generate heat in response to exposure to an alternating magnetic field (AMF), which can cause local modification of its properties, such as thermal treatment or binding properties. Additionally, these IO MNPs can be regenerated through purification processes that do not require harmful solvents or generate secondary byproduct. [21-29,150] Most importantly, IO MNPs can be easily synthesized with readily available materials and low cost methods, making them ideal for large-scale operations.

Furthermore, the surface of the IO MNPs can be easily modified to incorporate a variety of materials, such as organic molecules, polymers, surfactants, oligonucleotides, among others, that improve the stability of the MNPs in solution and help prevent their aggregation, as well as providing additional functionalities for tailored applications. The incorporation of the IO MNPs into core-shell structures has been widely exploited because of its versatility in shell materials that can provide desired functionality, while the magnetic core functions as the means for magnetic separation. In order to obtain the desired functionalities, there are several strategies that have been used either as ‘grafting to’ or ‘grafting from’ the MNP surface. Of particular interest are methods which involve surface initiated atom transfer radical polymerization (ATRP), a ‘grafting from’ approach widely used today. [151-1544] ATRP is a controlled “living” radical polymerization which allows for the synthesis of core-shell nanoparticles with tunable thickness. The magnetic properties

of this nanocomposites have enabled their use in environmental applications for capture and/or separation where they can be easily decanted out of solution.^[151-155, 158]

To obtain larger adsorption capacities for a specific compound, various functional monomers or crosslinkers can be incorporated in the ATRP reaction, which will modify the chemical composition of the adsorbent via its shell. Plant derived polyphenols, such as quercetin and curcumin, are a well-known class of naturally occurring antioxidants rich in aromatic and phenolic moieties. The prevalence of these types of functionalities have been observed in computational analysis of the monoclonal antibody S2B1, which possesses high selectivity and nanomolar binding affinities for coplanar, non-ortho-chlorinated PCB congeners. The sterically constrained deep binding pocket present in this antibody presents aromatic residues of tyrosine and arginine, where pi-cation interactions with the center of the PCB molecule take place.^[159] This pi-pi stacking interactions between PCB and aromatic residues have also been observed in other antibodies, as well as in water-sediment interactions where humin and humic matter act as PCB sinks.^[160-1644] Therefore, by incorporating plant derived polyphenols into core-shell magnetic nanoparticles, their aromatic and phenolic moieties will improve the adsorption behavior for organic contaminants such as PCBs.

In this work, core-shell magnetic nanoparticles were prepared using ATRP to coat IO MNPs with a PEG-based polymer shell crosslinked with acrylated plant derived polyphenols. Two different polyphenols, curcumin and quercetin, were acrylated and incorporated in the core-shell magnetic nanoparticles to enhance their adsorption capacity for PCBs. The functionalized nanoparticle systems were characterized for size, shell coating percent, response to a static magnetic field and stability. The binding isotherm for

a model contaminant, PCB 126, was studied, and the binding constants for the four systems synthesized were evaluated using the Langmuir adsorption model.

3.2.1 Experimental details

3.2.1.1 Materials

Iron (III) chloride hexahydrate ($\text{FeCl}_3 \cdot 6 \text{H}_2\text{O}$); iron chloride tetrahydrate ($\text{FeCl}_2 \cdot 4 \text{H}_2\text{O}$); 2-bromo-2-methyl propionic acid (BMPA); 2,2' bipyridine (Bpy); copper(I) bromide (CuBr); copper powder (<425 micron), triethyl amine (TEA), acryloyl chloride, and potassium carbonate (K_2CO_3) were obtained from Sigma Aldrich (St Louis, MO). Ammonium hydroxide (NH_4OH) was purchased from EMD Chemicals (Gibbstown, NJ). Poly(ethylene glycol) 400 dimethacrylate (PEG400DMA) was obtained from Polysciences INC. (Warrington, PA). Curcumin was purchased from Chem-Impex International, Inc. (Bensenville, IL) and quercetin was purchased from Cayman Chemicals (Ann Arbor, MI). 3,3',4,4',5-Pentachlorobiphenyl (PCB-126) in isooctane was purchased from Accustandard (New Haven, CT). All solvents (Isooctane, ethanol HPLC grade, tetrahydrofuran (THF); dichloromethane (DCM), acetonitrile (ACN)) were obtained from Fisher Scientific (Hannover Park, IL). All materials were used as received

3.2.1.2 Curcumin multiacrylate synthesis and purification

Curcumin multiacrylate (CMA) was prepared by reacting curcumin with acryloyl chloride according to the protocol described by Patil et al.^[165,166] Briefly, curcumin was dissolved in THF at a concentration of 50 mg/mL. Both acryloyl chloride and TEA were added at a 3:1 ratio with respect to curcumin. The reaction mixture was purged with nitrogen for 20 min and allowed to react overnight. The reaction mixture was then filtered

to remove the byproduct salts formed. The THF was evaporated and the remaining solid was re-dissolved in DCM. This solution was then purified by washing three times with K_2CO_3 0.1 M to remove any unreacted acryloyl chloride, and again with HCl 0.1 M (three washes) to remove unreacted TEA. Finally the DCM was evaporated to obtain CMA.

3.2.1.3 Quercetin multiacrylate synthesis and purification

Quercetin multiacrylate (QMA) was prepared by the reaction of quercetin with acryloyl chloride according to the method described by Gupta et al.^[166] Briefly, quercetin was dissolved in anhydrous THF at a concentration of 100 mg/mL. Acryloyl chloride and K_2CO_3 were both added at a 6:1 ratio with respect to quercetin. The reaction vessel was purged with nitrogen for 20 min and allowed to react overnight. The reaction mixture was then filtered to remove the byproduct salts formed. The THF was evaporated and the remaining solid was re-dissolved in DCM. This solution was then purified by washing three times with K_2CO_3 0.1 M to remove unreacted acryloyl chloride. Finally the DCM was evaporated to obtain QMA

3.2.1.4 Iron oxide nanoparticle synthesis

Iron oxide magnetic nanoparticles (IO-MNPs) were synthesized via a one-pot co-precipitation method.^[17] A 2:1 molar ratio of $\text{FeCl}_3 \cdot 6 \text{H}_2\text{O}$ and $\text{FeCl}_2 \cdot 4 \text{H}_2\text{O}$, respectively, were dissolved in 40 mL of deionized (DI) water and combined in a sealed 3-neck flask under vigorous stirring and nitrogen flow to achieve an inert synthesis environment. The solution was heated to 85°C and, at this point, 5 mL of NH_4OH (30.0 % v/v) was injected dropwise into the vessel. The reaction was carried out for 1 h at this temperature. The nanoparticles were then magnetically decanted and washed three times with DI water.

Finally, the particles were re-suspended in 45 mL of DI water and dialyzed against water for 24 h. (100 kDA molecular weight cutoff).

3.2.1.5 Surface initiated polymerization

The core-shell nanoparticles were prepared by minor modifications of the previously reported method by Wydra et al.^[167] Briefly, the uncoated nanoparticles and the BMPA initiator were mixed at a 1:4 molar ratio in a 75-25 ethanol – DI water solution. The mixture was stirred for 24 h at room temperature. The particles were then washed three times with ethanol. The initiator coated particles (BMPA MNPs) were then suspended in ethanol for the ATRP reaction. The amount of catalyst used was determined based on a macromere ratio. The ratios used were 1:0.04 for Bpy and 1:0.01 for CuBr. Additionally, 2-3 crystals of Cu(0) were combined with the catalyst in 5 mL of ethanol. The catalyst solution and particles were then placed in a 3-neck flask under nitrogen bubbling and heated to 50°C. The acrylated polyphenol (CMA or QMA), was mixed with 8 mmol of the macromere in a 90:10 molar ratio, and injected into the reaction vessel once it reached a temperature of 50°C. The reaction was carried out for 24 h. After this, the particles were magnetically decanted and washed three times with ethanol, five times with a 50-50 % (v/v) ACN/DCM solution, and twice with a 50-50 % (v/v) ethanol/DI water solution. Finally, the particles were re-suspended in DI water.

3.2.2 Particle Characterization

3.2.2.1 Fourier transform infrared (FTIR) spectra

Attenuated total reflectance FTIR (ATR-FTIR) was used to determine the surface functionalization with a Varian Inc. 7000e spectrometer. Dried samples were placed on the

diamond ATR crystal and the spectrum was obtained between 700 and 4000 cm^{-1} using 32 scans.

3.2.2.2 Thermogravimetric analysis (TGA)

TGA was used to quantify the mass percent of the coating on the particle systems using a Netzsch Instruments STA 449A system. Approximately 5 mg of the dry sample was heated at a rate of 5°C/minute until a temperature of 120°C under constant nitrogen flow. The system was kept isothermal for 20 min to vaporize residual solvent and water vapors. The sample continued to be heated at 5°C/minute until a temperature of 600°C. The presented mass loss values are normalized to the mass after isothermal heating at 120°C.

3.2.2.3 Transmission electron microscopy (TEM)

TEM images of the samples were obtained using a JOEL 2010F at an accelerating voltage of 200 keV. The nanoparticles were diluted to a 1 mg/mL concentration in DI water and then dried on a lacey carbon TEM grids prior to analysis.

3.2.2.4 X-Ray Diffraction (XRD)

The X-ray patterns of the nanoparticles were obtained using a Siemens D-500 X-ray spectrometer with a $\text{CuK}\alpha$ radiation source ($\lambda = 1.54 \text{ \AA}$) at 40 kV and 30 mA scanning from 5° to 65°, at a scan rate of 1°/minute. The XRD patterns were used to estimate the particle's crystal domain using the Scherrer equation:^[168]

$$\tau = \frac{K\lambda}{\beta \cos\theta} \quad (1)$$

where τ is the mean size of the ordered, crystalline domains, K is a dimensionless shape factor with a value close to unity (for iron oxide, $K = 0.8396$), λ is the X-ray wavelength, β is the line broadening at half the maximum intensity (FWHM) after subtracting the instrumental line broadening, and θ is the Bragg angle, in radians (17.72°). Additionally, we use the XRD patterns to confirm the magnetic crystal structure of the iron oxide nanoparticles

3.2.2.5 Dynamic light scattering (DLS)

DLS measurements were obtained using a Malvern Zetasizer, Nano ZS90 instrument. The nanoparticle solutions were diluted to 200 $\mu\text{g/mL}$ and probe sonicated for 10 minutes prior to analysis.

3.2.2.6 Ultraviolet (UV)-visible spectroscopy

The stability of the nanoparticles was analyzed using a Cary Win 50 probe UV-visible spectrophotometer. The magnetic nanoparticles were diluted to 200 $\mu\text{g/mL}$ in DI water, and probe sonicated for 10 min. The samples were then placed in a quartz cuvette and their change in absorbance was read at 540 nm for a period of 12 h.

3.2.3 PCB 126 Binding Studies

The binding capacity of the MNPs to PCB 126 was conducted under equilibrium conditions, as determined by previous kinetic studies. All experiments were carried out using 0.1 mg of the core-shell nanoparticles (CMA MNPs, QMA MNPs, PEG MNPs, and IO MNPs), suspended in a 99:1 DI water to ethanol solvent in 3 mL borosilicate glass vials.

Different PCB 126 stocks of varying concentrations were freshly prepared in ethanol. Binding experiments were carried out in batch conditions: 0.1 mg of the freshly prepared core-shell MNPs were placed in a 3 mL borosilicate glass vial and dispersed in DI water. The samples were spiked with the PCB 126 stock solutions to obtain the initial concentrations ranging from 0.003 – 0.1 ppm, all while maintaining a solvent ratio of 99:1 of DI water to ethanol. The samples were initially sonicated for 10 minutes to ensure a well dispersed sample and then subjected to orbital shaking for 24 h at 200 rpm and room temperature conditions, in order to evaluate the equilibrium binding. At the end of the binding study, the MNP suspension was separated by exposure to a static magnet for ~ 10 min, as seen in Figure 3-1. The supernatant containing the unbound PCB 126 was placed into a new borosilicate glass vial and a 1:1 liquid extraction using iso-octane was performed for 24 hours. Finally the organic phase, rich in PCB 126, was collected using a Hamilton syringe and transferred to a glass chromatography vial for analysis. At this point each sample was spiked with the internal standard, 5'-fluoro-3,3',4,4',5-pentachlorobiphenyl (F-PCB 126). The PCB 126 concentration before and after binding were determined using an Agilent 6890N gas chromatography coupled to electron capture detection (GC-ECD),

equipped with an Agilent HP-5MS UI column (30x0.25x0.25). All binding studies were carried out in triplicates.

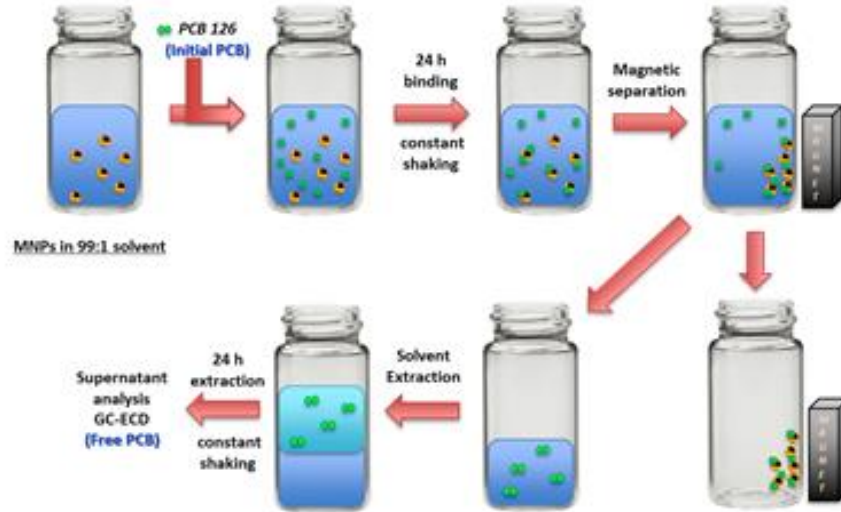


Figure 3-1 Schematic representation of the binding studies conducted with PCB 126 in a 99:1 DI water ethanol solvent

The equilibrium adsorption of PCB 126 was evaluated according to the Langmuir isotherm model. This model assumes a monolayer adsorption on a homogeneous surface where all existing binding sites are energetically equivalent. These sites are all identical, and once a site is filled, no interactions occur between the adsorbed molecules.^[169] The Langmuir model is represented by the following equation:

$$q_e = \frac{B_{max}K_D C_e}{1 + K_D C_e} \quad (2)$$

where q_e (mg/g) represents the adsorption capacity at equilibrium, C_e (mg/L) is the equilibrium concentration of the adsorbate, K_D (L/mg) is the adsorption coefficient of the adsorbant related to the energy of adsorption, and B_{max} (mg/g) is the maximum binding capacity of the adsorbant.

3.3 Results and discussion

Core-shell magnetic nanoparticles were prepared via surface initiated atom transfer radical polymerization. Two acrylated polyphenols, curcumin multiacrylate and quercetin multiacrylate, were selected as functional crosslinkers due to their unique properties and structure similarity to PCB binding domains in antibodies and humin matter. The reaction process followed a 3 step process. First, the uncoated nanoparticles were synthesized using the co-precipitation method, where Fe (III) and Fe (II) salts were dissolved in DI water in a 2:1 ratio and heated to 85°C, at which NH₄OH was added to precipitate the iron oxide magnetic nanoparticles. In the second step, the uncoated nanoparticles, suspended in ethanol, and were mixed with bromomethyl propionic acid in a 1:4 molar ratio for 24 hours at room temperature. Finally, the BMPA-coated nanoparticles were reacted with polyethylene glycol and the acrylated polyphenol in an inert environment, using bipyridine and copper salts as a catalyst, to obtain core-shell magnetic nanoparticles.

FTIR analysis confirms the successful ATRP reaction. The spectrum in Figure 3-2 demonstrates the incorporation of the polyphenol-based moieties, QMA and CMA, and the PEG400DMA. The presence of peaks at ~1750 cm⁻¹ and ~1100cm⁻¹ in all the synthesized core-shell MNPs correspond to the carbonyl band (C=O) stretching and ether band (C-O-C) stretching from the PEG400DMA. For the CMA and QMA core-shell systems, the appearance of additional peaks is seen, confirming the incorporation of the polyphenols onto the coating. In the CMA MNPs spectra, the presence of three peaks between 1604 cm⁻¹ and 1400 cm⁻¹ are attributed to the symmetric ring vibrations of the benzene rings present in CMA. Furthermore, less intense peaks 1026 cm⁻¹ and 964.4 cm⁻¹ correspond to the enol (C-O-C) peak, and the benzoate C-H vibrations of the aromatic rings. Similarly,

the QMA MNPs spectrum exhibits the presence of a broad peak at 1600 cm^{-1} and two shorter peaks at 1432 cm^{-1} and 1404 cm^{-1} that correspond to the aromatic ring vibrations of the benzene rings present in QMA. Additionally, the enol group peak of QMA is observed at 1122 cm^{-1} .

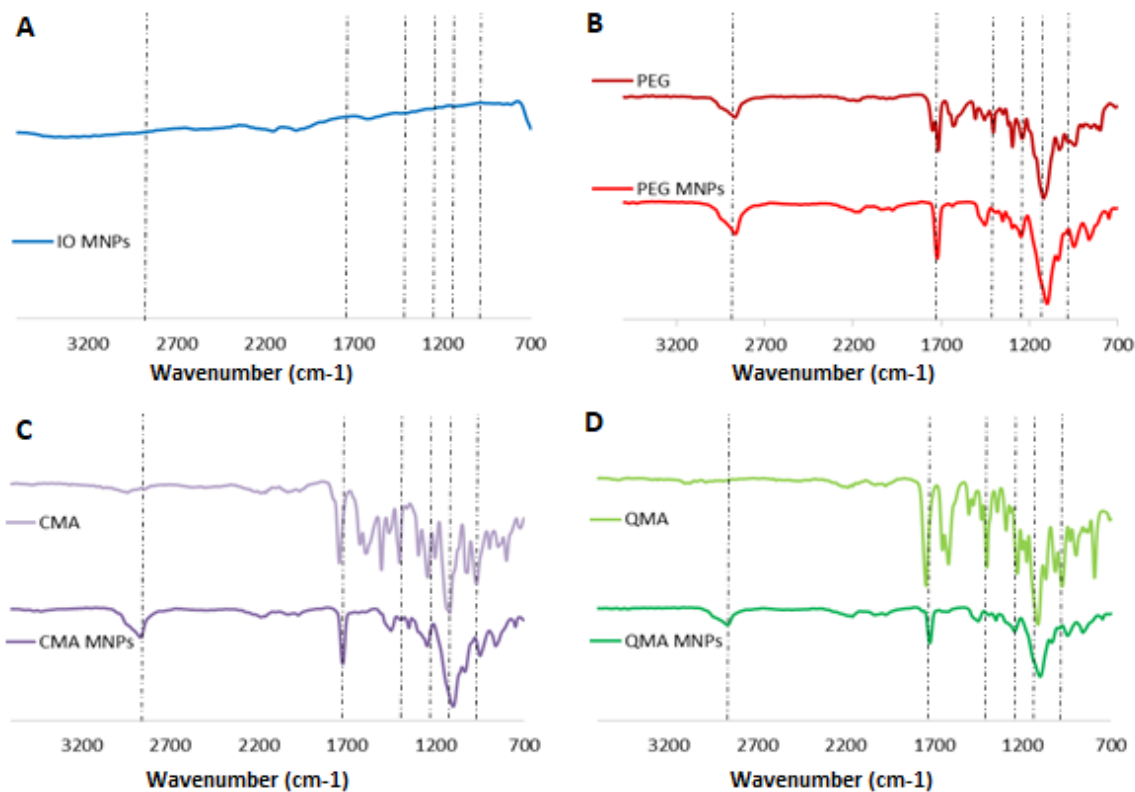


Figure 3-2 FTIR spectra of the synthesized core-shell magnetic nanoparticles

To further characterize the coating on the core-shell MNPs, quantification of this coating was conducted using thermogravimetric analysis (TGA), as shown in Figure 3-3. Minimal weight loss was observed for the uncoated iron oxide nanoparticles. However, a significant weight loss of 9.7%, 8.3 % and 3.2 % was observed for the CMA, QMA and PEG400DMA coated magnetic nanoparticle systems, respectively, suggesting the successful ATRP reaction being conducted on the surface of magnetic nanoparticles.

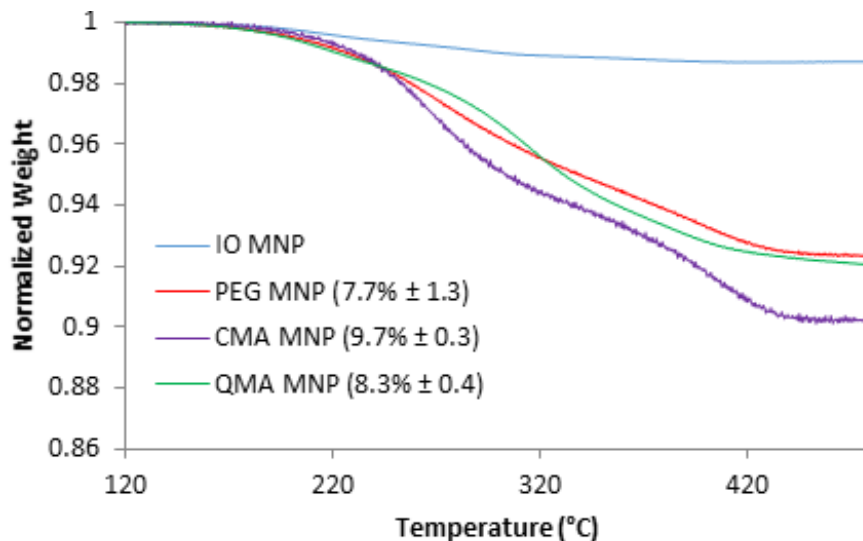


Figure 3-3 . Mass loss profile with increasing temperature of the synthesized core-shell magnetic nanoparticles

The core-shell MNPs exhibit a tendency to be attracted to a static magnet, as can be seen in Figure 3-4. The black aqueous dispersion of MNPs is rapidly magnetically decanted, leaving a transparent solution after exposure to a nearby magnet. This indicates that the core of the MNPs remains superparamagnetic after the ATRP synthesis. Additionally, the XRD patterns of the iron oxide core-shell MNPs synthesized are in agreement with the JCPDS card (19-0629) associated with magnetite. Similarly, the broad diffraction lines in the XRD patterns suggest the nano-crystallite nature of the magnetite particles.^[171,172] The sharp peaks present in the diffractograms in Figure 5 indicate the formation of a crystalline magnetite structure. The highest intensity peak seen for the 35.5° (2θ) corresponds to the (3 1 1) reflection plane of the iron oxide crystalline structure, which was used in the Scherrer equation to calculate the crystallite size of the core-shell MNPs. The calculated crystallite size from the XRD spectra is depicted in Table 3-1.



Figure 3-4 Suspended solution of CMA MNPs and capture of CMA MNPs in a static magnetic field (right).

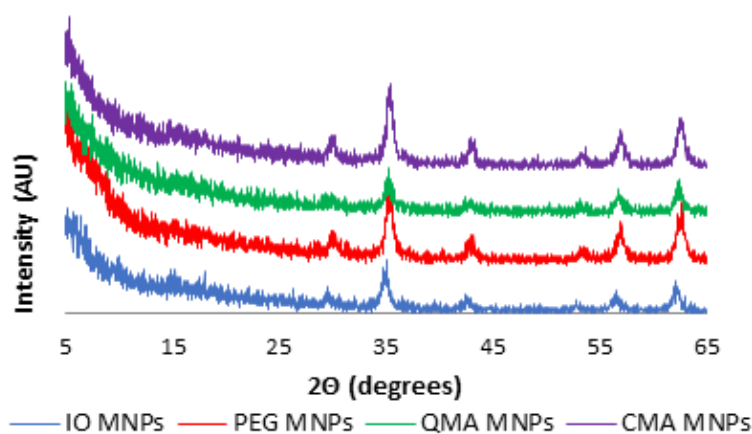


Figure 3-5 XRD patterns of the synthesized core-shell magnetic nanoparticles

Table 3-1 T Size analysis from XRD diffractograms using the Scherrer equation and hydrodynamic size analysis via dynamic light scattering of the synthesized core-shell MNPs (mean \pm std dev. for three independent batches and three samples from each batch)

MNP system	XRD crystal size (nm)	Hydrodynamic size (nm)*	PDI
IO MNPs	13.4 \pm 0.9	126.5 \pm 0.9	0.12 \pm 0.02
BMPA MNPs	10.8 \pm 0.7	141.0 \pm 0.3	0.14 \pm 0.05
PEG MNPs	12.9 \pm 1.6	222.7 \pm 10.6	0.18 \pm 0.10
CMA MNPs	9.5 \pm 1.2	254.6 \pm 19.4	0.15 \pm 0.05
QMA MNPs	9.0 \pm 1.4	232.8 \pm 9.6	0.20 \pm 0.03

The TEM images of the core-shell nanoparticles in Figure 3-6 demonstrate that the core iron oxide nanoparticle size is between 8 - 12 nm. This size is in accordance with values previously reported by our lab group.^[17,168,173] As seen in Table 3-1, these values are similar to those obtained for the crystal size using the Scherrer equation.

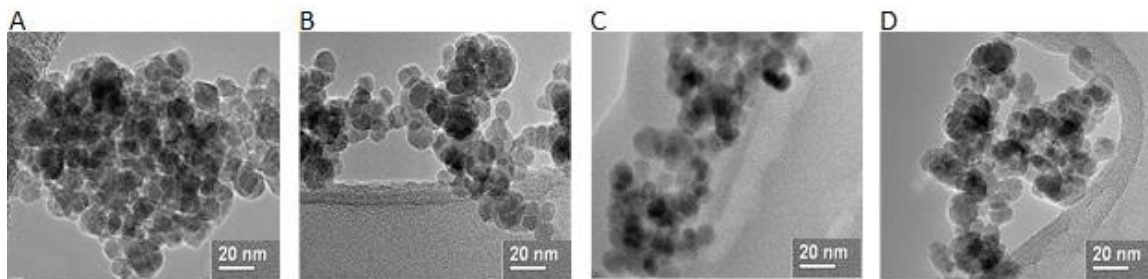


Figure 3-6 TEM images of (a) iron oxide magnetic nanoparticles, (b) PEG coated magnetic nanoparticles, (c) CMA coated nanoparticles and (d) QMA coated magnetic nanoparticles.

The hydrodynamic diameter of the core-shell MNPs was determined via dynamic light scattering (DLS) and reported as Z-average, with the variability in particle size within the batches being quantified by the polydispersity index (PDI), as presented in Table 3-1. The coated MNPs demonstrated a slightly larger aggregate size than the uncoated nanoparticles. It was observed that the hydrodynamic size of the uncoated particles is significantly larger than the size reported from the TEM (Figure 3-6) and XRD analysis (Table 3-1). This is due to the agglomeration of the iron oxide particles in the dispersed state, and it suggests that the core-shell systems are most likely small agglomerates of IO MNPs which are encapsulated within the PEG400DMA-polyphenol-based coatings.

In order to maximize the pollutant binding capacity of the core-shell MNPs in aqueous environments, their stability in solution is very important as further agglomeration could cause the nanoparticles to fall out of solution and limit the available surface for

adsorption to occur. Thus, the stability of the core-shell systems in DI water was analyzed for a period of 12 h, after probe sonication for 10 minutes. All the synthesized systems demonstrated good stability over the period of time studied, as seen in Figure 3-7.

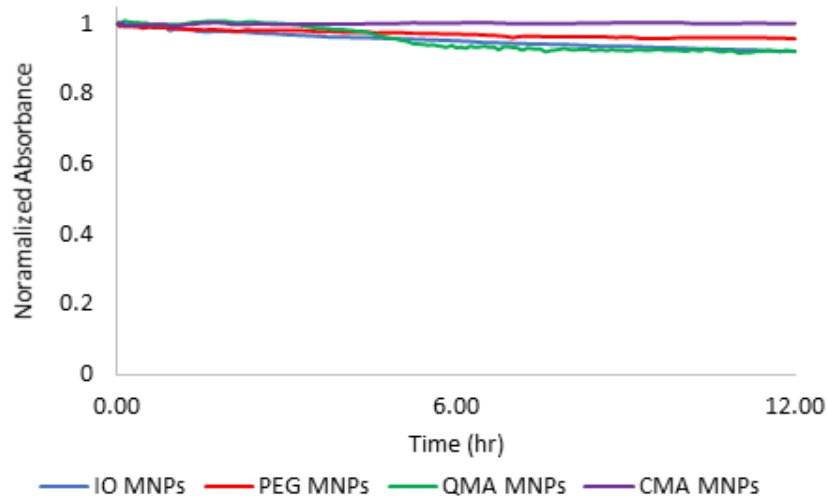


Figure 3-7 Normalized absorbance (at 540 nm) of the MNPs in DI water for 12 hours using UV-visible spectroscopy.

The binding capacity of the nanoparticles for PCB 126 was studied under equilibrium conditions and constant shaking at room temperature. Seven different PCB 126 concentrations were used at a loading of 0.1 mg/mL of the nanoparticles to obtain a binding isotherm. The equilibrium time of 24 hours was determined from previous kinetic studies where the contact time varied from 30 minutes to 1 week. The adsorption isotherm for PCB 126 onto the IO MNPs, PEG MNPs, CMA MNPs and QMA MNPs is shown in Figure 3-8. It can be seen that for all systems the amount of PCB 126 adsorbed increases as the free concentration of PCB increased, until an adsorption plateau was reached. The CMA MNPs bind more PCB at lower free adsorbate concentrations, and as the plateau is reached, it behaves very similarly to the other three systems. The Langmuir model provides a good fit for the experimental data ($R^2 > 0.95$), and thus can be used to describe the adsorption

behavior of the MNP systems. The use of the Langmuir model suggests that the adsorption of PCB 126 onto the MNP systems occurs through monolayer adsorption where there is little to no interaction between the adsorbed PCB molecules. This can be explained due to the planar nature of PCB 126. Previous studies have demonstrated that planar molecules, such as PCB 126, can more closely approach the sorption surface of the adsorbent material, which allows for a favorable π -cloud interaction between the aromatic groups present in the adsorbent and those in the sorbate molecules.^[174-175] The maximum adsorption capacity (B_{\max}) and Langmuir adsorption coefficients (K_D) for each system were calculated and are presented in Table 3-2.

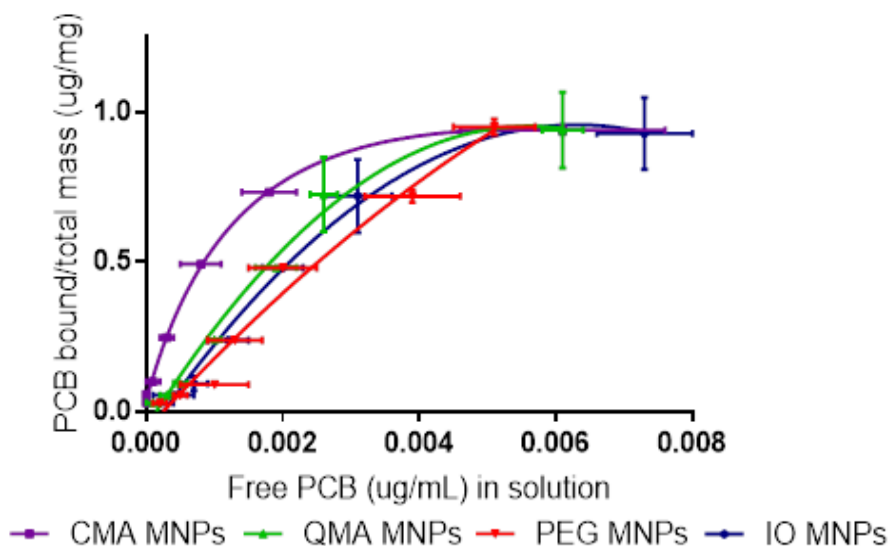


Figure 3-8 Adsorption isotherms for PCB 126 of the core-shell systems at room temperature. PCB 126 initial concentrations from 0.003 – 0.1 ppm fitted using the Langmuir model.

Table 3-2 Langmuir binding constants for the binding isotherms of PCB 126 for the four nanoparticle systems synthesized (n = 12, except for PEG MNPs where n = 15)

MNP system	B_{max} (mg/g)	95% CI	K_D (nM)	95% CI	R²
IO MNPs	0.99	0.98 to 1.01	6.23	6.10 to 6.37	0.963
PEG MNPs	1.91	0.98 to 2.75	8.42	6.54 to 14.24	0.980
CMA MNPs	1.06	1.02 to 1.09	2.72	2.50 to 3.00	0.993
QMA MNPs	1.06	1.02 to 1.10	5.88	5.58 to 6.24	0.956

The binding isotherms were obtained by running four independent studies with newly synthesized materials and preparing three independent samples for each concentration in each of these studies. Although there is some variability between each batch, the amount of PCB bound per total mass at the lower end of the binding isotherm for CMA MNPs is significantly higher than the other curves based on the confidence intervals, indicating a higher affinity for PCB 126. However, because of this batch to batch variability, there is no significant difference in the behavior of the other three systems (IO MNPs, QMA MNPs and PEG MNPs). This behavior is further confirmed when looking at the scatter plots with confidence intervals for each individual initial concentration, where the confidence intervals indicate that the CMA MNPs have a significantly higher affinity than the other systems (see Appendix 1 Figure A1-S1 – S7). For each initial concentration level, from the confidence intervals, differences between the systems can be observed. For example, when the initial PCB concentration level is 0.003 ppm, the estimate difference between CMA MNPs and IO MNPs is of 0.0022 with p-values less than 0.0001.

The maximum binding capacity of all the magnetic nanomaterials is relatively the same for all of the systems and close to 1 mg/g, with the only exception being the PEG

MNPs which is closer to 2 mg/g. These values are all much lower than those normally reported for other carbonaceous materials, specifically activated carbon, which normally present values of maximum loading of higher orders of magnitude.^[174,176] However, the Langmuir adsorption coefficients obtained for the IO MNPs, PEG MNPs, CMA MNPs and QMA MNPs are 8.23 nM, 8.42 nM, 2.72 nM and 5.88 nM, respectively. These values are lower than the reported K_D of 15.2 nM for activated carbon made of coconut shell binding specifically to PCB 126,^[177] showing promising adsorption capacities for our newly synthesized materials to outcompete activated carbon, which the gold standard in environmental remediation/biding of organic contaminants. Additionally, the K_D values obtained for our acrylated polyphenol containing core-shell MNPs are very close to what is reported for specific binding of PCB 126 by the monoclonal antibody S2B1 (2.5 ± 0.01 nM) [39], which further demonstrated the high affinity of these materials for PCB 126.

More closely examining the K_D values in table 2, it is seen that their affinity for PCB 126 is as follows: PEG MNPs < IO MNPs < QMA MNPs < CMA MNPs. This order demonstrates that the presence of the acrylated polyphenols, CMA and QMA, as crosslinkers enhances the binding affinity for PCB 126. This can be explained because of their aromatic rich nature which provides sites for $\pi - \pi$ stacking interactions between the nanoparticle surface and the PCB in solution. In contrast, the PEG MNPs present a lower affinity for PCB 126 than the IO MNPs. This was expected as the hydrophilic nature of the PEG400DMA is expected to hamper the adsorption of the hydrophobic PCB 126 onto the nanoparticle surface.^[178] Furthermore, this emphasizes the important role that the aromatic rich acrylated polyphenols have in enhancing PCB 126 binding by not only allowing for π - π interactions with the adsorbate but also increasing the hydrophobic nature of the

nanomaterial. These results show the great promise for our magnetic nanomaterials to be used as remediation alternatives for harmful contaminants in the environment.

3.4 Conclusions

This study reports the successful synthesis of novel core-shell magnetic nanoparticles using ATRP to coat iron oxide nanoparticles with a PEG-based polymer shell with and without acrylated plant derived polyphenols as additional functional crosslinkers. The curcumin multiacrylate and quercetin multiacrylate were incorporated to enhance pollutant binding capacity of the core-shell nanoparticles. Equilibrium binding studies were conducted at seven different PCB concentration, and binding isotherms for each MNP system synthesized were obtained. The Langmuir model was used to obtain binding coefficients and the maximum binding capacity of the nanoparticles. It was seen that the maximum binding capacity of these materials was lower than what is reported for carbonaceous materials. However, it was demonstrated that these materials possess higher binding affinity coefficients for PCB 126 than activated carbon, which is the gold standard for organic pollutant adsorption. Furthermore, we were able to demonstrate the binding enhancement for PCB 126 by incorporating only 10 mol% of the acrylated naturally occurring polyphenols, curcumin and quercetin, and obtaining binding affinities similar to those observed for antibodies. This materials can be further optimized to enhance the binding capacity by modifying the loading of the polyphenol, and these materials can be further explored as capture agents for other organic contaminants in the environment. Overall, we have obtained novel nanomaterials that can bind PCB 126 in aqueous media and are feasible alternatives for environmental remediation of harmful organic contaminants.

CHAPTER 4. SYNTHESIS OF MAGNETIC NANOCOMPOSITE MICROPARTICLES FOR BINDING OF CHLORINATED ORGANICS IN CONTAMINATED WATER SOURCES

4.1 Abstract

In this work, the development of novel magnetic nanocomposite microparticles (MNMs) via free radical polymerization for their application in the remediation of contaminated water is presented. Acrylated plant-based polyphenols, curcumin multiacrylate (CMA) and quercetin multiacrylate (QMA), were incorporated as functional monomers to create high affinity binding sites for the capture of polychlorinated biphenyls (PCBs), as a model pollutant. The MNMs were characterized by Fourier transform infrared spectroscopy, thermogravimetric analysis, scanning electron microscopy, dynamic light scattering, and UV-visible spectroscopy. The affinity of these novel materials for PCB 126 was evaluated and fitted to the nonlinear Langmuir model to determine binding affinities (KD). The results suggest the presence of the polyphenolic moieties enhances the binding affinity for PCB 126, with KD values comparable to that of antibodies. This demonstrates that these nanocomposite materials have promising potential as environmental remediation adsorbents for harmful contaminants.

4.2 Introduction

In recent years, nanotechnology has become one of the fastest growing topics of interest given its potential to greatly improve areas in telecommunications, electronics, manufacturing technologies, health, and environmental remediation. The benefits associated with using nanomaterials result from their large specific surface area and high reactivity, when compared to their bulk counterparts.^[179] Additionally, physical properties of nanomaterials, such as size, porosity, morphology and chemical composition, can be

tuned to specifically target molecules of interest, depending on the desired application. This combined with a rich surface chemistry modification capacity allows for significant advantages over traditional materials. Nanocomposites are comprised by two or more materials, combining the desired properties from each individual component into the composite system in order to develop more efficient, stable or selective materials.^[9] A subclass of these, magnetic nanocomposite materials, have attracted significant interest in recent years because of their potential application in fields like magnetic resonance imaging, catalysis, biomedicine, and environmental remediation.^[180,181]

Magnetic nanocomposite materials are generally composed of a magnetic nanoparticle embedded within a non-magnetic matrix, commonly made up of polymers, surfactants, or different forms of carbon. These materials combine the properties of an organic matrix with the intrinsic magnetic properties of the nanoparticles, leading to a fast and facile separation method. Magnetic separation is a simple and low-cost method for removing pollutants from contaminated water or slurries, and often times more efficient than more cumbersome methods like centrifugation and membrane filtration. The most commonly used magnetic nanoparticle is iron oxide (IO MNPs) or magnetite (Fe_3O_4), and Fe_3O_4 is superparamagnetic.^[16,47] More so, these magnetic nanoparticles can be produced with readily available materials through well-known methods, facilitating their scale up process. These magnetic composites have found their main area of application in environmental remediation, specifically their use as adsorbents for organic pollutants, heavy metals and other emerging contaminants.^[126,182,183]

Water pollution is a major threat worldwide, which continues to become more complex, difficult and costly, due to the vast majority of chemicals being discharged into

the environment. This is a result of rapid developing economies and technologies, and the inability of regulatory agencies to keep up with the various innovations and their effects in the environment and human health.^[184,185] As harmful contaminants continue to be distributed worldwide, the need to remove them from the environment and increase access to safe drinking water becomes increasingly important. Polychlorinated biphenyls (PCBs) are a group of chlorinated aromatic compounds with a large number of isomers or congeners.^[186] PCBs are some of the most persistent organic pollutants in the environment, despite their production ban in the US in 1979 and further priority classification in the Stockholm Convention on Persistent Pollutants held in 2001.^[133,136,187] PCBs are ubiquitous in the environment, have low solubility and low volatility, and can bioaccumulate throughout the food chain, making their extraction from soil and water especially challenging.^[133,188,189] The most common remediation techniques employed nowadays consist of using physical caps on contaminated areas or dredging of the area and its deposition on a landfill, both of which can result in further leaching of the contaminant into the environment. Alternatively, they are degraded via incineration of stocks, which can result in incomplete combustion and further environmental exposure.^[137] There is a need for other remediation techniques for PCBs that limit the production of harmful by-products and reduce the possibility of further contamination to the environment in their application.

Adsorption is a popular method for water treatment due to its simplicity and vast sorbent variety. Features of the adsorbent such as large surface area, porosity, mechanical strength, tunable shape and morphology, and the presence of a variety of surface functional groups allow for their targeting towards specific contaminants.^[144,145] One way to increase

the affinity for hydrophobic molecules, such as PCBs, is by incorporating hydrophobic components into the polymeric matrix of the magnetic nanocomposite. Of particular interest to our group are plant derived polyphenols, curcumin and quercetin, because they are a well-studied group of naturally occurring antioxidants rich in aromatic moieties. The prevalence of aromatic groups has been detected in other molecules that present very high affinities for PCBs, such as the monoclonal antibody S2B1. Through computational analysis, a sterically hindered deep binding pocket rich in aromatic residues from tyrosine and arginine was discovered, demonstrating a high selectivity for non-ortho chlorinated PCBs congeners.^[12] Within this pocket, π - π interactions between the antibody and the PCB molecule thrive. These types of interaction have also been observed between water and sediment in the environment, especially with humin and humic matter and PCB molecules.^[145,163] Therefore, the incorporation of aromatic rich molecules, such as plant derived polyphenols, into the polymer matrix of the magnetic nanocomposites will increase the affinity of these materials for PCBs in solution.

The proposed study focuses on the development of magnetic nanocomposite microparticles using free radical polymerization to synthesize PEG-based crosslinked polymers with functional monomers from acrylated plant derived polyphenols and magnetic iron oxide nanoparticles. Both curcumin multiacrylate and quercetin multiacrylate were be used in order to enhance the binding affinity of the systems towards PCBs 126, our model contaminant. Binding isotherms were fitted using the Langmuir model obtaining the binding constants and the maximum binding capacities of the synthesized MNM systems.

4.3 Experimental

4.3.1 Materials

Iron (III) chloride hexahydrate ($\text{FeCl}_3 \cdot 6 \text{H}_2\text{O}$); iron chloride tetrahydrate ($\text{FeCl}_2 \cdot 4 \text{H}_2\text{O}$), ammonium persulfate (APS), N,N,N'-Trimethylethylenediamine 97% (TEMED), triethyl amine (TEA), acryloyl chloride, and potassium carbonate (K_2CO_3) were obtained from Sigma Aldrich (St Louis, MO). Ammonium hydroxide (NH_4OH) was purchased from EMD Chemicals (Gibbstown, NJ). Poly(ethylene glycol) 400 dimethacrylate (PEG400DMA) was obtained from Polysciences INC. (Warrington, PA). Curcumin was purchased from Chem-Impex International, Inc. (Bensenville, IL) and quercetin was purchased from Cayman Chemicals (Ann Arbor, MI). 3,3',4,4',5-Pentachlorobiphenyl (PCB-126) in isooctane was purchased from Accustandard (New Haven, CT). 5'-fluoro-3,3',4,4',5-pentachlorobiphenyl (F-PCB 126) was purchased from Resolution Systems Inc. (Holland, MI). All solvents (Isooctane, ethanol HPLC grade, tetrahydrofuran (THF); dichloromethane (DCM), acetonitrile (ACN), acetone) were obtained from Fisher Scientific (Hannover Park, IL). All materials were used as received.

4.3.2 Iron oxide nanoparticle synthesis

Iron oxide magnetic nanoparticles (IO MNPs) were synthesized via a one-pot co-precipitation method.^[17] In a 3-neck flask a 2:1 molar ratio of $\text{FeCl}_3 \cdot 6 \text{H}_2\text{O}$ and $\text{FeCl}_2 \cdot 4 \text{H}_2\text{O}$, respectively, were dissolved in 40 mL of deionized (DI) water. The flask was sealed purged with nitrogen flow to achieve an inert synthesis environment. Under vigorous stirring and constant N_2 flow, the solution was heated to 85°C under and, at this point, 5 mL of NH_4OH (30.0 % v/v) was injected dropwise into the vessel. The reaction was carried

out for 1 h under these conditions. The nanoparticles were then magnetically decanted and washed thrice with DI water. Finally, the particles were re-suspended in 45 mL of DI water and dialyzed against water for 24 h. (100 kDa molecular weight cutoff).

4.3.3 Curcumin multiacrylate synthesis and purification

Curcumin multiacrylate (CMA) was prepared according to the protocol described by Patil et al.^[165,166] Briefly, curcumin was dissolved in THF at a concentration of 50 mg/mL. Acryloyl chloride and TEA, both, were added at a 3:1 ratio with respect to curcumin. The reaction mixture was then purged with nitrogen for 20 min and allowed to react overnight. Following, byproduct salts formed during reaction were removed through filtration and the THF was evaporated. The remaining solid was re-dissolved in DCM and purified by washing three times with K_2CO_3 0.1 M to remove any unreacted acryloyl chloride, and again thrice with HCl (0.1 M) to remove unreacted TEA. Finally, the DCM was evaporated to obtain CMA.

4.3.4 Quercetin multiacrylate synthesis and purification

Quercetin multiacrylate (QMA) was prepared according to the method described by Gupta et al.^[167] Briefly, quercetin was dissolved in anhydrous THF at a concentration of 100 mg/mL. Both acryloyl chloride and K_2CO_3 were added at a 6:1 ratio with respect to quercetin. The reaction vessel was purged with nitrogen for 20 min and allowed to react overnight. The byproduct salts formed were then filtered out from the reaction mixture. The THF was evaporated and the remaining solid was re-dissolved in DCM. This solution was then purified by washing three times with K_2CO_3 0.1 M to remove unreacted acryloyl chloride. Finally, the DCM was evaporated to obtain QMA.

4.3.5 Magnetic nanocomposite microparticle synthesis

In order to make the MNMs, we first synthesized a gel with the desired functionalities in glass templates via free radical polymerization. The functional monomer, CMA or QMA, was dissolved in DMSO and added to the polyethylene glycol 400 dimethacrylate (PEG400DMA) in a 1:9 ratio. The uncoated MNPs (1 wt %), dispersed in DI water, were then incorporated into this mixture, and quickly vortexed to ensure a good dispersion. The initiator was then added to the mixture, closely followed by the accelerator. The mixture was again vortexed and added to the glass template where the polymerization took place. Ammonium persulfate dissolved in ethanol (APS, 2 wt %) was used as the initiator for the reaction, and N,N,N',N'-tetramethylethylenediamine (TEMED, 0.67 wt %) as the accelerator. Once polymerization occurs, the polymer was cut into small pieces and washed once with ethanol, three times with a 50-50 % (v v⁻¹) ACN/DCM solution, twice with a 50-50 % (v v⁻¹) ethanol/DI water solution and finally once with water. The polymer pieces were then placed overnight in a freezer at -4°C and then lyophilized for a period of 24 hours to remove any excess solvent.

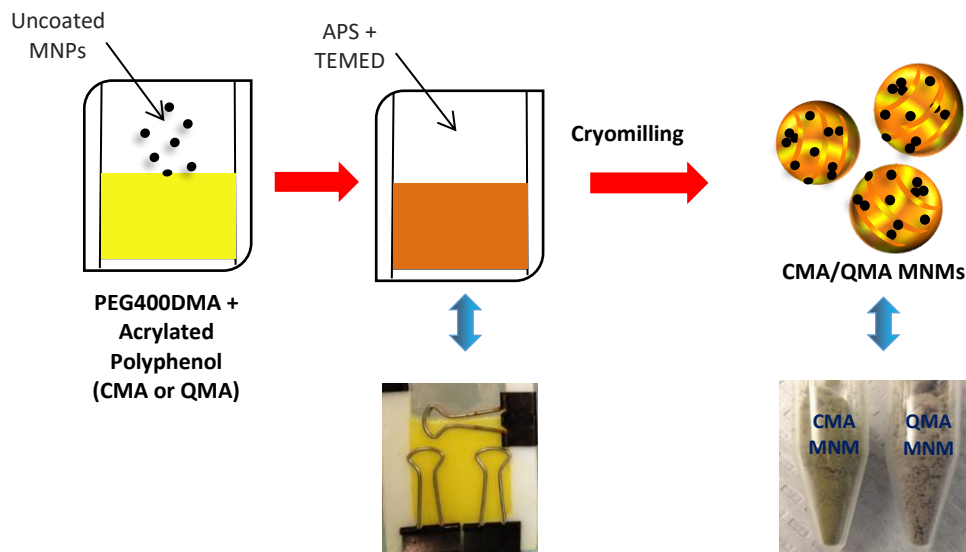


Figure 4-1 Schematic representation of the overall synthesis of magnetic nanocomposite polymers and their cryomilling to obtain magnetic nanocomposite microparticles (MNM).

4.3.6 Cryomilling

The polymers were placed in stainless steel vials and cryomilled under liquid nitrogen using a SPEX SamplePrep 6770 Freezer/Mill Cryogenic Grinder. The process began with a 5 minute pre-cool, followed by two 10 minute cycles at 10 rpm and completed with a 2 minute cool down. The microparticles obtained followed a uniform distribution.

4.3.7 Microparticle characterization

4.3.7.1 Fourier transform infrared (FTIR) spectra

Attenuated total reflectance FTIR (ATR-FTIR) was used to determine the incorporation of the acrylated polyphenols into the polymers with a Varian Inc. 7000e spectrometer. Dried samples were placed on the diamond ATR crystal and the spectrum was obtained between 700 and 4000 cm^{-1} using 32 scans.

4.3.7.2 Thermogravimetric analysis (TGA)

A Netzsch Instruments STA 449A system was used to conduct a TGA of the nanocomposites and quantify the mass percent corresponding to the iron oxide nanoparticles incorporated. Under constant nitrogen flow, approximately 5 mg of the dry sample was heated at a rate of $5^{\circ}\text{C min}^{-1}$ until a temperature of 120°C . The system was kept isothermal for 20 min to vaporize residual solvent and water vapors. Then, the sample continued to be heated at $5^{\circ}\text{C min}^{-1}$ until a temperature of 600°C . The presented mass loss values are normalized to the mass after isothermal heating at 120°C .

4.3.7.3 Particle sizing using a micron sizer

A Systat SigmaScanTM 5.0 software was used to digitally determine the mean size of the microparticle sample and perform the dynamic light scattering analysis of the MNMs in DI water as solvent. The nanocomposite systems were probe sonicated to solubilize at approximately 1mg mL^{-1} . All measurements were conducted in triplicates.

4.3.7.4 Scanning electron microscopy (SEM)

SEM was completed using a Hitachi S4300 microscope in order to observe the particle size. Double-sided adhesive carbon tabs were adhered onto aluminum studs (Ted Pella) and carefully dabbed against a weigh paper containing the dry sample. For all systems, three independent samples were prepared and multiple images were examined for each sample.

4.3.7.5 Ultraviolet (UV)-visible spectroscopy

The stability of the nanoparticles was analyzed using a Cary Win 50 probe UV-visible spectrophotometer. The MNMs were suspended in DI water at a concentration of 0.1 mg g⁻¹ and probe sonicated for 10 min. The samples were placed in a quartz cuvette and their change in absorbance was studied for 12 hours at a wavelength of 540 nm.

4.3.8 PCB 126 binding studies

The capacity of the MNMs to bind PCB 126 was studied under equilibrium conditions, determined by previous kinetic studies. All experiments were carried out using 0.1 mg of the microparticle systems (CMA MNMs, QMA MNMs, and PEG MNMs), suspended in a 99:1 DI water to ethanol solvent in 3 mL borosilicate glass vials.

All binding experiments were carried out in batch conditions where 0.1 mg of dry MNMs were weighed into 3 mL borosilicate glass vials and dispersed in DI water. The samples were then spiked using one of the freshly prepared PCB stocks at one for seven different concentrations (0.0003, 0.0005, 0.001, 0.0025, 0.005, 0.0075, 0.01 ppm), all whilst maintaining a 99:1 DI water to ethanol solvent ratio. All samples were bath sonicated for 10 minutes and then placed in an orbital shaker at 200 rpm and room temperature for 48 hours. After the equilibrium binding study finalizes, the samples are exposed to a static magnet for approximately 20 minutes to make sure all suspended particles are decanted, as seen in Figure 4-2. The supernatant containing the unbound PCB was transferred into a new borosilicate glass vial and a 1:1 liquid extraction using isoctane was conducted for a period of 24 hours. Following this, the organic phase, rich in PCB 126, was collected using a Hamilton syringe and deposited directly into a gas chromatography vial. Each sample

was then spiked with a known amount of the internal standard, 5'-fluoro-3,3',4,4',5-pentachlorobiphenyl (F-PCB 126). Using an Agilent 6890N gas chromatograph coupled with electron capture detection (CG-ECD), equipped with an Agilent HP-5MS UI column (30x0.25x0.25), was used to determine the PCB 126 concentration before and after equilibrium binding studies. All studies were carried out in triplicates, as was each sample per study.

Similarly, batch experiments were conducted for microparticles (MPs) prepared following the same synthesis and characterization procedure as the MNMs, however, without the incorporation of the magnetic nanoparticles. These MPs are used as controls during the binding studies to determine the effect the magnetic component has in binding. For this purpose, three systems were evaluated: CMA MPs, QMA MPs and PEG MPs.

The Langmuir model is the most commonly used model to evaluate the interactions between a molecular adsorbate and a surface site on an adsorbent, and accurately describes many adsorption processes.^[170-190] This model assumes uniform energy for all adsorption sites at localized sites occurring on a homogeneous surface and monolayer adsorption.^[170] The Langmuir model is represented by the following equation:

$$q_e = \frac{B_{max}K_D C_e}{1 + K_D C_e} \quad (1)$$

where q_e (mg g^{-1}) represents the quantity of adsorbate bound at equilibrium, C_e (mg L^{-1}) is the equilibrium concentration of the adsorbate, K_D (L mg^{-1}) is the adsorption coefficient of the adsorbant related to the energy of adsorption, and B_{max} (mg g^{-1}) is the maximum adsorption capacity of the adsorbent, also known as the equilibrium monolayer capacity.

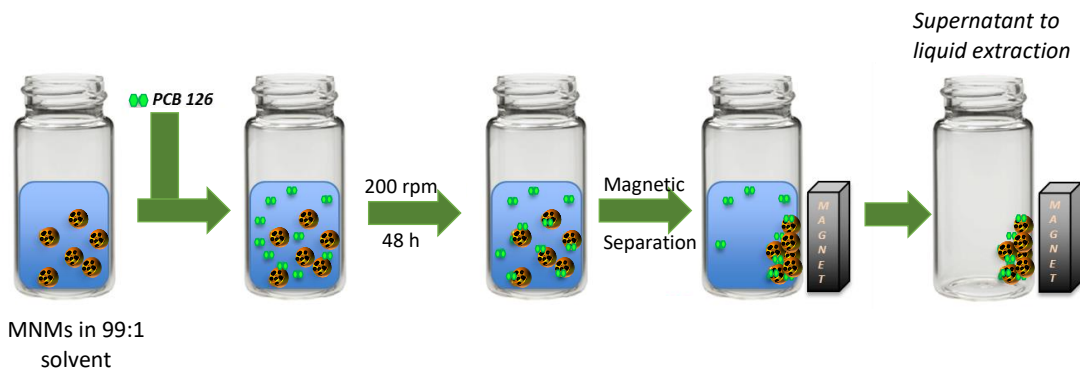


Figure 4-2 Schematic representation of the binding studies conducted with PCB 126 in a 99:1 DI water ethanol solvent

4.4 Results and discussion

Magnetic nanocomposite microparticles were prepared via chemically initiated free radical polymerization. FTIR analysis confirms a successful polymerization for all systems. Figure 3 shows the resulting spectra for the MNM systems where characteristic peaks for PEG400DMA and the functional monomers, CMA and QMA, can be observed. The acrylated polyphenols used in synthesis contain aromatic rings in their structure. Evidence of this functional group in the CMA MNMs is the presence of three peaks between 1604 cm^{-1} and 1400 cm^{-1} , attributed to symmetric ring vibrations, as well as peaks at 1026 cm^{-1} and 964.4 cm^{-1} of lesser intensity that correspond to the enol (C-O-C) functionality and the benzoate C-H vibrations of the aromatic rings, respectively. Likewise, the presence of the benzene rings in the QMA MNMs are confirmed by a broad peak at 1600 cm^{-1} and two shorter peaks at 1432 cm^{-1} and 1404 cm^{-1} , corresponding to the aromatic ring vibrations, in addition to the presence of a peak observed at 1122 cm^{-1} attributed to the enol group present. Finally, the presence of peaks at $\sim 1750\text{ cm}^{-1}$ and $\sim 1100\text{ cm}^{-1}$ in all the spectra in Figure 4-3, respectively corresponding to carbonyl bond (C=O) stretching

and ether bond (C-O-C) stretching, demonstrate the presence of PEG400DMA within the MNM systems.

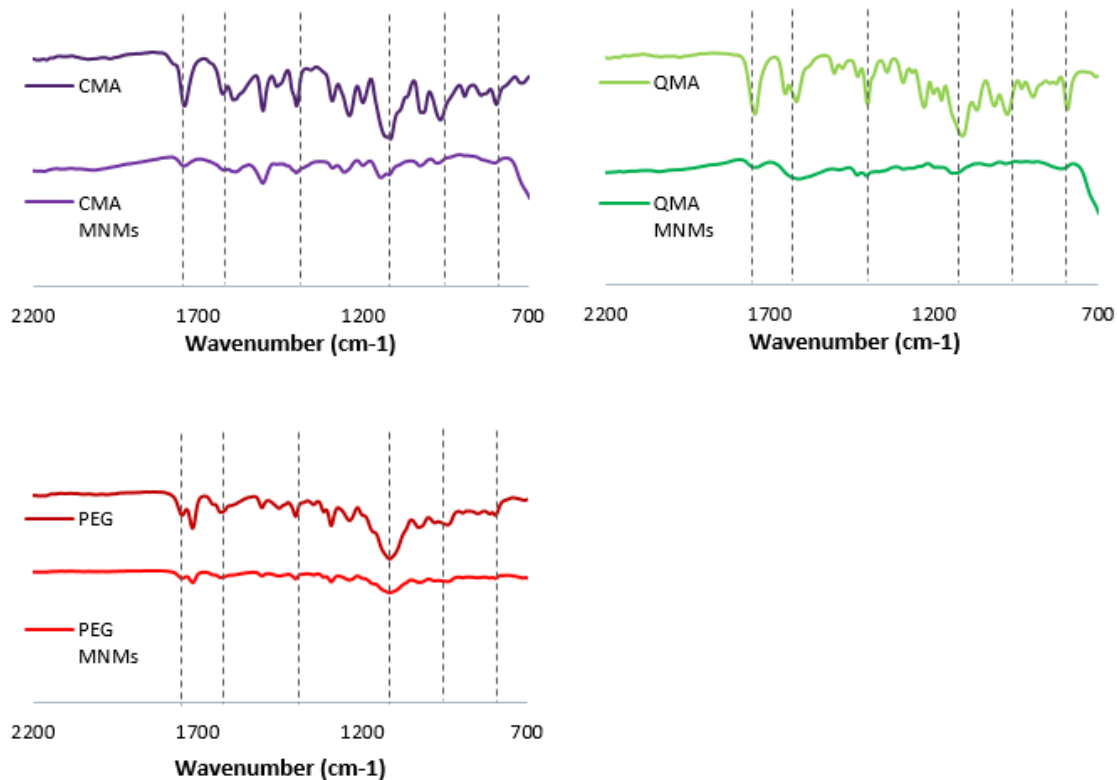


Figure 4-3 FTIR spectra of the synthesized magnetic nanocomposite microparticles. A) CMA MNMs, B) QMA MNMs and C) PEG MNMs.

Thermogravimetric analysis has been established as an effective technique to determine inorganic components in a polymer composite. In the case of the synthesized MNMs, the polymer matrix should completely decompose over the temperature range, leaving only the iron oxide magnetic nanoparticles. The TGA curves for the synthesized MNM systems are presented in Figure 4-4. Here it can be seen that all systems exhibit a single stage thermal decomposition that takes place over a wide range of temperature. The PEG MNMs start to start decompose at a temperature of 218.6°C reaching full decomposition at 420°C. This behavior agrees with what has been reported for the other

PEG400 polymers with ranges of decomposition going from 200°C to 420°C, with a highest weight loss at 340°C.^[168,191] The total weight loss for the PEG MNMs is of 86.7%, and the remaining 13.3% corresponds to the magnetic nanoparticles in the system. Both the CMA MNMs and QMA MNMs begin to decompose at 285.8°C following an almost identical thermogram until a complete polymer pyrolysis is reached at 420°C. In this thermogram, the biggest weight change is seen at 340°C. This onset in initial decomposition temperature can be explained by the presence of the polyphenol moieties. Patil et al.^[166] studied the thermal stability of the CMA monomer reporting the biggest decomposition at around 350°C, which is akin to the temperature observed in the CMA MNMs TGA curve. Similarly, within the temperature range of the QMA MNMs thermogram, previous published studies for quercetin and polyquercetin systems have reported a maximum weight change at a temperature of 340°C which is in accordance to what is observed here.^[167,192] The final weight loss for the CMA MNMs was of 89.6% and for the QMA MNMs of 90.2%, meaning the iron oxide nanoparticles represent 10.4% and 9.8% of the respective systems. Overall, the synthesis and further processing to obtain the MNM systems produces microparticles with an approximately 90:10 polymer network to magnetic nanoparticle composition.

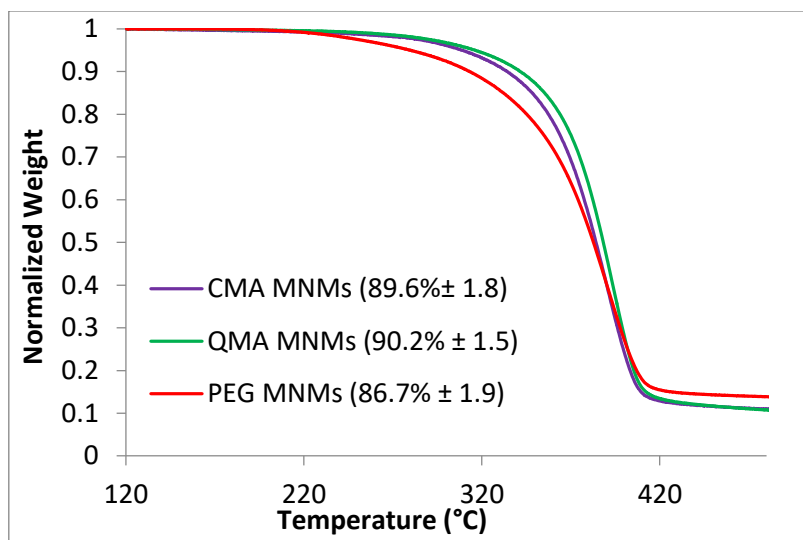


Figure 4-4 Mass loss profile with increasing temperature of the synthesized magnetic nanocomposite microparticles.

The loading of magnetic nanoparticles into the MNMs needs to be enough to enable the MNMs to be pulled out of a dispersed solution upon exposure to a static magnetic field. Figure 4-5 shows how the MNMs dispersed in water forming an opaque solution are rapidly decanted when exposed to a magnetic field, resulting in a transparent solution and the MNMs collected on the side of the magnet.



Figure 4-5 Suspended solution of CMA MNMs in water (left) and capture of CMA MNMs upon exposure to a static magnetic field (right).

The hydrodynamic size of the microparticles was determined using a Systat SigmaScan™ 5.0 software to digitally determine the mean size of the microparticle sample suspended in DI water at a concentration of 1 mg mL⁻¹. The average size for the MNM systems is reported as an average with the variability in particle size within the cryomilling processes being quantified by the polydispersity index (PDI) presented in Table 4-1. All the MNM systems presented a uniform distribution with a size of around 20 μm. The variation in size between the systems comes from the cryomilling process where the polymer films are milled into a fine powder. Because of the aggressiveness of the milling process, the resulting MNMs have random shapes and non-uniform surfaces, as can be seen in the SEM images (Figure 4-6). The average diameter for the MNM systems as determined from the SEM images is approximately 10 μm, even though some particles can be seen to be larger or smaller in the images.

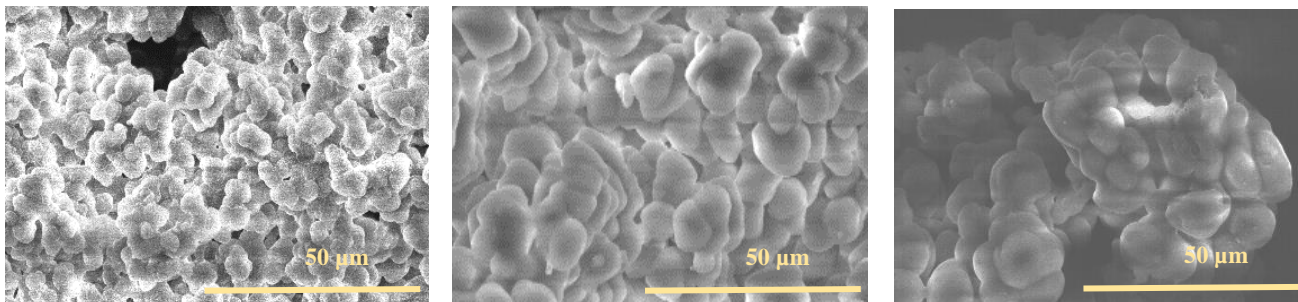


Figure 4-6 SEM images of (a) CMA MNMs, (b) QMA MNMs and (c) PEG MNMs

Table 4-1 Size analysis from SEM images and hydrodynamic size analysis via dynamic light scattering of the synthesized MNMs

MNM System	SEM Diameter (μm)	Hydrodynamic size (μm)	PDI
CMA MNMs	10 ± 1.6	20.6 ± 0.4	0.27
QMA MNMs	11 ± 1.5	15.3 ± 0.6	0.31
PEG MNMs	10 ± 2.0	18.2 ± 0.2	0.22

Furthermore, the stability of the MNM systems in an aqueous environment plays an important role during the binding process. In order to maximize the surface interactions between the MNMs and the pollutant, it is necessary to make sure no further aggregates form in solution. The stability of the MNM systems in DI water was studied for a period of 12 hours after an initial 10 minute probe sonication. It can be seen from Figure 4-7 that all the MNM systems fall out of solution within the first hour. Consequently, it is necessary to introduce some mechanical agitation into the system during the binding studies and for their ultimate application as environmental adsorbents, in order to avoid microparticle aggregation or sedimentation of the MNMs and, hence, maximize pollutant binding.

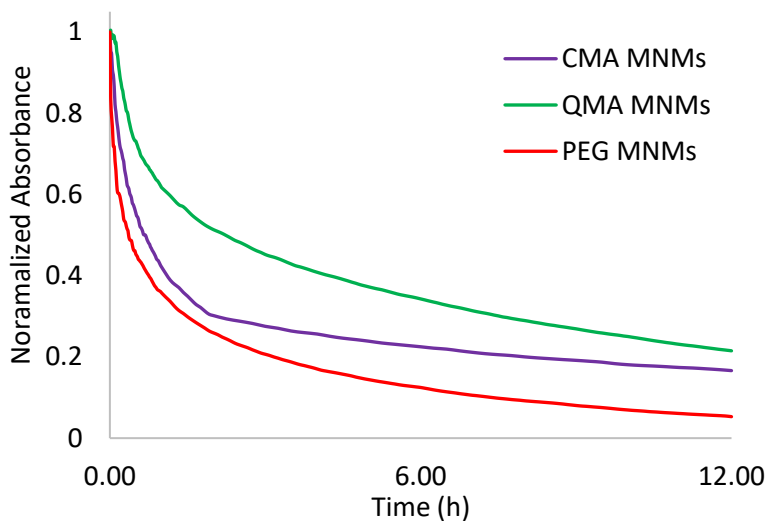
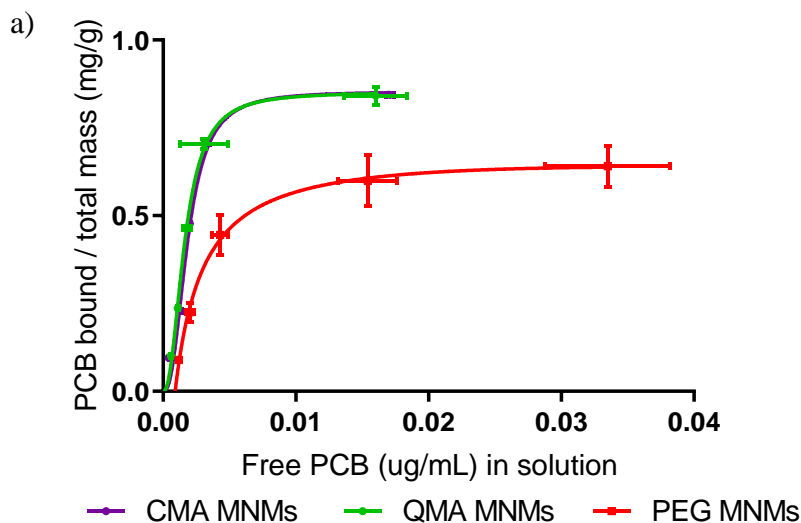


Figure 4-7 Normalized absorbance (at 540 nm) of the MNMs in DI water for 12 hours using UV-visible spectroscopy.

The binding capacity of the MNM systems towards PCB 126 was studied at equilibrium conditions, room temperature and under constant shaking. The equilibrium time for the study was of 48 hours, as determined by previous kinetic studies where the contact time ranged from 30 minutes to 1 week. The binding isotherm was obtained for all

the systems was obtained using a loading of 0.1 mg mL^{-1} and seven different PCB 126 concentrations, from 0.003 ppm to 0.1 ppm. The adsorption isotherms for the MNM systems are presented in Figure 4-8A. For all systems, as the concentration of the free PCB in solution increases, the amount of PCB bound per total mass of adsorbent increases as well until a plateau is reached. This plateau is also known as the equilibrium monolayer capacity.^[193] In order to understand the behavior of the synthesized microparticles, the Langmuir model is used to fit the experimental data and obtain the maximum adsorption capacity (B_{max}) and Langmuir adsorption coefficients (K_D) for each system (presented in Table 2). According to the values of nonlinear R^2 presented in Table 4-2, the Langmuir model provides a good fit to describe the systems and suggests the adsorption process is homogeneous and occurs as a monolayer, implying there is no interactions between PCB molecules bound at the surface of the MNMs. The binding isotherm for both CMA MNMs and QMA MNMs behaves almost identically, showing higher binding at all concentrations when compared to the PEG MNMs. Previous studies have demonstrated that the sorption of hydrophobic organic chemicals, like PCBs, show strong absorption to aromatic-carbon based materials as a result of hydrophobic interactions and, most importantly, π - π interactions at the aromatic surface.^[194, 195] Moreover, PCB 126 is a planar molecule, which can closely approach the sorption sites of the adsorbent material allowing for the formation of favorable π -cloud interaction between the aromatic groups present in the adsorbent and those in the sorbate molecules.^[174, 175] Hence, the presence of the acrylated polyphenol, rich in aromatic groups, in the CMA MNMs and QMA MNMs appears to enhance binding for PCB 126.

The binding isotherms from Figure 4-8A show some variability between in the concentration of free PCB in solution. This comes from to the preparation of 12 independent samples per concentration proceeding from three different microparticle batches. At the lower concentrations, all the MNM systems behave very similarly, having a rapid increase for PCB bound and continue to increase until a maximum capacity is reached. At this point, the PEG MNMs visibly are saturated at a lower amount of PCB bound. This can be confirmed by the scatter plots presented in the supportive information (Figures A2-S1 – S5), where confidence intervals for each individual initial concentration are shown, demonstrating than only at the highest concentration of the present study (0.1 ppm), the PEG MNMs behave significantly differently from the other two MNM systems.



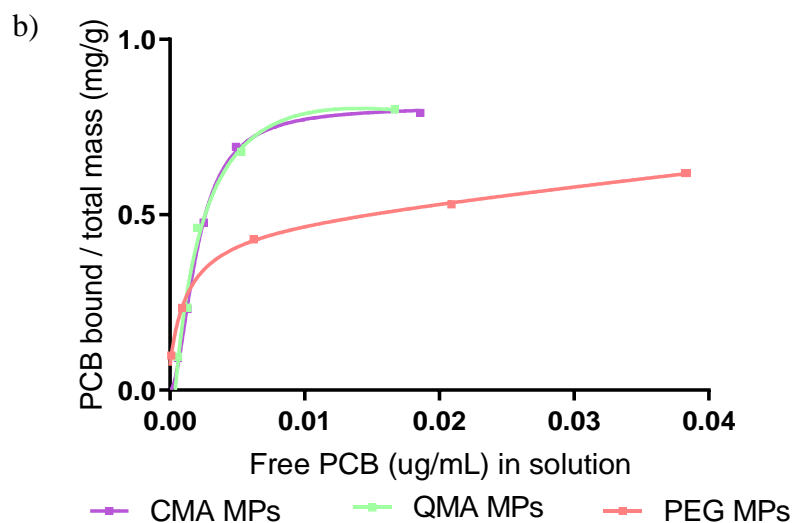


Figure 4-8 Room temperature adsorption isotherms for PCB 126 of the A) MNM systems and B) MP systems. PCB 126 initial concentrations from 0.003 – 0.1 ppm fitted using the Langmuir model.

Table 4-2 Langmuir binding constants for the binding isotherm of PCB 126 for the microparticle systems synthesized (n = 12 independent samples ^a n = 9 independent samples. ^b n = 15 independent samples. ^c values reproduced from [46] with permission from the authors.

System ID	K_d (nM)	95% CI	B_{max} (mg g ⁻¹)	95% CI	R^2
CMA MNMs	1.20	0.98 to 1.47	0.96	0.94 to 1.01	0.983
QMA MNMs	1.28	1.05 to 1.55	1.02	0.94 to 1.04	0.995
PEG MNMs	1.84	1.72 to 1.97	0.74	0.71 to 0.79	0.949
CMA MPs ^a	1.06	0.86 to 1.30	0.96	0.89 to 1.04	0.999
QMA MPs ^a	1.06	0.88 to 1.28	0.97	0.91 to 1.04	0.986
PEG MPs ^a	1.71	1.24 to 2.32	0.60	0.57 to 0.64	0.999
CMA MNPs ^c	2.72	2.50 to 3.00	1.06	1.02 to 1.09	0.993
QMA MNPs ^c	5.88	5.58 to 6.24	1.06	1.02 to 1.10	0.956
PEG MNPs ^{b,c}	8.42	6.54 to 14.24	1.91	0.98 to 2.75	0.980

As mentioned above, the maximum binding capacity of the presented MNMs appears to be enhanced by the presence of the acrylated polyphenol moieties. From the

confidence intervals presented in Table 4-2, obtained from the nonlinear models in JMP statistical software, it is clear that the value for B_{\max} for the PEG MNMs (0.74 mg g^{-1}) is significantly lower than those for the CMA MNMs (0.96 mg g^{-1}) and QMA MNMs (1.02 mg g^{-1}). This can again be explained by the ability of the aromatic moieties present in the CMA MNMs and QMA MNMs to form π - π interactions at the surface with the PCB molecules, resulting in a higher binding capacity towards PCB compared to the PEG MNMs, where only hydrophobic interactions can occur. There is no significant difference in the binding capacity between either the CMA MNMs or the QMA MNMs, both having a maximum binding capacity for PCB 126 of approximately 1 mg g^{-1} . These values are within error of reported saturation capacities for other engineered microplastics and magnetic composites developed for the adsorption of organic pollutants.^[112, 196] However, the B_{\max} of all the MNM systems are lower than those reported for other carbon-based materials, specifically a couple orders of magnitude lower than activated carbon.^[197,198] The Langmuir adsorption coefficients obtained for the CMA MNMs, QMA MNMs and PEG MNMs are 1.20 nM , 1.28 nM and 1.84 nM , respectively. These K_D values are all in the same order of magnitude as what has been reported for the monoclonal antibody S2B1 binding to PCB 126 ($2.5 \pm 0.01 \text{ nM}$), demonstrating the high affinity of the synthesized MNMs for this contaminant.^[199] Moreover, the obtained Langmuir constant values are lower than values found in literature specifically for PCB 126 being adsorbed by activated carbon (6.12 nM), the gold standard for non-specific adsorption of organic contaminants, and micron sized charcoal (15.2 nM), another commonly used material for pollutant remediation.^[44,177] This further demonstrates the applicability of the newly synthesized

MNMs as adsorbent materials with the possibility to outcompete current remediation materials in the adsorption of specific contaminants, like PCBs.

In order to determine if the presence of the magnetic nanoparticles within the polymeric matrix of the MNM systems, a set of microparticles (MPs) was synthesized without this magnetic component. The synthesis process followed was the same as previously described for the MNMs. The binding studies were conducted in the same manner, with the exception of the magnetic decantation step due to the absence of magnetic nanoparticles within the MPs. In this case, the MPs were left to sediment out of solution and a sample of the supernatant was taken from the top of the vials. The results for the binding isotherms are shown in Figure 8B. It can be seen that the CMA MPs and QMA MPs follow a similar behavior, reaching a maximum amount of PCB bound per total mass close to 1 mg g^{-1} , almost the same as what was observed for their corresponding MNM systems. From the confidence intervals shown in Table 4-2, it can be seen that all for polyphenol containing systems have maximum binding capacities within error of each other, which suggest the presence of the magnetic nanoparticles does not negatively affect the capacity of the MNM or MP systems for PCB 126 at the studied conditions. Regarding the PEG MPs, the binding isotherm does increase as the concentration of free PCB in solution increases, as does the other two MP systems, but reaches a lower maximum binding capacity at 0.6 mg g^{-1} . This behavior is similar to what is observed for the PEG MNMs, however, the maximum binding capacity for this system is in fact greater and statistically different to the PEG MPs, as determined from the confidence intervals shown in Table 2. In this case, the magnetic nanoparticles appear to be increasing the maximum binding capacity of the PEG MNMs by providing additional surface area for binding to

occur, and reducing the possible hydrophilic interactions the PEG polymer may be having with the water molecules in solution.^[178] Examining the K_D values of the MP systems presented in Table 4-2, all fall within the confidence intervals of each other and the MNM systems, demonstrating they are not adversely affected by the presence of the magnetic nanoparticles in the material.

Taking a closer look at the Langmuir constant for PCB 126 of all the synthesized systems in this work, from lowest affinity to highest, the order is as follows: PEG MNPs < PEG MPs < QMA MNMs < CMA MNMs < QMA MPs = CMA MPs. The PEG systems present a lower affinity for PCB 126 in the aqueous solution most likely due to the hydrophilic nature of the PEG400DMA, therefore impeding interactions with the hydrophobic PCB 126 molecules.^[200] The CMA and QMA containing systems exhibit a higher binding affinity for the PCB molecule, which can be explained on the basis of the presence of π - π stacking interaction between the aromatic rings in the adsorbate and the adsorbant. This result demonstrates the important role the incorporation of the functional monomers, CMA and QMA, imparts into the microparticle systems by increasing the affinity of the material via the introduction of π -electron rich sites that allow for π -electron coupling/stacking, and lead to an overall increase in hydrophobicity.

Recently, our group developed nanoadsorbent materials containing these functional acrylated monomers, CMA and QMA, to be used in environmental remediation.^[200] Briefly, the core-shell systems consisting of a magnetite nanoparticle core was coated using a grafting from approach (atom transfer radical polymerization) with PEG400DMA and either CMA or QMA. The adsorption for PCB 126 for these magnetic nanoparticles was subsequently analyzed and fit to the Langmuir model. From the data in Table 4-2, it can be

seen that the CMA MNPs and QMA MNPs have higher affinity for PCB 126, than the PEG MNPs, as is the case with the MNM and MP systems in this work. However, by examining the confidence intervals, it becomes evident that the K_D values for the CMA MNMs, QMA MNMs, CMA MPs and QMA MPs indicate a greater affinity for PCB 126. This result seems counter intuitive given that it is expected that the nano-sized MNPs with an average size 240 nm compared to an average size of 18 μ m for the MNM and MP systems, would translate into a higher surface where adsorption of the contaminant molecule can occur. However, the amount of functional polymer consisting of PEG and CMA/QMA present in the MNP systems represents only 10 wt% of the total mass in comparison to 90 wt% in the MNMs and 100% in the MPs. Given this considerable difference in composition, it is possible that the available sites for a combination of π - π interactions, primarily, and hydrophobic interactions at the particle surface are significantly reduced ensuing a lower affinity for PCB 126 at the studied conditions. These results provide significant promise for the use of our magnetic nanocomposite microparticle systems to be used as high affinity adsorbents for specific harmful contaminants in the remediation of contaminated sites.

4.5 Conclusions

This work presents the promising application of the synthesized magnetic nanocomposite microparticles as high affinity adsorbents for harmful organic pollutants in environmental remediation. The synthesized MNMs incorporated curcumin multiacrylate or quercetin multiacrylate in order to provide the microparticles with π -electron rich sites and, hence, enhance the pollutant binding capacity. The magnetic nanoparticles served as a means of magnetic separation throughout the binding process and do not adversely affect the binding properties of the MNM systems. The Langmuir model adequately fit the

adsorption data, providing information about the maximum binding capacity of the systems and their binding coefficients. The saturation capacity proved to be consistent to available literature of other engineered polymer based micro-adsorbents used for organic contaminants but lower than reported values for carbon-based materials. It was demonstrated that the synthesized MNMs possess a higher binding affinity for PCB 126 than activated carbon and charcoal, which are the most commonly used materials for capture of organic pollutants. Additionally, the incorporation of a small amount (10 mol %) of the functional monomer, CMA or QMA, into the microparticles resulted in an increase in affinity due to the ability to form π - π interactions, resulting in affinities comparable to those observed in antibodies. Finally, the MNM systems combine the increased affinity provided by these plant derived monomers with the magnetic separation capabilities of the magnetic nanoparticles, and they offer a unique advantage for their use in the environment: micron size allows for an easier manipulation and control of their fate in comparison to nanoparticles. Overall, we have developed novel nanocomposite materials with high affinities for PCBs that show promising potential for use as environmental remediation adsorbents for harmful contaminants.

CHAPTER 5. ALTERNATING MAGNETIC FIELD MODULATED BINDING IN MAGNETIC NANOCOMPOSITES AS A LOW ENERGY REGENERATION STRATEGY IN ENVIRONMENTAL REMEDIATION

5.1 Abstract

Adsorption is one of the most widely used remediation techniques for water and waste-water treatment of organic contaminants. Regeneration of these materials often times involve the use of harsh organic solvents, which in themselves can be environmental pollutants; or require high temperatures, long duration, high energy consumption due to heat loss (to surroundings, equipment, adsorbent, production of volatile components), resulting in high costs. In this work, a low energy regeneration strategy based on an alternating magnetic field (AMF) modulated binding in magnetic nanocomposites is presented. Magnetic nanocomposite microparticles (MNMs) interact with an AMF to generate localized energy dissipation. This associated local generation of heat is dissipated through the MNMs causing the destabilization of bound contaminants. Here, polychlorinated biphenyls (PCBs) are chosen as model pollutants due to their ubiquitous nature and designation as a national priority contaminant. When the MNMs in isooctane are exposed for just 5 minutes to an AMF operated at 55 kA m^{-1} and a frequency of 300 kHz, over 90% of the bound PCBs is desorbed. The proposed regeneration strategy allows for low energy regeneration of the MNMs, reducing operating costs and providing significant advantages over existing technologies.

5.2 Introduction

Activated carbon (AC) represents the most widely used technology for environmental remediation and water treatment by means of adsorption, specifically for organic contaminants.^[5,6] The highly porous structure of ACs provide high surface area for

adsorption to occur, therefore providing high, non-selective, removal efficiency.^[7] Additionally, the vast variety of low cost source materials enable it to be made with low production costs.^[44,201] Regeneration of AC is an important factor to restore its adsorption capacity for reuse without adversely affecting its porosity. Current regeneration treatments include the use of the following methods: thermal, solvent extraction, electrochemical, biological, ultrasound, microwaves and solar.^[52,108,202-208] Among these, thermal regeneration is still viewed as most effective and environmentally acceptable.^[209] Thermal regeneration can amount to almost 85% of the total operation cost in a six month period, due to the need for high temperatures (700 – 1000°C).^[210] Aside from the high energy consumption, concerns regarding physical changes of the AC leading to loss of adsorption capacity, material being burnt in the regeneration process, and the potential to generate even more harmful byproducts, need to be taken into consideration.^[37,108,211] Therefore, there is a need for other water treatment options coupled with low-cost regeneration methods that can meet the ever growing needs for sustainable, efficient, and cost-effective technologies.

Magnetic nanocomposites adsorbents have led to a new class of magnetic separation strategies for water treatment that can also have a low production costs, high surface area, and ease of operation.^[15] Magnetic nanocomposites are composed of a magnetic nanoparticles, most commonly iron oxide nanoparticles (IO MNPs), embedded within a non-magnetic matrix. This results in a functional material that combines the properties of both components that can be targeted for a specific application.^[212] Polymeric matrixes are of particular interest in environmental remediation given their ability to impart unique chemistries for specific molecular interactions.^[9,118,213] Additionally, due to the intrinsic

magnetic properties of the embedded IO MNPs, nanocomposites can be quickly separated from solution when a static magnetic field is applied, improving their control and recovery from aqueous media.^[16] Furthermore, these magnetic nanocomposites can respond to an alternating magnetic field (AMF) and dissipate heat through magnetic relaxation processes.^[16,20] These relaxation processes occur through: Neel paramagnetic switching in which the magnetic moment changes with respect to the crystal lattice and Brownian motion where the particles physically rotate to align themselves with the magnetic field.^[16] The effect generated from these interactions converts magnetic work into internal energy that is then dissipated from the IO MNPs to their surroundings. Herein we present a low energy regeneration strategy using an AMF to remotely heat magnetic nanocomposites used in environmental remediation in order to generate a local desorption of the contaminant back into solution, allowing for further reuse of the adsorbent

Although there has been a report in literature regarding the interaction of a magnetic nanoadsorbent with an AMF to generate localized heat and induce the evaporation of bound toluene, the feasibility of this regeneration method for other adsorbents and for less volatile compounds has yet to be explored.^[214] Polychlorinated biphenyls (PCBs) are a class of persistent organic pollutants with stable physical and chemical properties, and PCBs are not readily biodegradable.^[6] Furthermore, they are semi-volatile or non-volatile and partition between the aqueous and solid phase resulting in their widespread contamination in the environment.^[42] The US EPA lists over 500 sites contaminated with PCBs already, or in the process of being, designated on the Superfund National Priority List, and the safe drinking water act establishes a maximum PCB contamination level of 0.0005 mg L^{-1} in

public drinking water sources.^[215] This brings forward the need to evaluate regeneration methods for adsorbents used in the remediation of priority contaminants like PCBs.

In this work, we used magnetic nanocomposite microparticles (MNMs), previously synthesized by our group, to demonstrate the ability of the AMF to trigger the desorption of PCB 126, as model contaminant.^[22] These MNMs contain acrylated polyphenols which have been shown to increase affinity for aromatic rich molecules through the formation of π - π interactions.^[200,213,216,217]

5.3 Experimental

5.3.1 Materials

Iron (III) chloride hexahydrate ($\text{FeCl}_3 \cdot 6 \text{H}_2\text{O}$); iron chloride tetrahydrate ($\text{FeCl}_2 \cdot 4 \text{H}_2\text{O}$), ammonium persulfate (APS), N,N,N'-Trimethylethylenediamine 97% (TEMED), triethyl amine (TEA), acryloyl chloride, and potassium carbonate (K_2CO_3) were obtained from Sigma Aldrich (St Louis, MO). Ammonium hydroxide (NH_4OH) was purchased from EMD Chemicals (Gibbstown, NJ). Poly(ethylene glycol) 400 dimethacrylate (PEG400DMA) was obtained from Polysciences INC. (Warrington, PA). Curcumin was purchased from Chem-Impex International, Inc. (Bensenville, IL) and quercetin was purchased from Cayman Chemicals (Ann Arbor, MI). 3,3',4,4',5-Pentachlorobiphenyl (PCB-126) in isooctane was purchased from Accustandard (New Haven, CT). 5'-fluoro-3,3',4,4',5-pentachlorobiphenyl (F-PCB 126) was purchased from Resolution Systems Inc. (Holland, MI). All solvents (Isooctane, ethanol HPLC grade, tetrahydrofuran (THF); dichloromethane (DCM), acetonitrile (ACN), acetone) were obtained from Fisher Scientific (Hannover Park, IL). All materials were used as received.

5.3.2 Magnetic nanocomposite microparticle synthesis

The magnetic nanocomposite microparticles (MNMs) were synthesized via chemically initiated free radical polymerization using poly(ethylene glycol) 400 dimethacrylate (PEG400DMA) and an acrylated polyphenol, following the method described in previous work from our lab.^[213] Briefly, polymer gel containing the desired functionalities was synthesized via free radical polymerization. The functional monomer, curcumin multiacrylate (CMA) or quercetin multiacrylate (QMA), was dissolved in DMSO and added to polyethylene glycol 400 dimethacrylate (PEG400DMA) in a 1:9 ratio. The uncoated MNPs (1 wt %), dispersed in DI water, were incorporated into the mixture and vortexed. The initiator, ammonium persulfate (APS), was then added to the mixture, closely followed by the accelerator N,N,N',N'-tetramethylethylenediamine (TEMED, 0.67 wt %). Following polymerization, the polymer was cryomilled to obtain MNMs. The synthesis of the acrylated polyphenols, specifically curcumin multiacrylate (CMA) and quercetin multiacrylate (QMA), has been previously described in literature.^[29,30] A total of three nanocomposite systems, previously studied as adsorbents for PCB 126, were evaluated throughout this work: curcumin multiacrylate magnetic nanocomposite microparticles (CMA MNMs), quercetin multiacrylate magnetic nanocomposite microparticles (QMA MNMs) and poly(ethylene glycol) 400 dimethacrylate magnetic nanocomposite microparticles (PEG MNMs). All MNM systems contain 10 wt% of IO MNPs, and the CMA MNMs and QMA MNMs.

5.3.3 PCB 126 binding studies and AMF regeneration

The MNMs underwent a batch adsorption studies with PCB 126, under equilibrium conditions, where 1 mg mL^{-1} of the nanocomposite was suspended in a 99:1 DI water to ethanol solvent and spiked with a 0.05 ppm solution of PCB 126. The samples were placed in an orbital shaker at 200 rpm and room temperature for 48 h. Following, the MNM suspension was magnetically separated and the supernatant containing the unbound PCB was collected. Immediately after this, the MNMs were resuspended in the solvent of choice, a 99:1 DI water to ethanol or isooctane, and then placed directly in the coil of the AMF source, as seen in Figure 5-1. A Taylor Winfield alternating magnetic field source operating at a field amplitude of approximately 55 kA m^{-1} and a frequency of 300 kHz was used. The resuspended MNMs were exposed for a period of 5 min, and the heat produced was measured in real time with a Luxtron® optical thermometer interface. After 5 minutes had elapsed, the sample was taken out of the AMF coil and exposed to a static magnet for 20 seconds. The supernatant was collected and quantified to determine the amount of PCB 126 released. The supernatant of the MNMs that had been resuspended in the aqueous solvent was subjected to a liquid extraction using isooctane. All samples were analyzed in isooctane using an Agilent 6890N gas chromatograph coupled to electron capture detection (GC-ECD), equipped with an Agilent HP-5MS UI column (30x0.25x0.25). All binding studies were carried out in triplicates.

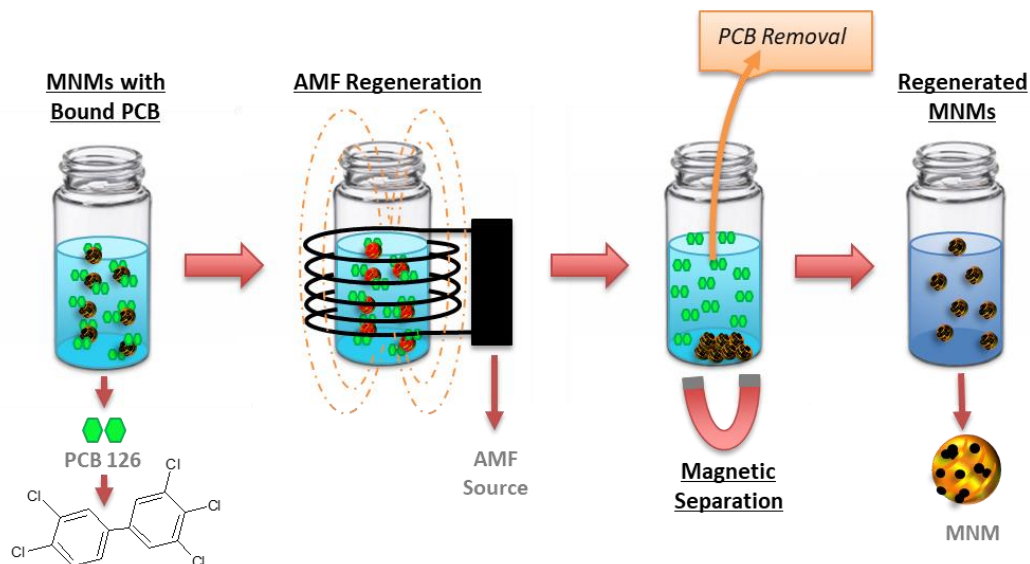


Figure 5-1 Schematic representation for the low energy regeneration strategy based on an alternating magnetic field for magnetic nanocomposites used in environmental remediation

5.4 Results and discussion

Magnetic nanocomposite microparticles (MNMs) were synthesized via chemically initiated radical polymerization producing microparticle systems where 10 wt% of the total mass corresponds to the iron oxide magnetic nanoparticle, and the remaining 90% to the functional polymer matrix.

The magneto-thermal response of the MNMs was studied during the regeneration studies. The temperature profiles as a function of time for all the MNM systems in both solvents, 99:1 DI water to ethanol and isooctane, can be seen in Figure 5-2. Once the AMF was turned on (at time zero), the temperature increased as a function of exposure time for all cases until after 5 minutes, the temperature reached steady state near 37°C. Once the AMF is turned off at 5 minutes, a rapid decrease in temperature is observed as the IO MNPs

are no longer generating localized heat within the nanocomposite. The sample cools off as the energy is dissipated to the surrounding environment until room temperature is reached again.^[218] Overall, it can be seen that the MNMs efficiently heat under the selected AMF conditions.

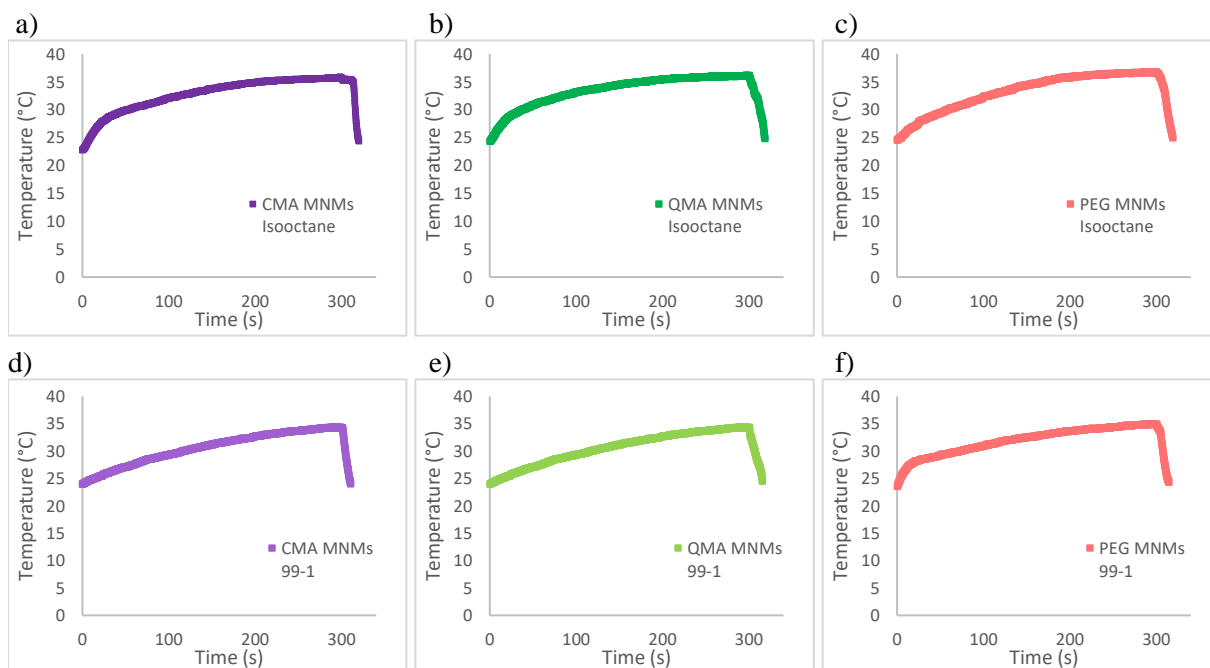


Figure 5-2 Temperature variation data as a function of time for the MNMs upon exposure to an AMF operating at 55 kA m⁻¹ and a frequency of 300 kHz. a) CMA MNMs, b) QMA MNMs, and c) PEG MNMs in isooctane. d) CMA MNMs, e) QMA MNMs, and f) PEG MNMs in 99:1 DI water to ethanol.

In order to determine if the release of the bound PCB 126 to the MNMs was a function of solution temperature, three different exposure temperatures were considered for release after the binding study: room temperature (RT), 37°C, and 60°C. For these studies, the two solvents of choice, 99:1 DI water to ethanol and isooctane, were placed in water baths each set at the aforementioned temperatures. Once the MNMs had undergone the binding study and the supernatant was collected, they were resuspended in the

corresponding solvent and temperature for period of 5 minutes followed by magnetic separation and supernatant GC-ECD analysis. The results for a 5 minute AMF exposure and 5 minute water bath treatments are shown in Figure 5-3a. It is clear that, for each individual solvent, when the regeneration of the MNMs occurs through exposure to an AMF, the amount of PCB 126 desorbed is statistically greater than at any of the other temperature treatments ($p < 0.05$ from a double tailed T-test), which is likely a result of the local temperature rise in the vicinity of the IO MNPs.^[219] When isooctane is used as the solvent for desorption of PCB 126, it can be seen that over 90% of the bound PCB to the MNMs were released after a 5 minute exposure to the AMF for all the MNM systems. Similarly, at the three different release temperatures (RT, 37°C, and 60°C), the amount of PCB released was higher in isooctane, increasing as the solution temperature increased. In the aqueous solvent, the MNMs exposed to an AMF for 5 minutes are significantly different from all the temperature treatments ($p < 0.05$ from a double tailed T-test), indicating that the release is not just a function of the solution temperature, but probably a result of the creation of localized heat within the MNMs due to interactions with the AMF.^[220, 221] At the three temperature treatments, the amount of PCB 126 released does not exceed ~ 20-25%. This behavior could be attributed to the low solubility of the PCB in water.

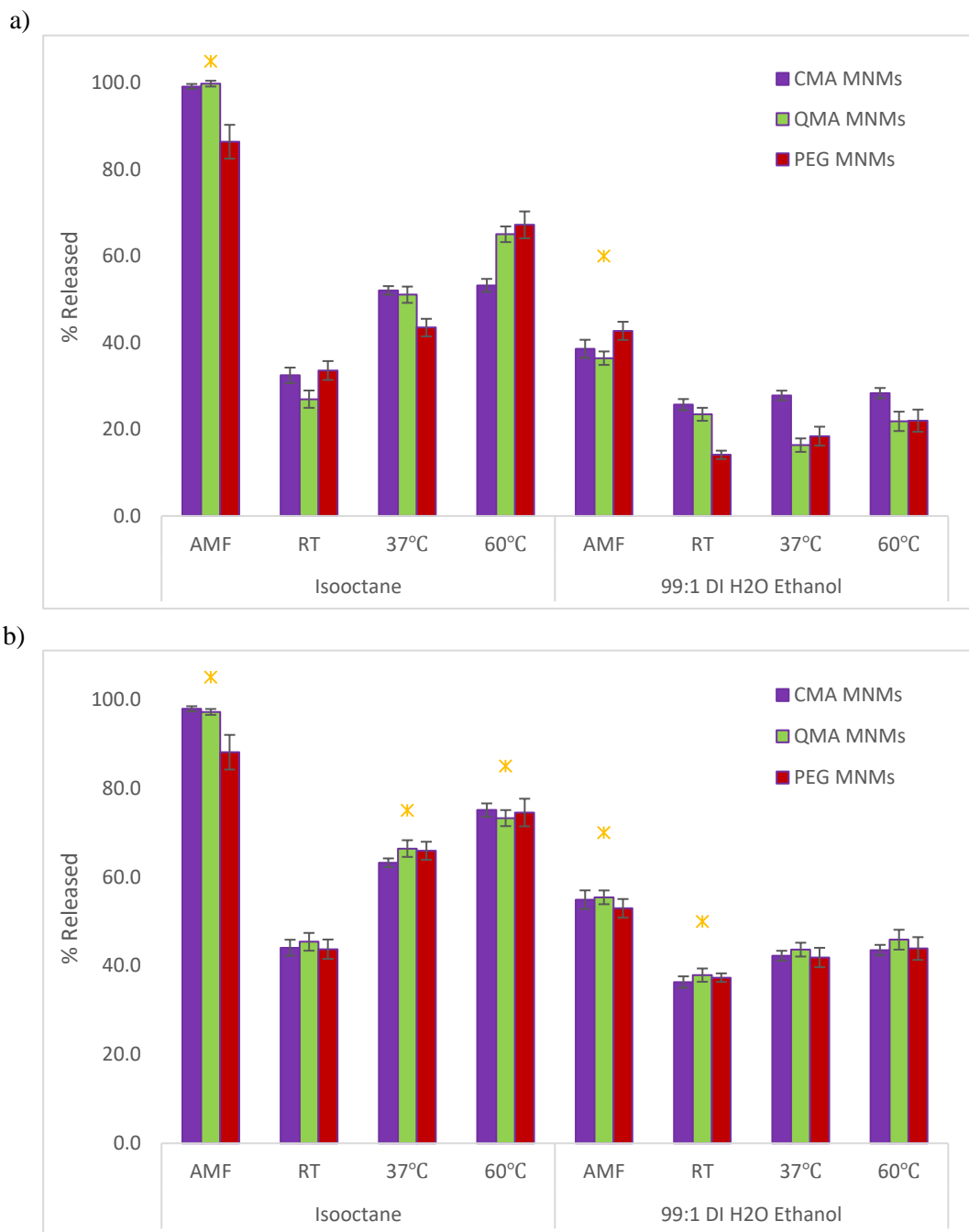


Figure 5-3 Percentage of PCB 126 released from the MNM systems upon exposure to different remediation strategies. a) 5 minute AMF exposure regeneration method and temperature release treatments b) 5 minute AMF exposure regeneration method and 30 minute temperature release treatments. (AMF operating at 55 kA m⁻¹ and a frequency of 300 kHz)

To further determine if the release of PCB 126 is a function of solution temperature, the duration of the temperature treatments in isooctane and the aqueous solvent was extended to 30 minutes for all the MNM systems, whilst maintaining a 5 minute AMF exposure. From Figure 5-3b, it can be seen that the overall trend observed for the 5 minute release treatments remains the same despite increasing the temperature treatments to 30 minutes. In isooctane, the amount of PCB released increase in the following order: RT (43.9%) < 37°C (64.1%) < 60°C (74.9%) < AMF (94.5%), all statistically different from each other ($p < 0.001$). These results display a trend of increasing percentage of PCB released as a function of increasing bulk solution temperature. The increase in the solvent temperature means an increase in its kinetic energy which can destabilize the interactions binding the PCBs to the MNMs, most likely π - π stacking and/or hydrophobic interactions, resulting in the PCB desorption. Additionally, the hydrophobic nature of isooctane and its high affinity for PCB increases the desorption likelihood. In the aqueous solvent, the 5 minute AMF regeneration strategy still desorbs a significantly greater percentage of PCB 126 compared to the three temperature treatments ($p < 0.05$). Here, the amount of PCB released presents the following order: RT (37.2%) < 37°C (42.5%) \leq 60°C (44.5%) < AMF (54.4%). Even though the amount of PCB released increased for the temperature treatments in 99:1 DI water to ethanol, it still remained at less than 50% desorbed after 30 minutes. One explanation for this can be the nature of the solvent. The solubility of PCB 126 in water is of 1.33 ng mL⁻¹ at RT and 1.60 ng mL⁻¹ at 35°C.^[222] Even as the increase in temperature provides kinetic energy to the solvent to potentially disrupt the PCB-MNM interactions, the low solubility of PCB in water will prevent its full desorption leaving some of it still bound to the nanocomposite.

The exposure of the MNMs to an AMF has demonstrated the interaction of the IO MNPs with the magnetic field to generate localized heat. This intrinsic behavior of the IO MNPs in response to an AMF further elucidates why the MNMs that underwent a 5 minute exposure were able to release more bound PCB than those incubated at different temperatures and time intervals. Moreover, by incorporating the IO MNPs into the magnetic nanocomposite microparticles, the local energy generated is not immediately dissipated to the bulk solution. Instead, it is transferred to the polymer network and dissipated through the MNM system proving to be enough to destabilize the π - π interactions and hydrophobic interactions with the PCB molecules.

5.5 Conclusions

An optimal regeneration strategy completely desorbs the pollutant from the adsorbent, does not modify the initial properties of the adsorbent (chemical/ physical), allows for complete recovery of the adsorbent, requires low energy consumption, has short regeneration times, does not generate harmful byproducts, and is easy to operate. None of the existing technologies or methods available today can achieve the aforementioned conditions. The presented low energy regeneration strategy based on an alternating magnetic field provides a viable alternative. Using a magnetic nanocomposite, the combined benefits of magnetic separability and responsiveness to an AMF were achieved. The MNM system was able to dissipate heat from the inside of the IO MNPs to the bulk solution upon a short 5 minute exposure to an AMF. This localized heat allowed for the disruption of the interactions between the adsorbent and the bound adsorbant, in this case PCB 126, triggering its desorption. The adsorbent is then collected in a sink solvent. Using isooctane as the solvent, an exposure of 5 minutes to an AMF operating at 55 kA m^{-1} and

a frequency of 300 kHz, $94.5\% \pm 3.87$ of the bound PCB was desorbed from the MNMs allowing for their efficient regeneration and further reuse. In conclusion, the AMF based regeneration strategy proposed in this work allows for, almost, a complete desorption of the pollutant, complete and easy recovery of the adsorbent thanks to its ability to be magnetically separated, has a short regeneration time of only 5 minutes, does not generate harmful byproducts, and reduces operation costs by eliminating the need to heat the solution to high temperatures. It is still necessary to evaluate the physicochemical characteristics of the adsorbent after several adsorption-regeneration cycles. The low energy regeneration strategy presented here can be readily extended to other contaminants and magnetic adsorbents, providing an efficient and high performance recycling technology with the potential to be used *in situ* or *ex situ*.

CHAPTER 6. THE IMPACT OF SOLUTION IONIC STRENGTH, HARDNESS AND PH IN THE ADSORPTION EFFICIENCY OF POLYCHLORINATED BIPHENYLS ON MAGNETIC NANOCOMPOSITE MATERIALS

6.1 Abstract

Environmental conditions of groundwater and surface water greatly vary as a function of location. Factors such as ionic strength, water hardness and solution pH can change the physical and chemical properties of the nanocomposites used in remediation and the pollutants of interest. In this work, magnetic nanocomposite microparticles (MNMs) are used as adsorbents for remediation of PCB 126, as a model organic contaminant. Three MNM systems are used: curcumin multiacrylate MNMs (CMA MNMs), quercetin multiacrylate MNMs (QMA MNMs), and polyethylene glycol 400 dimethacrylate MNMs (PEG MNMs). The effect of ionic strength, water hardness and pH was studied on the adsorption efficiency of the MNMs for PCB 126 by performing equilibrium binding studies. It is seen that as the ionic strength of the solution increases from 0 to 20 mM, there is a slight decrease in %PCB bound for all systems (4%), indicating that the ionic strength has a relatively small effect on the adsorption. Similarly, there was minimal effect on adsorption of the MNM systems for PCB 126 when the water hardness increased from 0 to 1.6 mM. However, a decrease in binding was observed when the pH increases from 6.5 to 8.5, attributed to anion- π interactions between the buffer ions in solution and the PCB molecules and the buffer ions in solution and the aromatic rings of the MNM systems. Overall, the results indicate that the developed MNMs can be used as magnetic adsorbents for polychlorinated biphenyls in groundwater and surface water remediation provided solution pH is controlled.

6.2 Introduction

Water conservation and quality are some of the most important global challenges humans are facing in 21st century. Fast industrialization implies exhaustive consumption of fresh water and groundwater for agricultural, industrial and domestic purposes.^[223] Most of these uses have led to the contamination of water bodies with an array of pollutants. In order to mitigate the health and environmental risks associated with the contamination, stringent environmental regulations have been imposed worldwide.^[125,224,225]

Several chemical, physical and biological water treatment technologies exist for the removal of organic contaminants.^[37] Among them, adsorption processes have been widely used to remove a wide variety of pollutants due to their large surface areas, mechanical strength, tunable shapes and morphologies, high efficiencies and can be simply implemented.^[146,147] Of particular interest in recent years has been the development of nanocomposite adsorbent materials that combine properties of organic and inorganic materials. Specifically, magnetic nanocomposite materials, where iron oxide nanoparticles (IO MNPs) are embedded within a composite to impart the material magnetic properties, have been widely studied. These magnetic nanocomposite adsorbents allow for a fast, easy, and cost effective separation of the saturated adsorbent from the treated solution.^[126] Furthermore, the organic component of the nanocomposite can be tailored specifically to target the pollutant of interest. Common organic components used in nanocomposites for adsorption of polycyclic aromatic hydrocarbons (PAHs) contain aromatic groups that can allow for π - π interactions and hydrophobic interactions, indicating this is the mechanism through which adsorption occurs.^[101,118,127,128,214,229,230]

Contamination by polycyclic aromatic hydrocarbons (PAHs) is widely distributed in the environment. Because of environmental cycling, PAHs are found all over the world in groundwater, surface water, sediments, and the atmosphere. Polychlorinated biphenyls (PCBs) are a class of PAHs comprised of chlorinated biphenyl complexes with varying degree of chlorination, and hence physico-chemical properties and toxicity. In general, PCBs have poor aqueous solubility and low volatility, which makes their environmental remediation challenging.^[231] The U.S. Environmental Protection Agency (EPA) and the European Union (EU) have classified some PCBs as priority pollutants for monitoring and remediation purposes in natural waters.^[224,233] However, due to their trace concentration in environmental waters and the complexity of environment condition of natural waters, the use of a remediation technique with high capacity and stable under environmental conditions is necessary.

Environmental conditions in groundwater and surface water can change the physical and chemical properties of the adsorbent nanocomposites and the pollutant molecules. Conditions such as ionic content, water hardness and pH vary based on the geographical location of the water body where bedrock erosion, presence of igneous rocks, drainage regions with alkaline earths, presence of microbiota and microorganisms communities, and human influences on the water sheds can change this parameters. Therefore, it is of utmost importance to investigate the effect of the water environment on the adsorption behavior of magnetic nanocomposite materials. The main objective of this work was to evaluate the effects of different environmental factors on the adsorption capacity of magnetic nanocomposite materials (MNMs) previously developed by our group.^[214] Here, we studied the effect of carrying ionic strength, water hardness and solution pH on the

adsorption for PCB 126 of curcumin multiacrylate MNMs (CMA MNMs), quercetin multyacrilate MNMs (QMA MNMs), and polyethylene glycol 400 dimethacrylate MNMs (PEG MNMs).

6.3 Experimental

6.3.1 Materials

Iron (III) chloride hexahydrate ($\text{FeCl}_3 \cdot 6 \text{H}_2\text{O}$); iron chloride tetrahydrate ($\text{FeCl}_2 \cdot 4 \text{H}_2\text{O}$), ammonium persulfate (APS), N,N,N'-Trimethylethylenediamine 97% (TEMED), triethyl amine (TEA), acryloyl chloride, potassium carbonate (K_2CO_3), dibasic sodium phosphate (Na_2HPO_4), glycine ($\text{C}_2\text{H}_5\text{NO}_2$) were obtained from Sigma Aldrich (St Louis, MO). Ammonium hydroxide (NH_4OH) was purchased from EMD Chemicals (Gibbstown, NJ). Poly(ethylene glycol) 400 dimethacrylate (PEG400DMA) was obtained from Polysciences INC. (Warrington, PA). Curcumin was purchased from Chem-Impex International, Inc. (Bensenville, IL) and quercetin was purchased from Cayman Chemicals (Ann Arbor, MI). Citric acid monohydrate, sodium chloride (NaCl), calcium carbonate (CaCO_3), and sodium hydroxide (NaOH) were obtained from Fisher Scientific (Hannover Park, IL). 3,3',4,4',5-Pentachlorobiphenyl (PCB-126) in isooctane was purchased from Accustandard (New Haven, CT). 5'-fluoro-3,3',4,4',5-pentachlorobiphenyl (F-PCB 126) was purchased from Resolution Systems Inc. (Holland, MI). All solvents (Isooctane, ethanol HPLC grade, tetrahydrofuran (THF); dichloromethane (DCM), acetonitrile (ACN), acetone) were obtained from Fisher Scientific (Hannover Park, IL). All materials were used as received.

6.3.2 Magnetic nanocomposite microparticle synthesis

Magnetic nanocomposite microparticles (MNMs) were synthesized via chemically initiated free radical polymerization followed by cryomilling, as previously described by our group.^[214] Poly-(ethylene glycol) 400 dimethacrylate (PEG) and an acrylated polyphenol were reacted in DMSO using ammonium persulfate dissolved in ethanol was used as the initiator for the reaction, and N,N,N',N'-tetramethylethylenediamine as the accelerator, to create a crosslinked polymer network. Iron oxide nanoparticles (IO MNPs) were added as the reaction took place, resulting in their immobilization within the polymer matrix.

6.3.3 Particle characterization

The magnetic nanocomposite microparticles were characterized by Fourier transform infrared spectroscopy (FTIR), thermogravimetric analysis (TGA), dynamic light scattering, and UV-visible spectroscopy as described in previous work from our group.^[214]

6.3.4 PCB binding studies

Binding studies were conducted at equilibrium conditions. All samples were prepared by weighing 0.1 mg of the dry MNMs into 3 mL borosilicate glass vials and dispersing them in DI water. The MNMs systems studied were: CMA MNMs, QMA MNMs, and PEG MNMs. Due to the low solubility of PCB 126 in water, a concentrated stock solution was prepared in ethanol which was then used to spike each sample to obtain the desired concentration of 0.05ppm. Samples were placed in an orbital shaker for 48 hours at room temperature. Following, the samples were magnetically separated using a static magnet for approximately 20 minutes in order to guarantee all MNMs were decanted from solution.

The supernatant containing the free PCB 126 was collected and transferred to a new vial where a liquid extraction using isoctane was performed for 24 hours. Finally, the organic phase was transferred into a glass chromatography vial using a Hamilton syringe and spiked with a known amount of the internal standard, 5'-fluoro-3,3',4,4',5-pentachlorobiphenyl (F-PCB 126). The PCB 126 present in each sample was determined using an Agilent 6890N gas chromatograph coupled with electron capture detection (CG-ECD), equipped with an Agilent HP-5MS UI column (30x0.25x0.25).

The amount of PCB bound to the MNM systems was calculated as:

$$\% \text{ Bound} = \frac{C_o - C_e}{C_o} \times 100 \quad (1)$$

where C_o (mg L^{-1}) is the initial concentration of PCB 126 and C_e (mg L^{-1}) is the concentration of PCB 126 at equilibrium.

The influence of ionic strength, water hardness and pH on the adsorption efficiency of the MNMs was investigated. The influence of ionic strength was tested using NaCl at two different concentrations: 1.5 mM and 20 mM. The effect of water hardness was evaluated using CaCO_3 at two different concentrations: 0.8 mM and 1.6 mM. The pH of the solution was adjusted to 6.5 using a glycine-NaOH buffer, and to 8.5 using a phosphate-citrate buffer, in order to assess its effect on PCB 126 binding.

6.4 Results and discussion

Magnetic nanocomposite microparticles were prepared through chemically initiated free radical polymerization. The MNM systems obtained had an approximate 90 wt%:10 wt% polymer network to magnetic nanoparticle composition. This amount of IO MNPs

present proved to be enough to maintain magnetic separation abilities. The average hydrodynamic particle size for the MNMs ranged from 15 μm to 20 μm .^[214] A schematic representation of the crosslinked polymer matrix interaction with the iron oxide magnetic nanoparticles within the MNMs is depicted in Figure 6-1.

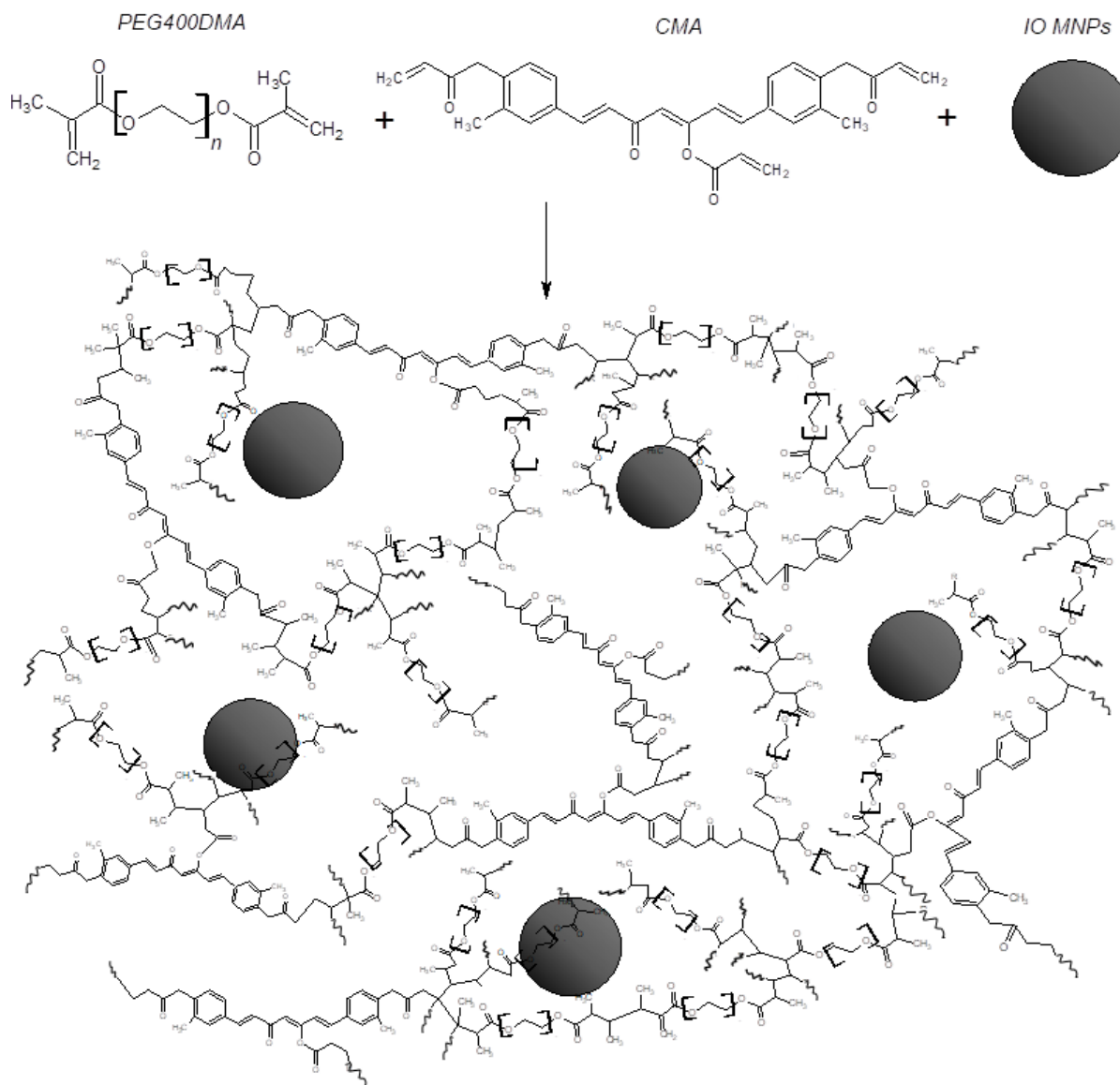


Figure 6-1 Schematic representation of the crosslinked polymer matrix interaction with the iron oxide magnetic nanoparticles within the magnetic nanocomposite microparticles (MNMs). Shown here is the CMA MNMs for representation purposes. Here, the squiggly line represents the continuation of the polymer chain.

The ionic strength of the solution is an important factor to study given the effect it can have on both, the nanocomposite and the contaminant. In the environmental water bodies, different ions will be present, with sodium tending to be the most common. These ions can interact with the surface of the contaminant through electrostatic interactions and, potentially, weaken the adsorption capacity.^[233] The effect of ionic strength on the adsorption capacity of the MNM systems using sodium chloride as the model electrolyte is shown in Figure 6-2. The ionic strengths studied represent salinity levels of freshwater, surface water and ground water (0, 1.5, and 20 mM, respectively).^[20] The general trend observed indicates that the effect of increasing the NaCl concentration does not appear to significantly impact the binding of the MNMs. It was speculated that an increase in NaCl concentration would increase the binding affinity of the MNMs for the PCB 126 due to the salting out effect, that is to say, the increase in ionic concentration makes the solution becomes more polar meaning the hydrophobic PCB molecule becomes less soluble.^[234,235] However, upon closer examination, when the ionic strength increases from 1.5 mM to 20 mM, there is a slight decrease in the binding for all three MNM systems, from 88 % (CMA MNMs, QMA MNMs) and 86% (PEG MNMs), to ~82% and 81%, respectively. Similar behavior has been observed for PCB 126 adsorption to silicone rubber adsorbents, where the sorption properties of the polymer decreased with increasing ionic strength of solution.^[237,238] This decrease in binding behavior has also been observed for other PCB congeners binding to glass surfaces as water salinity increases.^[x] Nonetheless, the overall decrease is less than 4%, therefore from this experiment it is possible to indicate that the ionic strength has a minimal effect on the adsorption of the developed MNMs in the range studied.

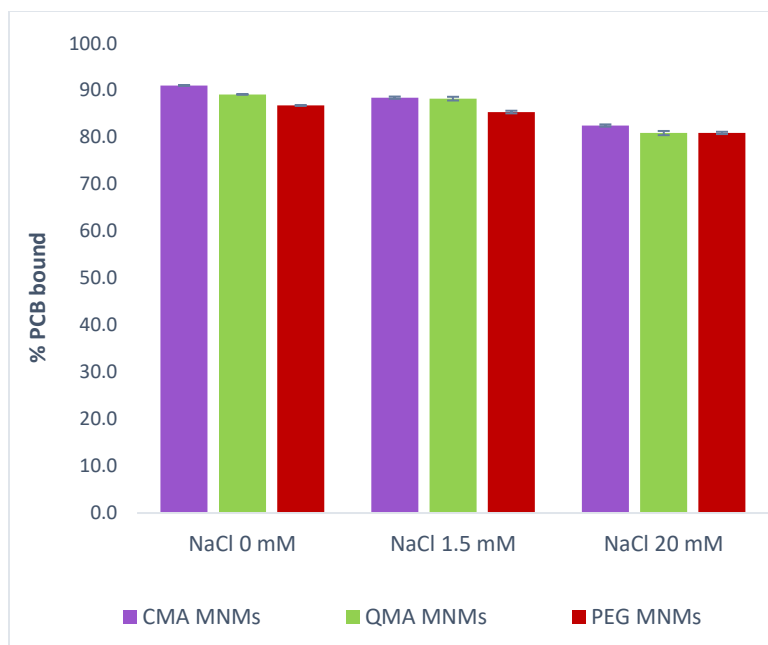


Figure 6-2 Effect of ionic strength on the adsorption efficiency of PCB 126 on CMA MNMs, QMA MNMs and PEG MNMs. The ionic strength concentrations represent fresh water (0 mM), surface water (1.5 mM), and ground water (120 mM).

Water hardness refers, mainly, to the amount of dissolved calcium and magnesium ions in water. The concentration of these ions varies depending on geographical location, because it depends on the mineral composition of the rock and soils in the area. General guidelines for classifying water hardness are defined in terms of calcium carbonate concentration where waters ranging from: 0 to 60 mg L⁻¹ are soft, 61 to 120 mg L⁻¹ are moderately hard, 121 to 180 mg L⁻¹ are hard, and those with a concentration higher than 180 mg L⁻¹ are very hard.^[238] Given that very hard waters tend to be localized in regions with alkaline earths, the experimental conditions studied did not focused on calcium concentration over 180 mg L⁻¹. Figure 6-3 shows the effect of different water hardness conditions is (soft, moderately hard and hard), on the percent of PCB bound by the MNM

systems. There appears to be no significant effect on the binding capacity of the MNM systems by changes in water hardness.

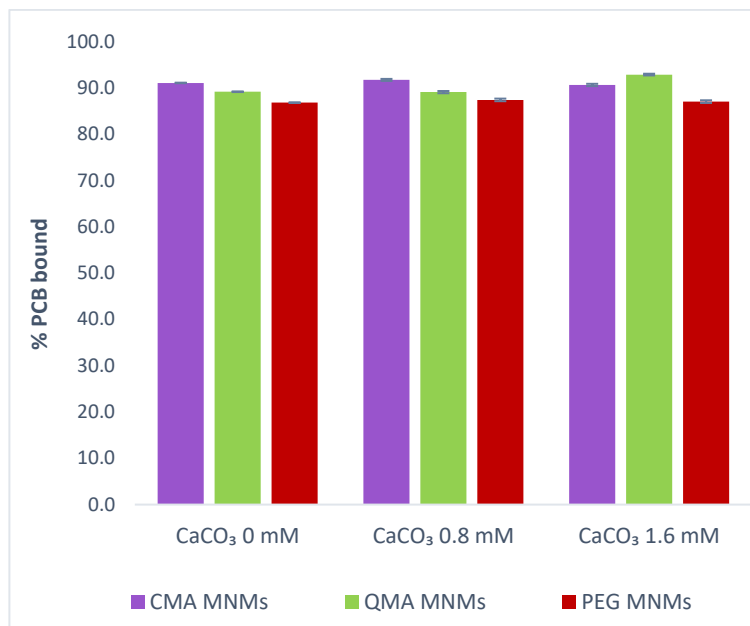


Figure 6-3 Effect of water hardness on the adsorption efficiency of PCB 126 on CMA MNMs, QMA MNMs and PEG MNMs. The water hardness concentrations represent soft (0 mM), moderately hard (0.8 mM), and hard (1.6 mM) waters.

The effect of pH on the adsorption efficiency of the nanocomposite is one of the most important factors to evaluate. Changes in the solution pH can alter the existing form of the adsorbate of interest, as well as the surface functional groups and density charges of the adsorption sites on the adsorbent. The pH of surface water has been described to range between 6.5 and 8.5, and the pH for shallow groundwater from 6 to 8.5.^[240] Therefore, the pH studied were comprised in this range. The effect of the different solution pH on the binding capacity of the MNM systems for PCB 126 is shown in Figure 6-4. The general trend observed is a decrease in the amount of PCB bound as the pH increases. Since PCB 126 is a neutral molecule and chemically stable under normal conditions therefore unlikely

to be affected by changes in pH. This behavior corresponds to what has been reported in a previous study where an increase in pH from 5 to 9 resulted in a decrease in binding for a group of 12 PCBs.^[241]

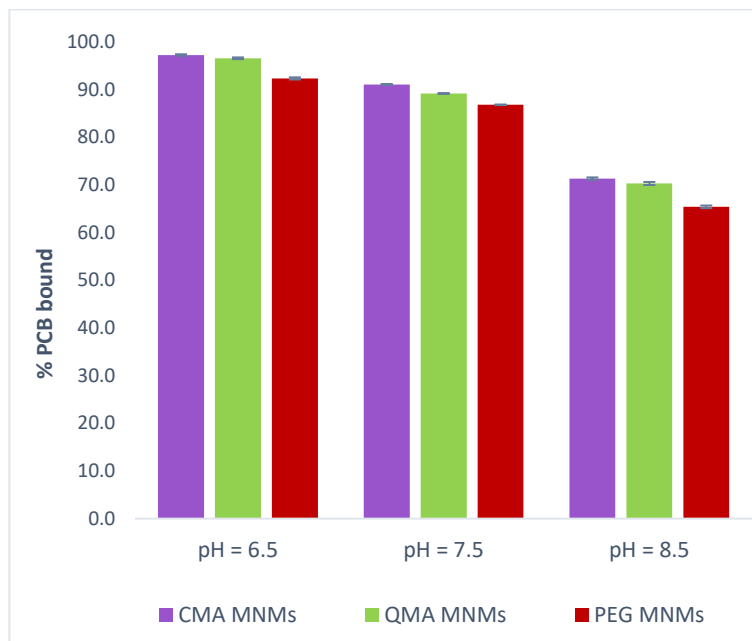


Figure 6-4 Effect of pH on the adsorption efficiency of PCB 126 on CMA MNMs, QMA MNMs and PEG MNMs.

To adjust the pH of the 99:1 DI water to ethanol solvent (where the binding studies were being carried out) to 6.5, a phosphate citrate was used. Here, the amount of PCB bound appears to slightly increase when compared to the standard binding conditions at a pH of 7.5. When the pH decreased from 7.5 to 6.5, the average increase in capacity for all the MNMs is of less than 6 %. This result is in agreement with previously published data showing that a pH between 6.5 and 7.5 was optimal for maximum adsorption of 8 PCB congeners to occur.^[242]

On the other hand, to adjust the pH to 8.5, a glycine sodium hydroxide buffer was used. Under these conditions, it was seen that as the pH increased from 7.5 to 8.5, the amount of PCB bound decreased from 91 to 71 % for the CMA MNMs, 89 to 70 % for the QMA MNMs, and 86 to 65 % for the PEG MNMs. Here, the average decrease in capacity for all the MNMs is almost 20 %. This significant decrease in binding capacity correlates to the general effect of ionic strength observed for the MNM systems. Because two different buffer solutions were employed in this study, it is reasonable to consider the combined effect of pH and presence of ions in solution to explain these results. With increasing pH, the presence of anion in solution increases allowing a different type of noncovalent interaction to occur: anion- π interactions. These kind of interactions are usually defined as attractive interactions between anions and the faces of π - rings.^[243,244] In the present work, anion- π interactions can occur between the aromatic rings of the PCB 126 molecules and the buffer anions. The formation of these interactions can then increase the solubility of the PCBs in solution and result in a decrease in the adsorption capacity. Likewise, the anion- π interactions can also occur between the aromatic rings within the MNMs network and create a competing effect for binding sites with the PCB molecules. Even though anion- π interactions are said to be weaker than π - π interactions, in some cases, there is a possibility these ‘complexes’ can be as strong in solution in this specific situation. Anion- π is a relatively newer type of noncovalent interaction and, as so, there is still not enough information available to make definitive conclusions.

Although different buffer solutions were added to the samples, it is not expected for the MNMs to be affected by the pH range studied due to the absence of ionizable functional groups on its surface and their stable chemical structure. These results indicate that the

solution pH is an important factor to consider in the application of the MNMs, and its controlled will be necessary when used to adsorb PCBs.

6.5 Conclusions

A water body is a complex system, and there are many factors that can influence the behavior of adsorbents used in water remediation. Here, the effect of ionic strength, water hardness and solution pH were evaluated on the adsorption capacity of PCB 126 on three magnetic nanocomposite microparticles (CMA MNMs, QMA MNMs, and PEG MNMs) previously synthesized by our group. The results showed that ionic strength and water hardness had minimal impact on the adsorption of the MNM systems towards PCB 126 in the range studied. However, the solution pH did affect the binding of the MNMs, resulting in a decreased in binding for PCB 126 as the pH increased from 6.5 to 8.5. These results indicate that the developed MNMs can be used as magnetic adsorbents for polychlorinated biphenyls in groundwater and surface water remediation provided solution pH is taken into consideration and controlled.

CHAPTER 7. EFFECT OF ATOM TRANSFER RADICAL POLYMERIZATION REACTION TIME ON PCB BINDING CAPACITIES OF STYRENE-CMA/QMA CORE-SHELL IRON OXIDE NANOPARTICLES

7.1 Abstract

Water pollution continues to be one of the greatest challenges humankind faces worldwide. Increasing population growth, fast industrialization and modernization risk the worsening of water accessibility and quality in the coming years. Nanoadsorbents have steadily gained attention as remediation technologies that can meet stringent water quality demands. In this work, core-shell magnetic nanoparticles (MNPs) comprised of an iron oxide magnetic core and a styrene based polymer shell were synthesized via surface initiated atom transfer radical polymerization (SI-ATRP), and characterized them for their binding of polychlorinated biphenyls (PCBs), as model organic contaminant. Acrylated plant derived polyphenols, curcumin multiacrylate (CMA) and quercetin multiacrylate (QMA), and divinylbenzene (DVB) were incorporated into the polymeric shell to create high affinity binding sites for PCBs. The affinity of these novel materials for PCB 126 was evaluated and fitted to the nonlinear Langmuir model to determine binding affinities (K_D). The K_D values obtained for all the MNP systems showed higher binding affinities for PCB 126 than carbonaceous materials, like activated carbon and graphene oxide, the most widely used adsorption materials for water remediation today. The effect of increasing ATRP reaction time on the binding affinity of MNPs demonstrated the ability to tune polymer shell thickness by modifying the reaction extent and initial crosslinker concentrations in order to maximize pollutant binding. The enhancement in binding affinity and capacity for PCB 126 was demonstrated by the use of hydrophobic, aromatic rich molecules like styrene, CMA, QMA and DVB, within the polymeric shell provides more sites for π - π

interactions to occur between the MNP surface and the PCB molecules. Overall, the high affinities for PCBs, as model organic pollutants, and magnetic capabilities of the core-shell MNPs synthesized provide a strong rationale for their application as nanoadsorbents in the environmental remediation of specific harmful contaminants.

7.2 Introduction

Atom transfer radical polymerization (ATRP) is one of the most frequently applied in the engineering of surfaces and interfaces with polymers brushes. ATRP is a powerful technique that allows to tune the chemical and physical properties of a surface/interface due to their simple experimental set up, performance under mild reaction conditions, tolerance for a variety of functional groups, and compatibility with organic and inorganic solvents.^[1] There are two main strategies to graft polymer brushes onto a surface: ‘grafting to’ or ‘grafting from’ approach. Of particular interest are methods on the ‘grafting from’ approach, where a surface initiator is first anchored, and then *in situ* polymerization occurs to generate a polymer brush.^[2,3] An example of this approach is surface initiated atom transfer radical polymerization (SI-ATRP). SI-ATRP is a well-established technique that offer control over the polymer thickness and densities. Additionally, it allows for the growth of polymer brushes on virtually any surface, as long as the surface initiator is properly selected.

Surface initiated ATRP has been widely used to grow polymers from a variety of nanoparticle surfaces, such as Au, Ni, MnFe₂O₄, BaFe₂O₃, Fe₃O₄, among others.^[4-8] These types of ATRP synthesis give rise to core-shell nanoparticles, an ideal composite system

that combines the advantages of the polymeric shell and the metallic core, that offers enhanced physical and chemical properties. Of particular interest is the formation of core-shell nanoparticles is the use of iron oxide nanoparticles (IO MNPs) to obtain magnetic nanoparticles. Herein, the core consists of magnetite (Fe_3O_4) or maghemite ($\gamma\text{-Fe}_2\text{O}_3$), which can be superparamagnetic, meaning that upon exposure to an external magnetic field the particles will rapidly aggregate together, yet able to redisperse back in solution once the magnetic field is removed.^[9-11] This characteristic allows the IO MNPs to be magnetically separated from solution with the use of a static magnetic field. Additionally, IO MNPs have the ability to respond to an alternating magnetic field (AMF) by converting magnetic work into internal energy, through magnetic relaxation processes, and dissipating it as heat.^[12,13] The polymeric coatings on the IO MNPs can improve the stability of the particles in solution, prevent their aggregation and protect them from oxidation. These functional polymer shells can provide the core-shell magnetic nanoparticles with desired functionalities to tailor their composition for specific applications. Polymer usually possess tunable porous structures, excellent mechanical properties, and a variety of functional groups. Because of this, core-shell nanoparticles have found application in a variety of areas like drug delivery, magnetic resonance, cancer treatment, rheology, energy storage, and environmental remediation, among others.^[14-20]

Core-shell magnetic nanoparticles have gained growing appeal in the environmental field for their versatility in polymer functionality, and core magnetic functions that allow for magnetic separation from the contaminated media. This grants the nanoparticles with a significant advantage over other remediation technologies: a fast and easy way to recover the sorbent material from raw environmental samples without the need of centrifugation or

filtration steps.^[21] In addition, nanoadsorbents have a very high specific surface, high associated sorption sites, tunable porosity, and have been successfully employed in environmental applications for pollutant mitigation and removal.^[22-24] The selection of the various functional monomers or crosslinkers to obtain the polymer shell is designed based on the final application. Studies have shown that the introduction of aromatic functional groups into the functional polymer shell increased the affinity of the core-shell nanoparticles for aromatic compounds.^[25,26] More specifically, styrene and divinylbenzene have been shown to be relatively selective for analytes with aromatic rings due to their specific π - π interactions, and have been used to remove aromatic pollutants from water.^[27] Given this information, it is expected that incorporating any aromatic rich molecule into the polymer shell will increase affinity for aromatic analytes. One such group is plant derived polyphenols, like curcumin and quercetin. These naturally occurring antioxidants can be acrylated to produce functional monomers to be used in SI-ATRP of core-shell nanoparticles.^[28-30]

One important use of core-shell magnetic nanoparticles is as nanoadsorbents in water treatment. Water pollution is a worldwide problem that needs to be addressed. Many persistent organic pollutants (POPs), persist in the environment despite their production having been banned decades ago or being under strict regulations today. One such class is polychlorinated biphenyls (PCBs). Despite their production being banned in 1979 in the United States and in 2001 by the Stockholm Convention on Persistent Organic Pollutants, concentrations of PCB congeners can still be found in water, sediment, soil, aquatic biota and other animals throughout the world.^[31-33] PCBs have low volatilities and poor aqueous solubility, making their extraction from water and soil very challenging. Current

remediation technologies are either too time consuming, not efficient enough at removal of the pollutant, and/or too costly.^[34,35]

In this work, core-shell magnetic nanoparticles were prepared using SI-ATRP to coat IO-MNPs with a styrene-based polymer shell crosslinked with acrylated plant derived polyphenols. Curcumin multiacrylate (CMA) and quercetin multiacrylate (QMA) were acrylated and incorporated in the core-shell magnetic nanoparticles to enhance their adsorption capacity for PCBs. Divinylbenzene (DVB) crosslinked systems were also studied as a comparison group. The effect of ATRP synthesis time on the shell thickness was studied at two different initial acrylated polyphenol or DVB loadings. The functionalized nanoparticle systems were characterized for size, shell coating percent, and stability. The binding isotherm for a model contaminant, PCB 126, was studied, and the binding constants for the four systems synthesized were evaluated using the Langmuir adsorption model.

7.3 Experimental

7.3.1 Materials

Iron (III) chloride hexahydrate ($\text{FeCl}_3 \cdot 6 \text{H}_2\text{O}$); iron chloride tetrahydrate ($\text{FeCl}_2 \cdot 4 \text{H}_2\text{O}$); 2-bromo-2-methyl propionic acid (BMPA); 4,4'-dinoyl-2,2'-dipyridil (DNDP); copper (I) bromide (CuBr); copper (II) dibromide (CuBr_2); triethyl amine (TEA), acryloyl chloride; and potassium carbonate (K_2CO_3) were obtained from Sigma Aldrich (St Louis, MO). Ammonium hydroxide (NH_4OH) was purchased from EMD Chemicals (Gibbstown, NJ). Styrene (Sty) and divinylbenzene (DVB) were obtained from Polysciences INC. (Warrington, PA). Curcumin was purchased from Chem-Impex International, Inc.

(Bensenville, IL), and quercetin was purchased from Cayman Chemicals (Ann Arbor, MI). 3,3',4,4',5-Pentachlorobiphenyl (PCB-126) in isooctane was purchased from Accustandard (New Haven, CT). All solvents (Isooctane, ethanol HPLC grade, xylene, toluene, tetrahydrofuran (THF); dichloromethane (DCM), acetonitrile (ACN)) were obtained from Fisher Scientific (Hannover Park, IL). All materials were used as received.

7.3.2 Iron oxide nanoparticle synthesis

Iron oxide magnetic nanoparticles (IO MNPs) were synthesized through a one-pot co-precipitation method.^[17] Iron chloride salts, $\text{FeCl}_3 \cdot 6 \text{H}_2\text{O}$ and $\text{FeCl}_2 \cdot 4 \text{H}_2\text{O}$, were dissolved in 40mL of DI water in a 2:1 molar ratio of respectively, and combined in a sealed 3-neck flask under vigorous stirring and nitrogen flow to achieve an inert synthesis environment. The flask was heated to 85°C and 5 mL of NH_4OH (30.0 % v/v) was injected dropwise into the vessel. The reaction was carried out for 1 h. The nanoparticles were magnetically decanted and washed three times against DI water. Finally, the particles were re-suspended in 45 mL of DI water and dialyzed for 24 h. (100 kDA molecular weight cutoff)

7.3.3 BMPA initiator addition

The iron oxide nanoparticles were mixed in a 1:4 molar ratio with the 2-bromo-2-methyl propionic acid (BMPA) initiator in a 75-25 ethanol – DI water solvent. The mixture was stirred for 24 h at room temperature. Following this, the particles were magnetically decanted and washed twice times with ethanol, and twice with xylene. The initiator coated particles (BMPA MNPs) were kept suspended in xylene.

7.3.4 Surface initiated atom transfer radical polymerization

The core-shell nanoparticles were prepared by adapting a the method reported by Li et al.^[36] The BMPA MNPs suspended in xylene were mixed with the catalyst mixture. The amount of catalyst used was determined based on a styrene ratio of: 70:1.1 for DNDP, 70:0.3 for CuBr and 70:0.015 for CUBr₂. The solution containing the BMPA MNPs and the catalyst had a total volume of 120 mL. This solution was placed in a 3-neck flask, under nitrogen bubbling, 325 rpm, and heated to 135°C. The crosslinker, in this case the acrylated polyphenol (CMA or QMA), or DVB, was dissolved/mixed in 15 mL of xylene and injected into the reaction vessel at 110°C. CMA and QMA were synthesized following the protocol described by Patil et al ^[165,166] and Gupta et al ^[167], respectively. Two different crosslinker feed were studied: 5 mol% and 10 mol%. The reaction was carried out for a total of 24 hours. Samples of 25 mL were drawn out at 2, 6, 12 and 24 hours using a stainless steel syringe. Each sample collected was transferred into a 30 mL borosilicate amber glass vial, magnetically decanted and washed twice with xylene, twice with acetone, three times with a 50-50 % (v/v) ACN/DCM solution, and twice with a 50-50 % (v/v) ethanol/DI water solution. Finally, the particles were re-suspended in DI water.

7.3.5 Particle characterization

A Varian Inc. 7000e spectrometer with attenuated total reflectance FTIR (ATR-FTIR) was used to determine the surface functionalization of the core shell nanoparticles. Dried samples were placed on the diamond ATR crystal and the spectrum was obtained between 700 and 4000 cm⁻¹ using 32 scans.

7.3.5.1 Thermogravimetric analysis

A Netzsch Instruments STA 449A system was used to quantify the mass percent of the coating on the nanoparticle systems. Approximately 5 mg of the dry sample was heated at a rate of 5°C per minute until a temperature of 120°C under constant nitrogen flow. The system was kept isothermal for 20 min to vaporize residual solvent and water vapors. The sample continued to be heated at 5°C per minute until a temperature of 600°C. The presented mass loss values are normalized to the mass after isothermal heating at 120°C.

7.3.5.2 X-ray diffraction

A Siemens D-500 X-ray spectrometer was used to determine the X-ray patterns of the nanoparticles using a with a CuK α radiation source ($\lambda = 1.54 \text{ \AA}$) at 40 kV and 30 mA, using scanning speed of 1° per minute from 5° to 65°. The XRD patterns were used to estimate the particle's crystal domain using the Scherrer equation:^[168]

$$\tau = \frac{K\lambda}{\beta \cos\theta} \quad (1)$$

where τ is the mean size of the ordered, crystalline domains, K is a dimensionless shape factor with a value close to unity (for iron oxide, $K = 0.8396$), λ is the X-ray wavelength, β is the line broadening at half the maximum intensity (FWHM) after subtracting the instrumental line broadening, and θ is the Bragg angle, in radians (17.72°). The XRD patterns were also used to confirm the magnetic crystal structure of the iron oxide nanoparticles.

7.3.5.3 Dynamic light scattering

A Malvern Zetasizer, Nano ZS90 instrument was used to obtain DLS measurements. Before analysis, the nanoparticle solutions were diluted to 200 µg/mL in DI water and probe sonicated for 10 minutes.

7.3.5.4 Ultraviolet (UV)-visible spectroscopy

A Cary Win 50 probe UV-visible spectrophotometer was used to study the stability of the nanoparticles. The magnetic nanoparticles were diluted to 200 µg/mL in DI water, and probe sonicated for 10 min. The samples were then placed in a quartz cuvette and their change in absorbance was read at 540 nm for a period of 12 h.

7.3.5.5 Alternating magnetic field (AMF) heating

Using a custom Taylor Winfield magnetic induction source the heating profiles of the nanoparticles were obtained. The temperature change in solution was recorded using a fiber optic temperature sensor (Luxtron FOT Lab Kit from LumaSense). A sample of 1.5 mL of the nanoparticles suspended in DI water at a concentration of 3 mg mL⁻¹ of iron oxide was placed in a microcentrifuge tube inside and in the center of the AMF induction coil. The alternating magnetic field source was operated at a field amplitude of approximately 55 kA m⁻¹ and a frequency of 300 kHz for 5 minutes. The specific absorption rate (SAR) values of the nanoparticles was calculated using the following equation:

$$SAR = \frac{C_{p,Fe}m_{Fe} + C_{p,H_2O}m_{H_2O}}{m_{Fe}} \frac{dT}{dt} \quad (2)$$

where $C_{p,Fe}$ is the heating capacity of iron, m_{Fe} is the mass of iron, C_{p,H_2O} is the heating capacity of iron, m_{H_2O} is the mass of water, and $dT (dt)^{-1}$ is the initial slope of the heating profile of the system.

7.3.6 PCB 126 binding studies

In order to determine the binding capacity of the core-shell nanoparticles to PCB 126, equilibrium binding studies were conducted. The process followed has been described by our group in previous publications.^[214,253] Briefly, 0.1 mg mL⁻¹ of the core-shell MNP systems suspended in a 99:1 DI water ethanol solvent were added in 3 mL borosilicate glass vials. Each sample was spiked with a known concentration of PCB 126 and sonicated for 10 minutes. PCB stocks were freshly prepared in ethanol to obtain 6 initial concentration ranging from 0.005 ppm to 1 ppm. The samples were placed in an orbital shaker (200 rpm, 25°C) for the duration of the study. Once the study finalized, the samples were magnetically decanted for ~ 10 min. The supernatant was collected and placed in a new vial for to extract the free PCB in solution using isooctane. After 24 h the organic phase, rich in PCB 126, was collected and placed in a gas chromatography vial. Here each sample was spiked with the internal standard, 5'-fluoro-3,3',4,4',5-pentachlorobiphenyl (F-PCB 126). All PCB 126 concentrations before and after the binding study were determined using an Agilent 6890N gas chromatography coupled to electron capture detection (GC-ECD), equipped with an Agilent HP-5MS UI column (30x0.25x0.25).

The MNP systems used for this studied were: styrene curcumin multiacrylate magnetic nanoparticles with 5 mol% initial acrylate loading at ATRP reaction times of 6h, 12h and 24h (Sty CMA MNPs_5%_6h, Sty CMA MNPs_5%_12h, Sty CMA MNPs_5%_24h); curcumin multiacrylate magnetic nanoparticles with 10 mol% initial acrylate loading at ATRP reaction time of 24h (Sty CMA MNPs_10%_24h); styrene quercetin multiacrylate magnetic nanoparticles with 5 mol% initial acrylate loading at ATRP reaction times of 6h, 12h and 24h (Sty QMA MNPs_5%_6h, Sty QMA

MNPs_5%_12h, Sty QMA MNPs_5%_24h); quercetin multiacrylate magnetic nanoparticles with 10 mol% initial acrylate loading at ATRP reaction time of 24h (Sty QMA MNPs_10%_24h); and styrene divinylbenzene magnetic nanoparticles with 5 mol% initial crosslinker loading at ATRP reaction times of 6h, 12h and 24h (Sty DVB MNPs_5%_6h, Sty DVB MNPs_5%_12h, Sty DVB MNPs_5%_24h).

The binding capacity of the nanoparticles was calculated using the following equation:

$$q_e = \frac{(C_0 - C_e)V}{m} \quad (3)$$

where q_e is the equilibrium binding capacity (mg g^{-1}), C_0 and C_e are the initial and equilibrium concentrations (mg L^{-1}), respectively, V is the total volume of the solution (L), and m is the mass of the adsorbent (g). The obtained data was fitted to the Langmuir isotherm model, as it is the most useful model to represent adsorption of polycyclic aromatic hydrocarbons from water onto adsorbents.^[43] The Langmuir model best represents monolayer adsorption on homogeneous surfaces, where there is a set number of binding sites that are all energetically equivalent and no interactions between adsorbed molecules occurs.^[168] The Langmuir model is represented by the following equation:

$$q_e = \frac{B_{\max} K_D C_e}{1 + K_D C_e} \quad (4)$$

where q_e (mg g^{-1}) represents the adsorption capacity at equilibrium, C_e (mg L^{-1}) is the equilibrium concentration of the adsorbate, K_D (L mg^{-1}) is the adsorption coefficient of the sorbent related to the energy of adsorption, and B_{\max} (mg g^{-1}) is the maximum binding capacity of the sorbent.

7.4 Results and discussion

Core-shell magnetic nanoparticles were successfully prepared via surface initiated atom transfer radical polymerization. The MNP synthesis can be broken down into 3 main steps: the preparation of the IO MNPS, the functionalization of the IO MNPs surface with an anchoring group for ATRP, in this case BMPA, and finally the SI-ATRP occurs under inert atmosphere. A schematic representation of this process and obtained core-shell nanoparticles is depicted in Figure 7-1

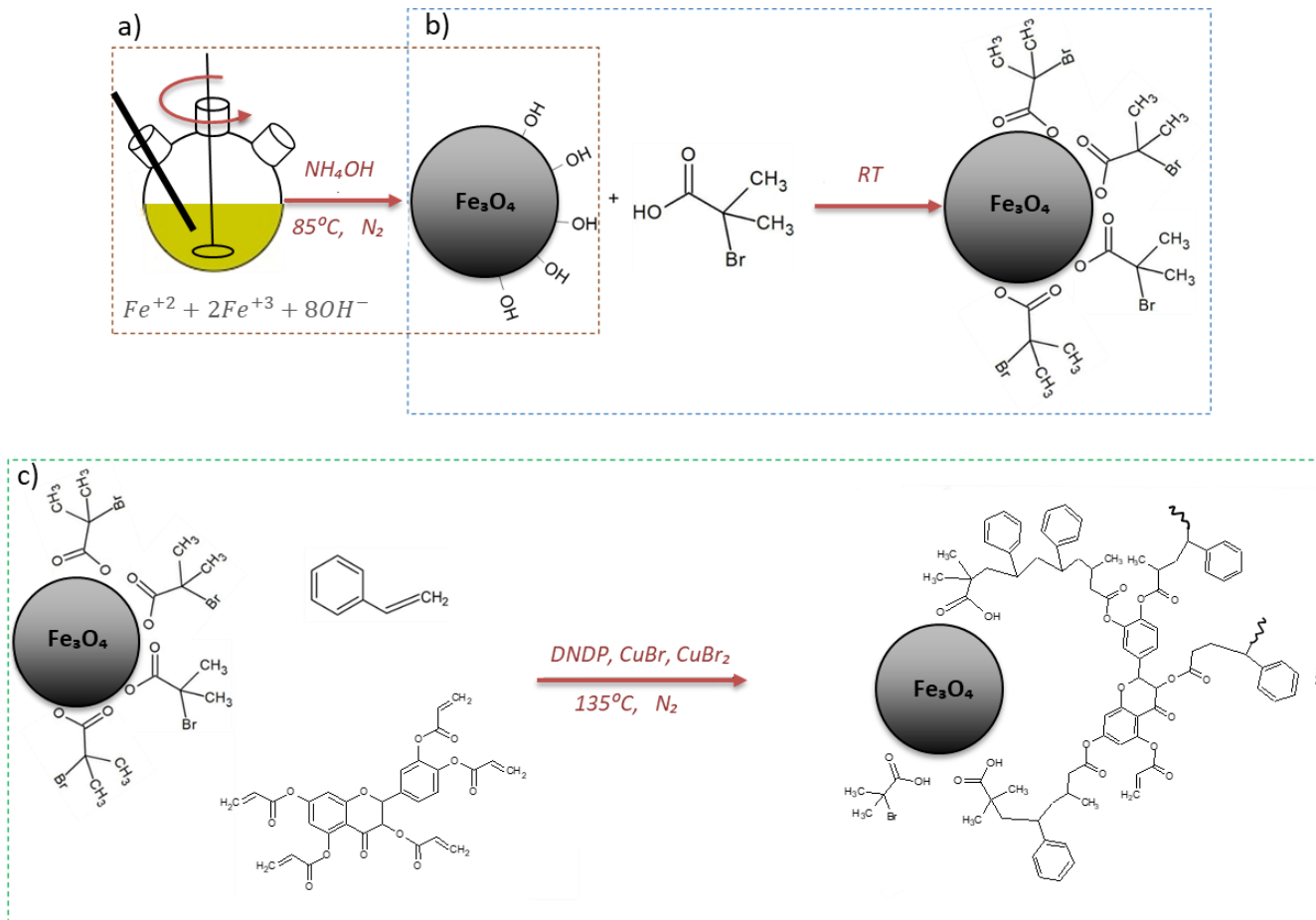
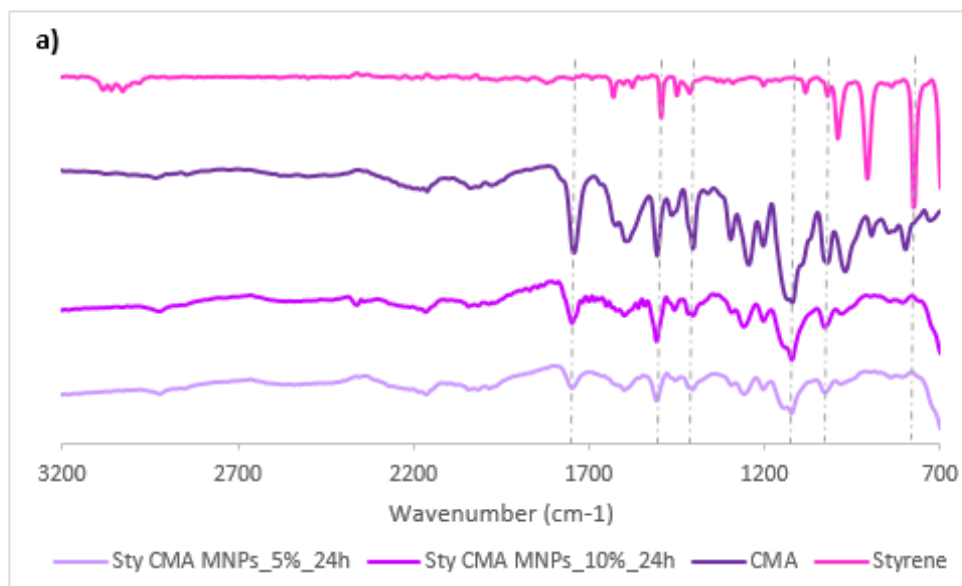


Figure 7-1 Schematic representation of the synthesis of the core-shell magnetic nanoparticles (MNPs): a) Co-precipitation synthesis of IO MNPs, shown inside the red rectangle b) Surface functionalization of the IO MNPs with BMPA to obtain BMPA MNPs, c) Atom transfer radical polymerization reaction with styrene (Sty) and curcumin multiacrylate (CMA) to obtain core-shell Sty-CMA MNPs.

FTIR analysis confirms the successful SI-ATRP reaction and the formation of a polymer shell on the IO MNPs. Figure 7-2a shows the spectra for the CMA containing MNPs at two different initial loadings, 5 mol% and 10 mol%, both after a complete 24h ATRP reaction time. The presence of three main peaks between 1800 cm^{-1} and 1400 cm^{-1} are attributed to the symmetric ring vibrations of the benzene rings present in CMA. The presence of a peak at 1100 cm^{-1} in both Sty CMA MNPs can be attributed to the ether C-O stretching of CMA. Additionally, peaks are seen at approximately 1000 cm^{-1} and 950

cm^{-1} corresponding to the enol (C-O-C) peak and C-H benzoate vibrations of the aromatic rings. Because styrene also presents aromatic rings, the peaks between 1600 cm^{-1} and 1400 cm^{-1} also provide evidence for the presence of styrene on the IO MNP polymer shell. Similar results are observed in Figure 7-2b, where the acrylated polyphenol present in QMA. Again, the aromatic ring vibration of the benzene are observed by broader peaks between 1800 cm^{-1} and 1400 cm^{-1} , as well as a peak at 1200 cm^{-1} for ether stretching. Once again, the presence of the styrene on the Sty QMA MNPs can also be inferred from the aromatic peaks, and by the presence of small peaks around 830 cm^{-1} corresponding to aromatic ring bending. Figure 3c shows the spectra for the core-shell MNPs made without polyphenols. In this case, divinylbenzene was used as the crosslinker. The presence of both monomers can be seen in the appearance of peaks corresponding to the C-H deformation vibrations of the benzene ring around $1000 - 800\text{ cm}^{-1}$.



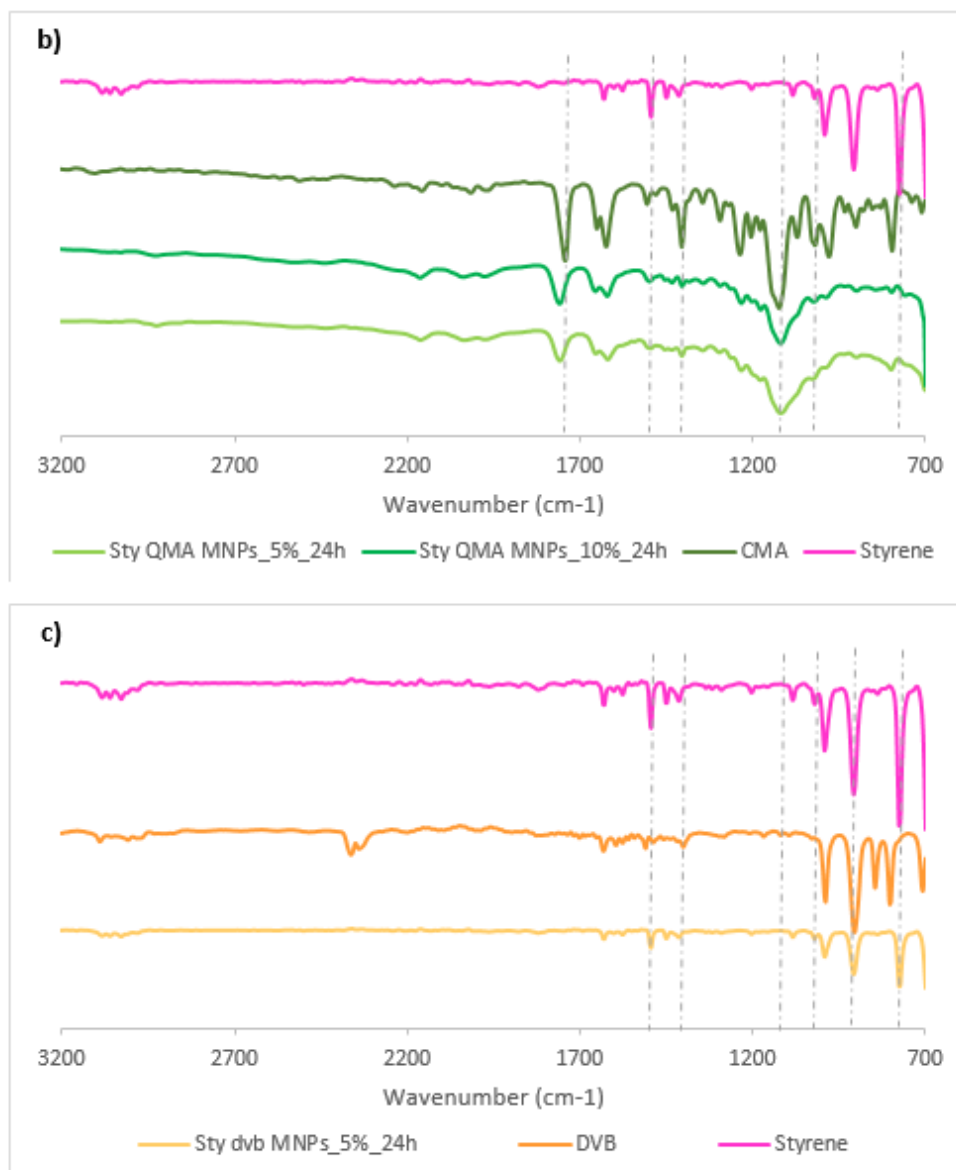
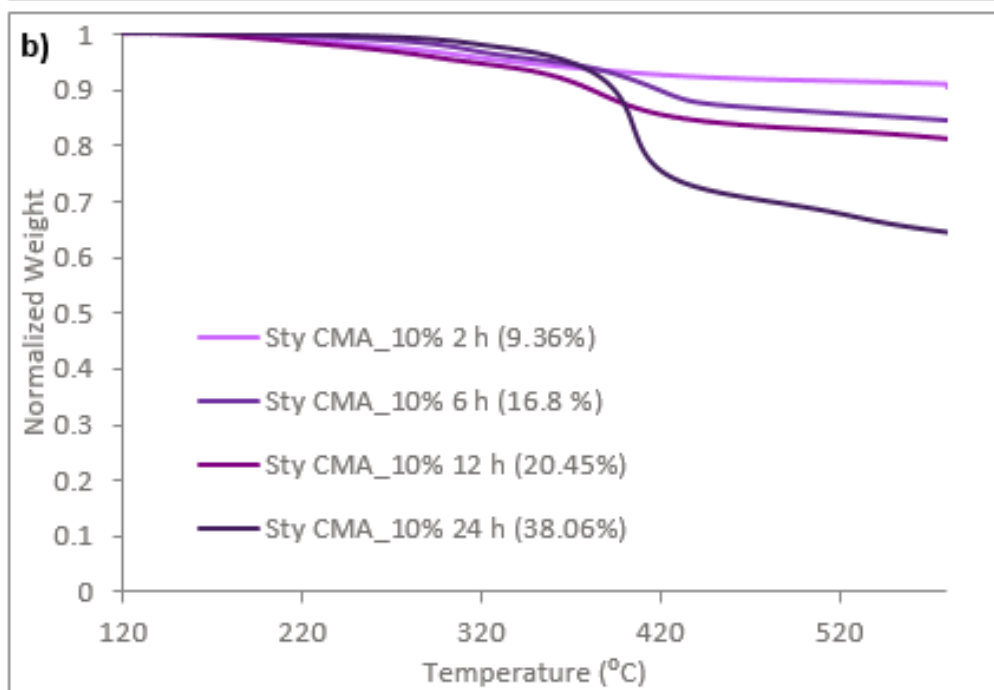
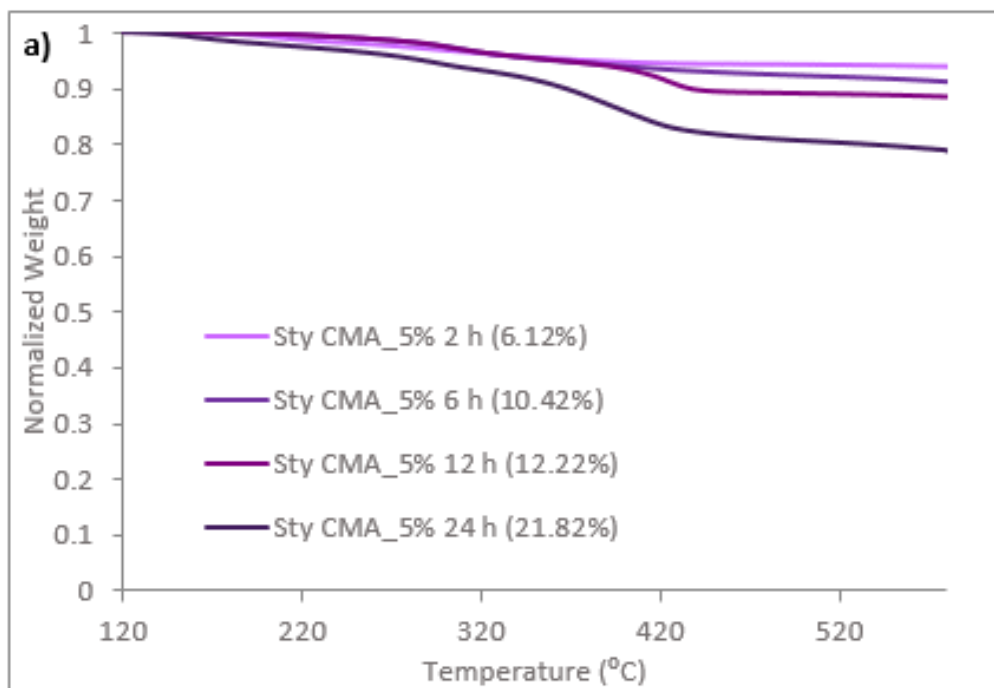
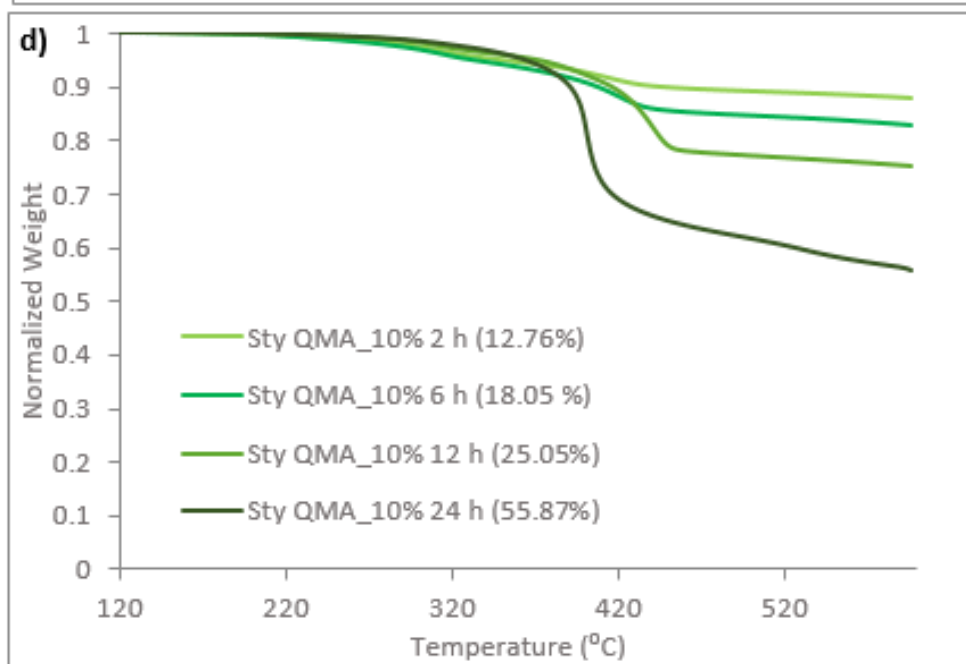
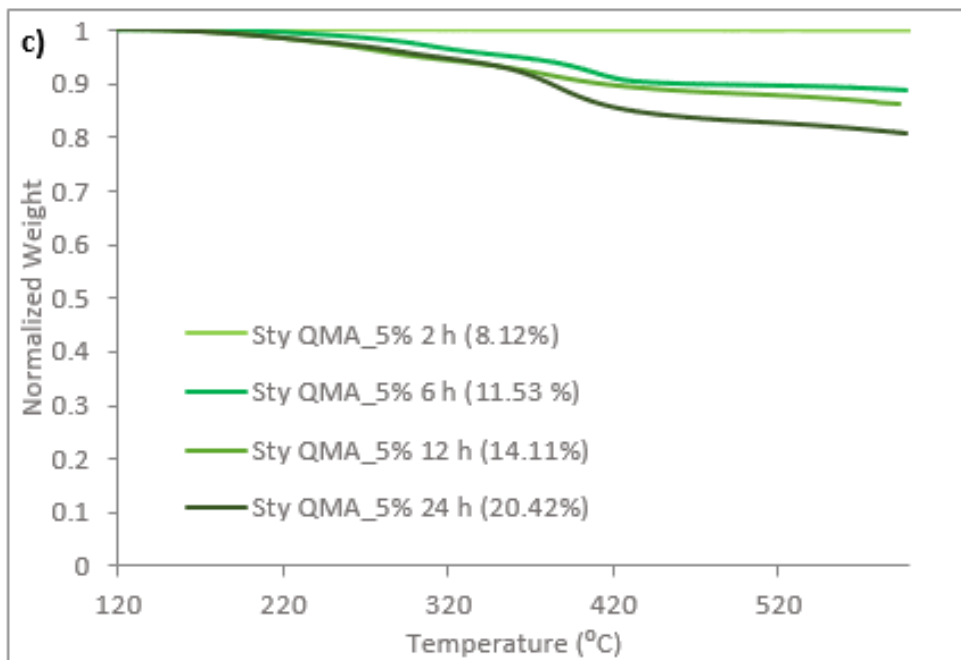


Figure 7-2 FTIR spectra of the synthesized magnetic nanoparticles. A) Sty CMA MNPs, B) Sty QMA MNPs and C) Sty DVB MNPs.

To begin to study the effect of ATRP reaction time on the growth of the shell on the IO MNPs, the determination of the amount of polymer grown needed to be determined. Thermogravimetric analysis was used to burn off the polymer shell over a selected temperature range, leaving the IO MNPs as residue. The TGA curves for the MNP systems

are presented in Figure 7-3. It can be seen that for all the MNPs the amount of polymer coating, or shell growth, increases as the ATRP reaction time increases. This was expected given that SI-ATRP has been shown to allow for precise control of polymer density, molecular weight, and shell thickness.^[238,254] For the 5 mol% of initial crosslinker/functional monomer initial loading (Figure 3a, c, e), the increase in polymer composition appears to be relatively the same for all three MNP systems where after 24h of reaction, the polymer shell represents close to 20% of the total mass. On Figure 3b and d the initial amount of functional monomer, CMA or QMA, was increased to 10 mol%. In both cases an increase in weight loss is seen in the thermogram, indicating a higher polymer composition in the resulting MNPs. After 24h, the polymer coating on the Sty CMA MNPs from 5 mol% to 10 mol% of initial loading has increased from 21.82% to 38.06%. Likewise, the polymer coating on the Sty QMA MNPs from 5 mol% to 10 mol% of initial loading has increased from 20.42% to 55.8%. In both cases the polymer mass has almost doubled, or in fact doubled, its mass compared to its counterpart at 5 mol%. This increase in polymer mass when the initial functional monomer is of 10 mol% continues to be seen at lower reactions times, but it is less pronounced the shorter the reaction time. For example, the Sty CMA MNPs at 5 mol% have a polymer growth of 6.12% at 2h, 10.42% at 6h and 12.22% at 12 h, compared to the Sty CMA MNPs at 10 mol% with a polymer growth of 9.36% at 2h, 106.8% at 6h and 38.06% at 12 h. This increase in polymer shell growth with increasing functional monomer loading has been observed by other groups, where the thickness obtained through SI-ATRP was dependent on the molecular weight of the monomer, and the amount of monomer present in solution.^[254-256]





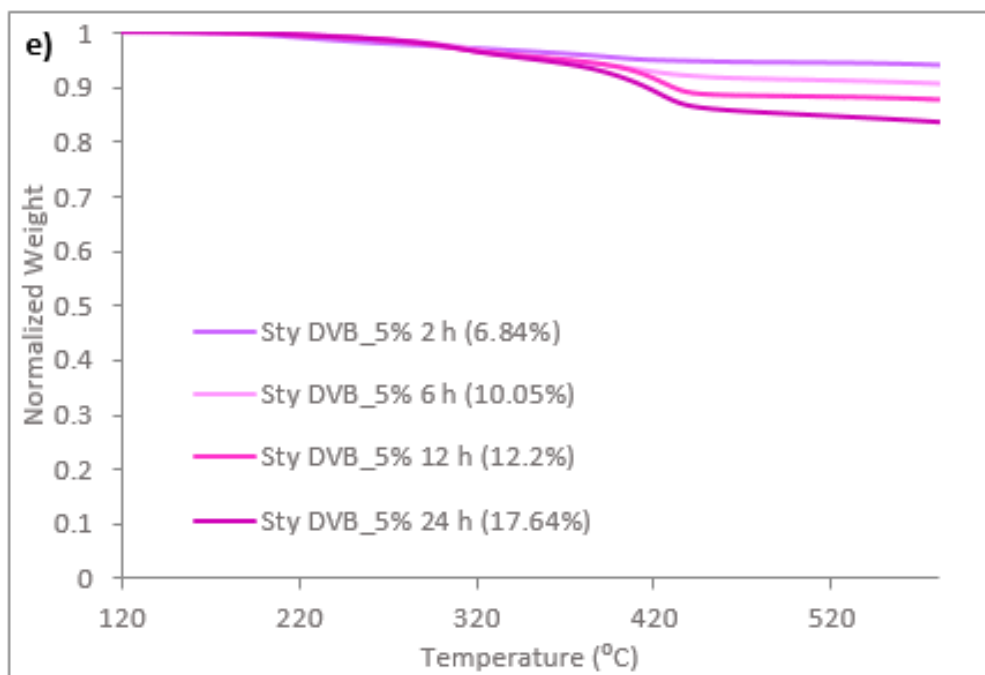


Figure 7-3 Mass loss profile with increasing temperature of the synthesized core-shell magnetic nanoparticles at different ATRP reaction times, A) Sty CMA MNPs at 5% initial loading, B) Sty CMA MNPs at 10% initial loading, C) Sty QMA MNPs at 5% initial loading, D) Sty QMA MNPs at 10% initial loading, and E) Sty DVB MNPs at 5% initial loading.

In order to verify the magnetic iron oxide nanoparticle core remained unchanged throughout the synthesis process, X-ray diffraction was performed. The XRD patterns for the prepared MNP systems, seen in Figure 4, are in agreement with the JCPDS card (19-0629) associated with magnetite. Furthermore, these XRD patterns present broad diffraction lines suggesting the nano-crystallite nature of the magnetite particles.^[168,170] The sharp peaks observed in the diffractograms indicate the formation of a crystalline structure, where the highest peak observed at 35.5° (2θ) corresponds to the (3 1 1) reflection plane of the iron oxide crystalline structure. This information can be used in conjunction

with the Scherrer equation to calculate the crystallite size of the core-shell MNPs. The iron oxide crystal size obtained from MNP for each system can be seen in Table 7-1.

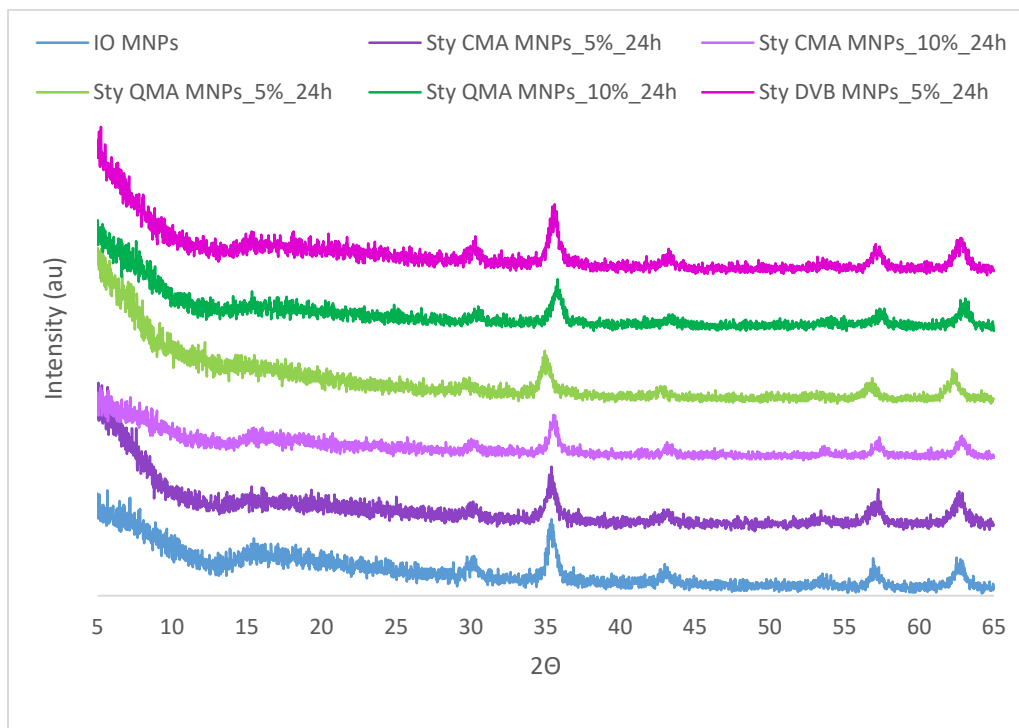


Figure 7-4 XRD patterns of the synthesized core-shell magnetic nanoparticles. Iron oxide nanoparticle XRD pattern included for reference

Table 7-1 Size analysis from XRD using the Scherrer equation; hydrodynamic size analysis of the synthesized core-shell MNPs (mean \pm std dev. for three independent batches and three samples from each batch); and SAR values from AMF heating)

MNP System	Hydrodynamic size (nm) [PDI]				XRD crystal size (nm)	SAR (W mg _{Fe} ⁻¹)
	<i>2h</i>	<i>4h</i>	<i>12h</i>	<i>24h</i>		
Sty CMA MNPs_5%	173.9 \pm 6.3 [0.06]	262.9 \pm 5.5 [0.1]	356.9 \pm 19.5 [0.1]	479.5 \pm 33.6 [0.11]	12.5 \pm 0.7	295.5 \pm 10.5
Sty CMA MNPs_10%	340.0 \pm 0.7 [0.07]	440.0 \pm 0.95 [0.1]	503.9 \pm 12.2 [0.11]	969.8 \pm 29.0 [0.1]	10.2 \pm 0.9	148.7 \pm 16.8
Sty QMA MNPs_5%	164.3 \pm 2.7 [0.05]	176.5 \pm 3.8 [0.1]	210.01 \pm 5.4 [0.1]	474.6 \pm 32.7 [0.1]	11.4 \pm 1.0	297.8 \pm 24.2
Sty QMA MNPs_10%	260.5 \pm 5.7 [0.04]	279.0 \pm 5.5 [0.1]	420.1 \pm 3.6 [0.11]	1558.7 \pm 36.8 [0.12]	9.8 \pm 0.8	93.4 \pm 9.8
Sty DVB MNPs_5%	262.6 \pm 1.0 [0.06]	278.2 \pm 4.6 [0.1]	272.4 \pm 7.3 [0.1]	285.5 \pm 3.2 [0.1]	10.6 \pm 1.1	309.5 \pm 22.9

The hydrodynamic size of the core-shell magnetic nanoparticles was determined using dynamic light scattering (DLS) and reported as Z-average, with the variability in particle size within the batches being quantified by the polydispersity index (PDI), as presented in Table 7-1. An increase in hydrodynamic size is observed for all MNP systems as the ATRP reaction time increases. Although it is known the nanoparticles aggregate in solution, the significant size increase observed in most cases would indicate an increase in the MNPs size as well. These results are in agreement with what was observed for the TGA results, where the increase in ATRP reaction time in fact increases the amount of polymer shell growth, hence increasing the size of the MNP system.

The stability of the core-shell MNPs in aqueous environment becomes an important factor for their application as nanoadsorbents. In order to maximize the binding capacity, it is ideal for the particles to remain suspended in solution so that all their surface area is available to interact with the contaminant of interest. In order to evaluate this, the MNP systems were suspended in DI water their change in absorbance was recorded for 12h (Figure 5). It can be seen that in Figure 7-5 a – d, as the ATRP reaction time increases the

MNP system becomes less stable in solution. This behavior can be explained by the increasing hydrophobicity of the MNPs as the polymer shell increases with increasing ATRP reaction time. Moreover, these systems show increasingly bigger hydrodynamic sizes as time progresses, suggesting aggregation is also occurring and most likely becoming a factor that pulls the MNPs out of solution. Accordingly, the use of mechanical agitation is necessary to make sure the MNPs remain suspended for the duration of the binding studies, and for their ultimate application as nanoadsorbents in water remediation.

Figure 7-5e shows the stability for the Sty DVB MNPs with initial 5 mol% loading. Here the stability of the MNPs does not seem to be affected by the increasing ATRP reaction time. Even though TGA data has confirmed the growth of a polymeric shell over time, DLS data suggests these particles are more stable in DI water and do not appear to aggregate as much, which would explain why they remain stable over a period of 12h.

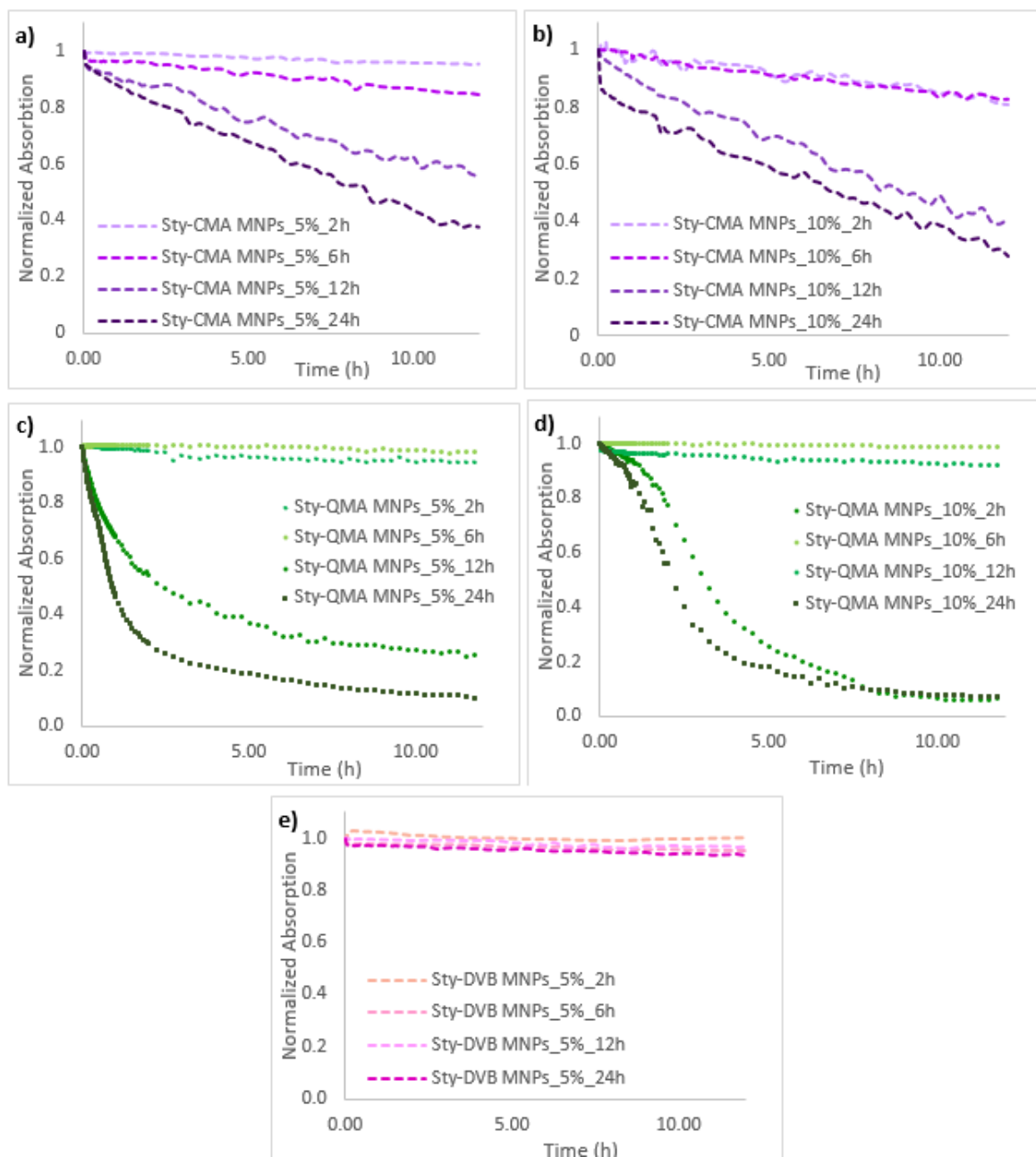


Figure 7-5 Normalized absorbance (at 540 nm) of the core-shell MNPs in DI water for 12 hours using UV-visible spectroscopy.

A unique property of IO MNPs is their ability to generate heat upon exposure to an alternating magnetic field (AMF). This heat dissipation can be used as a regeneration mechanism of the spent sorbent after a binding cycle.^[227,257] However, the thickness of the

polymeric shell coating the IO MNPs can negatively affect their heat dissipation ability. Thus the MNP systems in solution were exposed to an AMF for 5 minutes in order to obtain their heating profile and determine their specific absorption rate (SAR) values. The SAR values are reported in Table 7-1 and indicate the energy being produced per gram of iron oxide. Though the SAR values for the core-shell MNPs vary significantly between them, all MNP systems are still able to generate localized heat upon exposure to an AMF.

The binding capacity of the core-shell MNP systems for PCB 126 was studied at equilibrium conditions. The loading of the MNP systems utilized was of 0.1 mg mL^{-1} in a 99:1 DI water ethanol solvent, and six different PCB 126 concentrations were used. The MNP systems studied were: Sty CMA MNPs_5%_6h, Sty CMA MNPs_5%_12h, Sty CMA MNPs_5%_24h, Sty CMA MNPs_10%_24h, (The CMA MNP systems); Sty QMA MNPs_5%_6h, Sty QMA MNPs_5%_12h, Sty QMA MNPs_5%_24h, Sty QMA MNPs_10%_24h, (The QMA MNP systems); and Sty DVB MNPs_5%_6h, Sty DVB MNPs_5%_12h, Sty DVB MNPs_5%_24h, (The DVB MNP systems). The adsorption isotherms for all the studied MNP systems are presented in Figure 7-6.

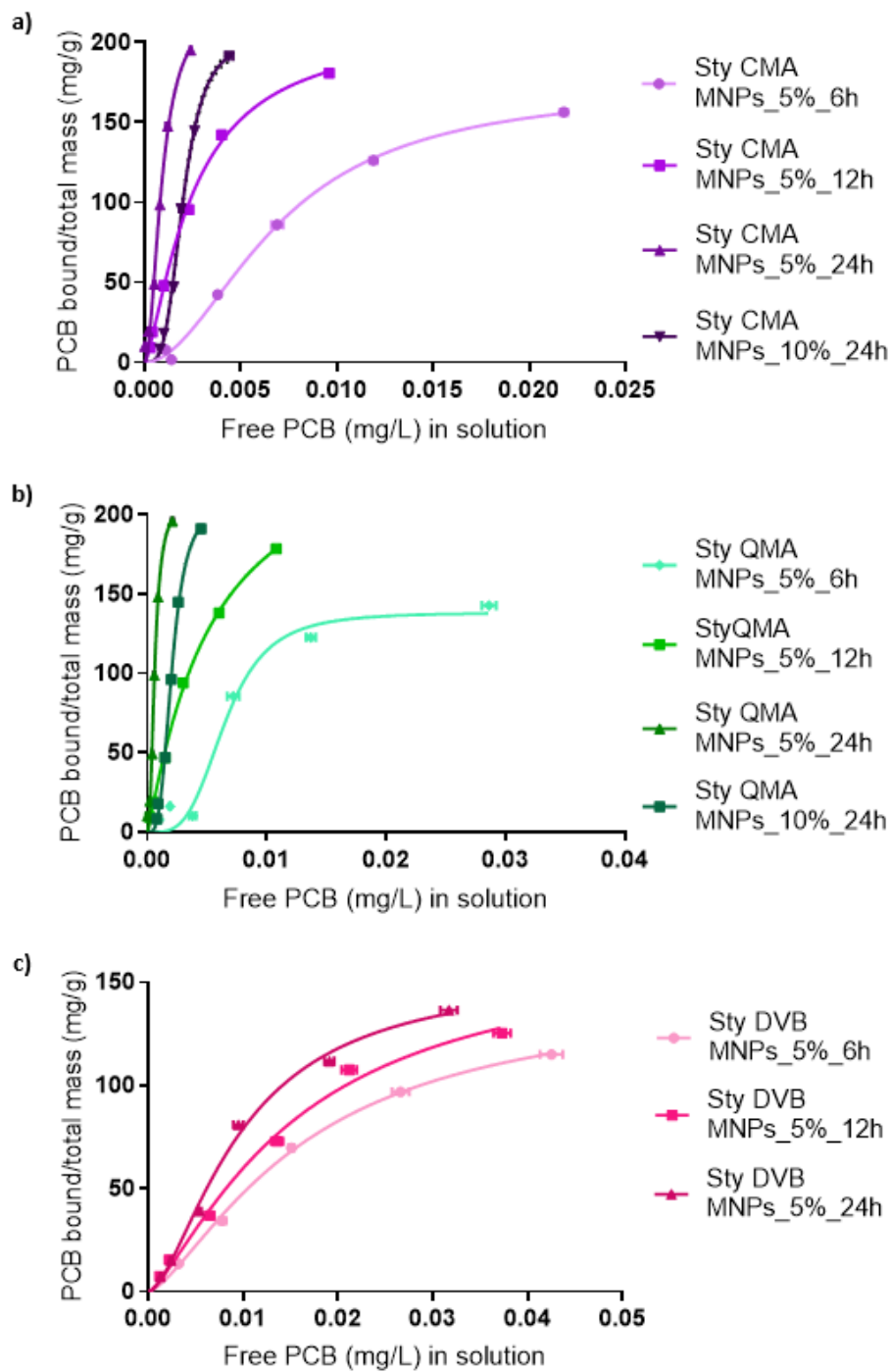


Figure 7-6 Adsorption isotherms for PCB 126 of the core-shell MNP systems in terms of total mass at room temperature. A) Sty CMA MNP systems, b) Sty QMA MNPs systems and c) Sty DVB MNPs systems. PCB 126 initial concentrations from 0.005 – 0.1 ppm fitted using the Langmuir model.

The adsorption isotherms for the CMA MNP systems studies are presented in Figure 8a. It is seen that for all the systems the amount of PCB 126 bound increases as the free concentration of PCB increased until reaching a plateau, or maximum binding capacity, at different values. The same behavior is seen in for the QMA MNP systems in Figure 8b. The DVB MNP systems behave in a similar manner, but the initial increase in the amount of PCB 126 bound as the free concentration of PCB increases has a lower slope. To better understand the adsorption phenomenon, the experimental data is fitted to the Langmuir model to obtain the maximum adsorption capacity (B_{max}) and Langmuir adsorption coefficients (K_D) for each system (presented in Table 7-2). The binding isotherms for the CMA MNP systems and the QMA MNP systems (Figure 7.6 a and 7.6 b, respectively) show higher binding at all free PCB concentrations in comparison to the DVB MNP systems. Previous works have demonstrated the importance of π - π interactions at the aromatic surface in the sorption of hydrophobic organic chemicals, such as PCBs, to aromatic-carbon based materials.^[51-53] In Addition, PCB 126 is a planar molecule which allows it to closely approach the approach the sorption sites of the adsorbent material and form favorable π -cloud interaction between the aromatic groups in the adsorbent and the PCB aromatic rings.^[54,55] Given the additional aromatic groups present in CMA and QMA in comparison to DVB, the binding isotherms indicate that the presence of the acrylated polyphenol groups enhance the binding of PCB 126.

Table 7-2 Langmuir binding constants for the binding isotherm of PCB 126 for the core-shell MNP systems synthesized (n = 9 independent samples). Confidence Intervals obtained from nonlinear regression using GraphPsd Prism

MNP system	B _{max} (mg g ⁻¹)	95 % CI	K _D (nM)	95 % CI	R ²
Sty CMA MNPs_5%_6h	172.8	167.6 to 178.6	2.13	2.03 to 2.24	0.998
Sty CMA MNPs_5%_12h	211.1	204.9 to 218.0	0.77	0.72 to 0.82	0.998
Sty CMA MNPs_5%_24h	223.7	211.0 to 240.7	0.27	0.25 to 0.30	0.992
Sty CMA MNPs_10%_24h	201.7	197.5 to 206.3	0.61	0.60 to 0.62	0.998
Sty QMA MNPs_5%_6h	138.3	131.4 to 146.9	2.00	1.87 to 2.16	0.978
Sty QMA MNPs_5%_12h	237.2	200.2 to 249.0	1.59	1.38 to 1.88	0.998
Sty QMA MNPs_5%_24h	207.6	206.0 to 209.3	0.19	0.18 to 0.20	0.994
Sty QMA MNPs_10%_24h	204.6	203.4 to 205.8	0.63	0.62 to 0.63	0.997
Sty DVB MNPs_5%_6h	145.1	137.4 to 154.8	5.03	4.58 to 5.63	0.997
Sty DVB MNPs_5%_12h	167.9	152.7 to 190.2	4.77	4.04 to 5.99	0.992
Sty DVB MNPs_5%_24h	155.2	147.3 to 165.0	2.99	2.74 to 3.34	0.995

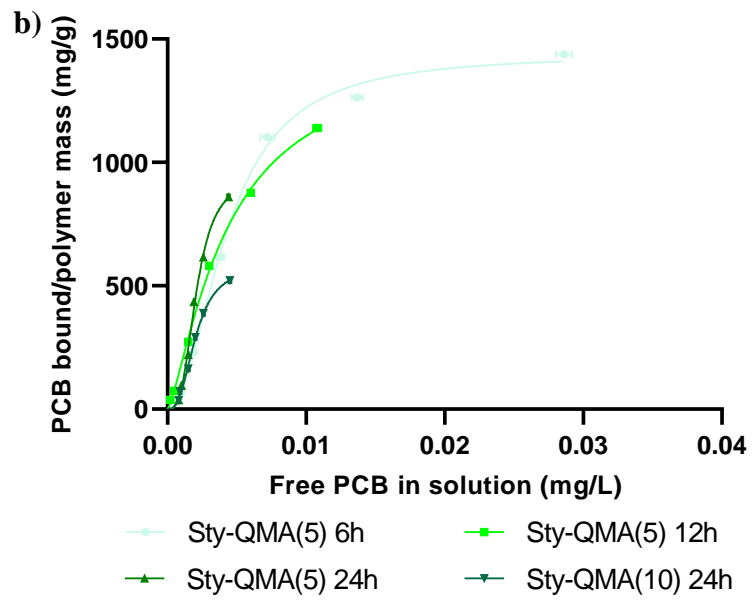
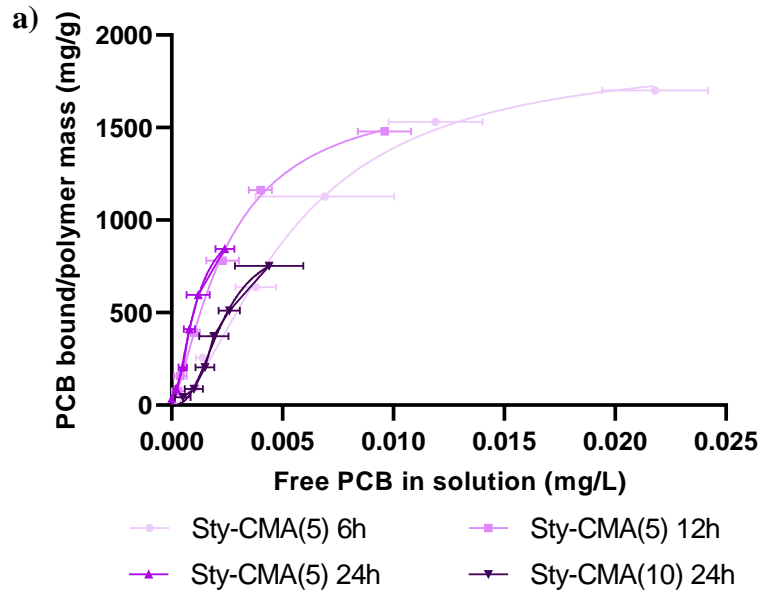
The maximum binding capacity for all the core-shell MNP systems can be seen in Table 7-2. The variation in the maximum capacity of the Sty DVB MNPs, with 5 mol% of initial crosslinker loading, remains relatively constant as the ATRP reaction increases, as seen from the confidence intervals. This behavior is the same for both the Sty CMA MNPs and the QMA MNPs, with 5 mol% of initial functional monomer loading. Focusing on the 5% initial loading after 24h of ATRP reaction, the confidence intervals obtained from a nonlinear regression in GraphPad Prism, indicate that the value for B_{max} for the Sty DVB MNPs (155.2 mg g⁻¹) is significantly lower than that for the Sty QMA MNPs (207.6 mg g⁻¹) and Sty CMA MNPs (223.7 mg g⁻¹). Again, this result suggests that the presence of the additional aromatic moieties in both the CMA and QMA allow for greater binding sites based on formation of π - π interactions at the surface with the PCB molecules. Maximum capacities for engineered magnetic nanomaterials and plastics have been reported for use in adsorption of organic pollutants in agreement with the values shown in Table 2.^[20,56-58] Likewise, the obtained values for B_{max} are also similar to those previously reported for

some carbon-based materials, yet still a couple orders of magnitude lower than activated carbon.^[56,59-61] Once the initial functional monomer molar% increased from 5% to 10%, there was no significant change on the binding capacity of Sty CMA MNPs or Sty QMA MNPs, meaning that at the conditions studied, there is no significant effect on the binding capacity of the system.

The Langmuir adsorption coefficients obtained for the Sty CMA MNPs and Sty QMA MNPs range from 0.19 nM to 2.19 nM, all which are smaller than those obtained for the Sty DVB MNPs (5.03 nM at 2 hour, 4.77 nM at 6h and 2.99 nM at 24 h). These smaller K_D values indicate greater binding affinities of the CMA and QMA systems for PCB 126. Once again, the core-shell systems containing the acrylated polyphenol moieties are shown to enhance the binding affinity for PCB 126. This difference in affinity could be based on structural differences of the polymer shell formed with the DVB versus the CMA/QMA functional monomers. The accepted structure-binding relationships for PCBs in protein and antibodies has been explained as a docking mechanisms which is can be highly selective.^[62] The presence of different side groups around the docking site have the ability to allow or impede the binding to occur. Extrapolating this to the core-shell MNPs, the CMA and QMA contain other functional groups within their molecular structure that could be aiding in the creation of better or higher affinity binding sites for PCB 126. Still, it is important to highlight here that the Langmuir adsorption coefficients obtained for all the synthesized MNPs are in the same order of magnitude as the binding affinity of the monoclonal antibody S2B1 presents for PCB126 (2.5 ± 0.01 nM), which demonstrates the high affinity the core-shell MNPs possess for this contaminant.^[63] Moreover, these K_D values are all lower than reported values in literature for the adsorption of PCB 126 by activated carbon

(6.12 nM), the most used adsorbent in water remediation for non-specific adsorption of organic contaminants, and micron sized charcoal (15.2 nM), another commonly used material for environmental remediation.^[59,64,65]

Looking more closely at the effect of reaction time on B_{\max} it is seen that for all the systems (Sty CMA MNPs, Sty QMA MNPs and Sty DVB MNPs) there is an increase in the maximum binding capacity of the systems with increasing reaction time. As reaction time increases, so does the growth of the polymer shell on the nanoparticle, resulting in particles having a greater fraction of their mass being the polymer coating, which in turn leads to a higher binding capacity. However, as the ATRP reaction time increases, it appears that the binding affinity for PCB 126 also increases (lower K_D values). Since we expect the composition of the polymer coating to not change significantly as the reaction process occurs, the observed increase in K_D with increasing reaction time for each system could be an artifact of the model fit where the total mass of the system was used to normalizing the data. To examine this further, the binding isotherms were also analyzed on a per polymer shell mass basis in the following.



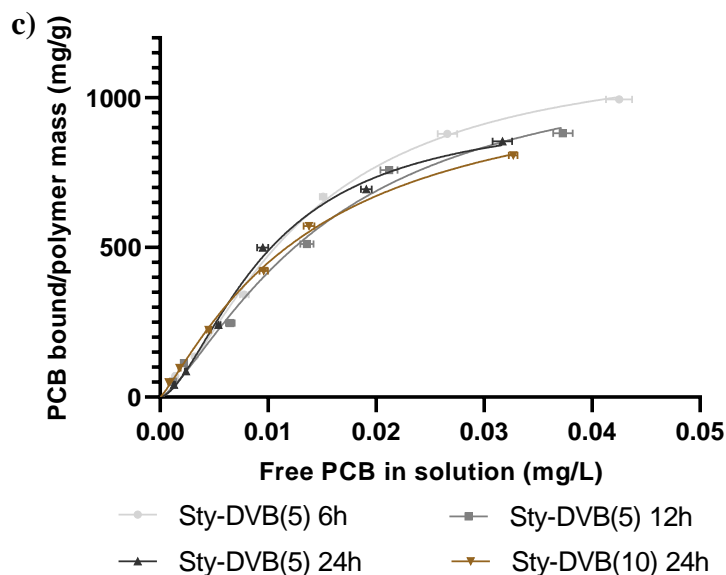


Figure 7-7 Adsorption isotherms for PCB 126 of the core-shell MNP systems in terms of polymer mass at room temperature. A) Sty CMA MNP systems, b) Sty QMA MNPs systems and c) Sty DVB MNPs systems. PCB 126 initial concentrations from 0.005 – 0.1 ppm fitted using the Langmuir model.

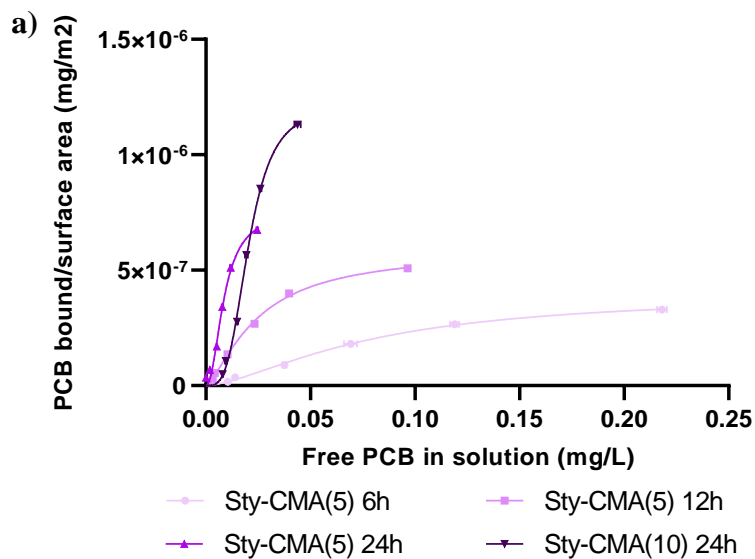
Table 7-3 Langmuir binding constants for the binding isotherm of PCB 126 for the core-shell MNP systems synthesized in terms of polymer mass (n = 9 independent samples). Confidence Intervals obtained from nonlinear regression using GraphPad Prism

MNP system	Bmax (mg g ⁻¹)	95 % CI	KD (nM)	95 % CI	R ²
Sty CMA MNPs_5%_6h	1902	1802 to 2025	1.67	1.52 to 1.88	0.996
Sty CMA MNPs_5%_12h	1728	1651 to 1818	0.77	1.70 to 0.85	0.998
Sty CMA MNPs_5%_24h	1048	941 to 1233	0.32	0.28 to 0.41	0.987
Sty CMA MNPs_10%_24h	880	811 to 982	0.69	0.64 to 0.78	0.994
Sty QMA MNPs_5%_6h	1438	1397 to 1484	1.31	1.24 to 1.39	0.997
Sty QMA MNPs_5%_12h	1471	1471 to 1587	1.33	1.18 to 1.53	0.999
Sty QMA MNPs_5%_24h	932	888 to 984	0.63	0.61 to 0.67	0.996
Sty QMA MNPs_10%_24h	580	556 to 608	0.62	0.59 to 0.65	0.997
Sty DVB MNPs_5%_6h	1170	1099 to 1264	3.97	3.56 to 4.56	0.997
Sty DVB MNPs_5%_12h	1169	1113 to 1422	4.01	3.54 to 5.57	0.991
Sty DVB MNPs_5%_24h	967	899 to 1063	3.03	2.67 to 3.58	0.996
Sty DVB MNPs_10%_24h	1485	1236 to 1947	3.91	3.18 to 4.85	0.998

Figure 7-7 shows the binding results normalized to the polymer mass of each system as reaction time increases. By normalizing the binding data to polymer mass, it is seen that the binding isotherms for the nanoparticle systems significantly collapse onto each other. By normalizing to the polymer shell mass, it can be seen that the maximum binding capacity of each nanoparticle system becomes more similar to each other. In Figure 7-7c, it can be seen that for the Sty DVB MNPs at the different reaction times the Langmuir curves in fact collapse onto each other and the B_{\max} for each reaction time falls within the confidence intervals of each other, as seen in Table 7-3, meaning there is no significant difference in their values. The same effect on K_D values is observed, where they all are in error of each other (as seen in Table 7-3 in the confidence intervals). In this specific case, the Sty DVB MNPs appear to bind less than the Sty CMA MNPs and Sty QMA MNPs, as observed in the values of free PCB in solution on Figure 7-7. Due to their lower affinity, the binding isotherm data spans a larger range of free concentrations resulting in the Langmuir model being able to fit a larger range of data than in the CMA and QMA systems and thus representing the system with a high level of confidence. In contrast, some of the data in the Sty CMA MNPs and Sty QMA MNPs has a much smaller range for the concentration of free PCB in solution, resulting in the Langmuir model fit and prediction of B_{\max} and K_D resulting from a limited range of concentrations, which might not accurately represent the system's behavior. For both, Sty CMA MNPs and Sty QMA MNPs, the amount of PCB bound increases as reaction time increases, reducing the range of free PCB in solution and further impacting the accuracy of the model.

To further examine the binding isotherms, the data was normalized to nanoparticle surface area. The surface area of each systems at the different reaction times was calculated

assuming a perfect sphere and additive densities of the nanoparticle components (iron oxide nanoparticle core and polymer shell constituents – Sty, DVB, CMA, and QMA). Figure 7-8 presents the Langmuir isotherms for the styrene nanoparticle systems based on surface area. Here, the curves for each nanoparticle system are visibly different from each other, suggesting that as reaction time increases so does the amount of PCB bound per surface area. This apparent increase in affinity and capacity suggest that the adsorption of PCB 126 to the styrene-based nanoparticles is not just an effect of surface area, given that the total surface area of the particles (seen in Table 7-4) decreases with increasing reaction time. Again, the phenomenon occurring during the binding studies appears to consist of more than just surface interactions between the nanoparticles and the PCB 126 molecules.



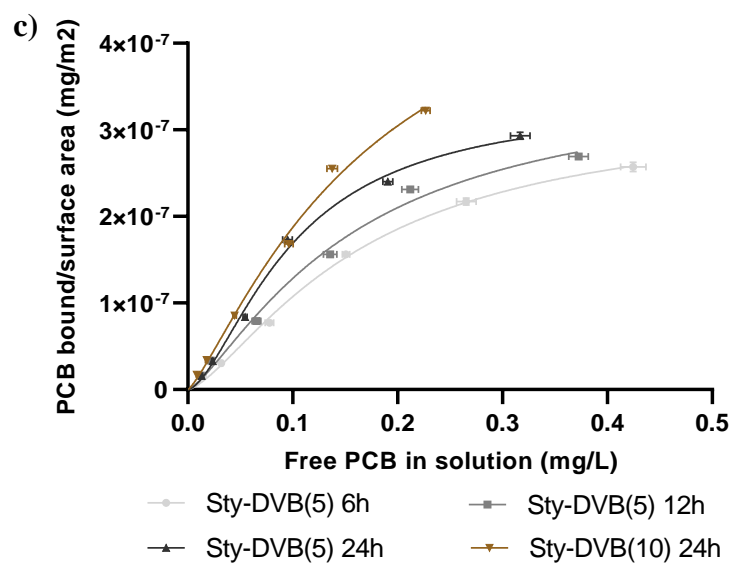
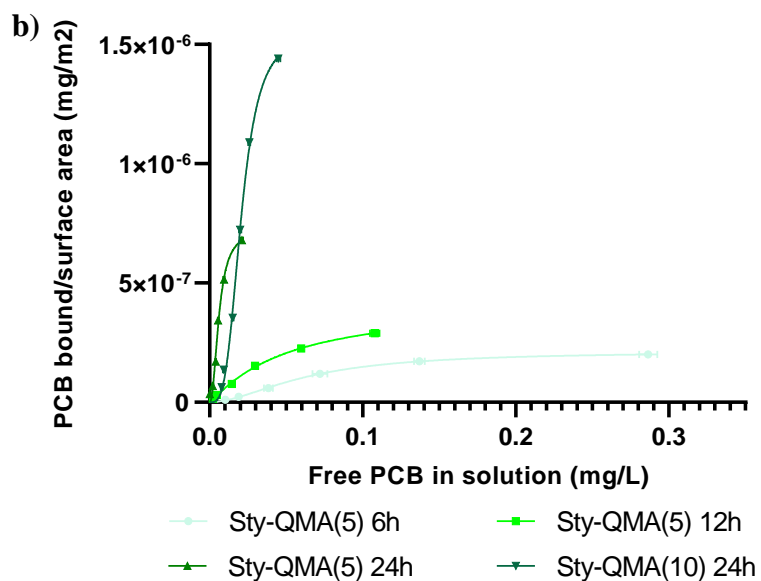


Figure 7-8 Adsorption isotherms for PCB 126 of the core-shell MNP systems in terms of surface area at room temperature. A) Sty CMA MNP systems, b) Sty QMA MNPs systems and c) Sty DVB MNPs systems. PCB 126 initial concentrations from 0.005 – 0.1 ppm fitted using the Langmuir model.

Table 7-4 Langmuir binding constants for the binding isotherm of PCB 126 for the core-shell MNP systems synthesized (n = 9 independent samples), in terms of surface area. Confidence Intervals obtained from nonlinear regression using GraphPad Prism

MNP system	Bmax (mg m ⁻²)	95 % CI	KD (nM)	95 % CI	R ²	Total SA (m ²)
Sty CMA MNPs_5%_6h	3.98E-07	3.75E-07 to 4.28E-07	0.504	0.457 to 0.568	0.998	4.75E+04
Sty CMA MNPs_5%_12h	5.87E-07	5.61E-07 to 6.17E-07	0.213	0.196 to 0.236	0.998	3.56E+04
Sty CMA MNPs_5%_24h	7.51E-07	6.87E-07 to 8.54E-07	0.092	0.075 to 0.075	0.990	2.89E+04
Sty CMA MNPs_10%_24h	1.21E-06	1.17E-06 to 1.25E-06	0.368	0.358 to 0.379	0.998	1.70E+04
Sty QMA MNPs_5%_6h	2.14E-07	2.10E-07 to 2.19E-07	0.272	0.546 to 0.546	0.999	7.15E+04
Sty QMA MNPs_5%_12h	4.17E-07	3.81E-07 to 4.67E-07	0.254	0.211 to 0.323	0.996	6.14E+04
Sty QMA MNPs_5%_24h	7.21E-07	6.80E-07 to 7.72E-07	0.065	0.060 to 0.072	0.993	2.88E+04
Sty QMA MNPs_10%_24h	1.54E-06	1.49E-06 to 1.61E-06	0.475	0.461 to 0.492	0.997	1.33E+04
Sty DVB MNPs_5%_6h	3.24E-07	3.00E-07 to 3.57E-07	1.117	0.979 to 1.329	0.997	4.47E+04
Sty DVB MNPs_5%_12h	3.59E-07	3.13E-07 to 4.44E-07	1.017	0.804 to 1.509	0.992	4.66E+04
Sty DVB MNPs_5%_24h	3.34E-07	3.09E-07 to 3.70E-07	0.648	0.567 to 0.777	0.995	4.67E+04
Sty DVB MNPs_10%_24h	5.56E-07	4.45E-07 to 8.34E-07	1.096	0.767 to 2.158	0.994	4.80E+04

Our group recently developed nanoadsorbent materials containing these functional acrylated monomers, CMA and QMA, as part of a core-shell structure to be used in environmental remediation.^[41] These core-shell MNPs were developed in a similar manner as to those described in this paper, with the exception of the use poly(ethylene glycol) 400 dimethacrylate (PEG400DMA) as part of the polymer shell, instead of styrene. The CMA and QMA containing MNP systems were synthesized for a period of 24h and an initial loading of 10 mol%, resulting in magnetic core-shell nanoparticles of uniform distribution with a polymer shell of roughly 10% of the total weight. Three systems were produced: CMA MNPs, QMA MNPs, and PEG MNPs (where the shell consisted of only a PEG400DMA). The binding capacity of these MNPs was also evaluated for PCB 126 under equilibrium conditions. The values obtained for the maximum binding capacity for the CMA MNPs and QMA MNPs was of 1.06 mg g⁻¹, and of 1.91 mg g⁻¹ for the PEG MNPs. Comparing these values to those presented in Table 2 for the styrene based MNPs on total mass, it becomes clear that by using a hydrophobic monomer like styrene in place of PEG400DMA, the maximum binding capacity of the core-shell MNPs was drastically

increased. Styrene is an organic monomer that can produce polystyrene polymers with a hydrophobic surface and high surface area per gram of material when crosslinked with other hydrophobic molecules like DVB or, in this case CMA or QMA.^[26,27,52,68] These styrene based polymers have shown to be particularly useful for the adsorption of molecules with aromatic rings because of the strong π - π interactions they can have. The Langmuir adsorption coefficients obtained for the CMA MNPs, QMA MNPs and PEG MNPs are 2.72 nM, 5.88 nM, and 8.42 nM, respectively. For the Styrene based systems synthesized under the same conditions (5 mol% initial loading and 24 h ATRP reaction), the K_D values are 0.27 nM, 0.19 nM and 2.99 nM for the Sty CMA MNPs, Sty QMA MNPs and Sty DVB MNPs respectively. Again, the values obtained indicate higher binding affinity for the styrene based MNPs compared to the PEG based MNPs further demonstrating the importance of the polymer shell composition for the targeting of PCB 126 removal. The use of a hydrophobic, aromatic rich molecule as styrene within the polymeric shell provides more sites for π - π interactions to occur between the MNP surface and the PCB molecules. This in turn, increases the maximum binding capacity of the MNP system for PCB 126. These results provide a strong rationale for the use of our magnetic core-shell nanoparticle systems to be used as high affinity adsorbents in the environmental remediation of specific harmful contaminants.

7.5 Conclusion

This study reports the successful synthesis of core-shell magnetic nanoparticles (MNPs) using surface initiated atom transfer radical polymerization (SI-ATRP). Herein, the

magnetic core is comprised of iron oxide nanoparticles which endow the MNP systems with magnetic decantation capabilities. The polymeric shell is composed by styrene and a crosslinker. Three different crosslinkers were used, all containing additional aromatic ring moieties to enhance pollutant binding capacity. Two of them were acrylated plant derived polyphenols, curcumin multiacrylate (CMA) and quercetin multiacrylate (QMA), and the third was divinylbenzene (DVB). The effect of ATRP reaction time was studied on the properties of the MNPs. Equilibrium binding studies were conducted at six different PCB 126 concentration, and binding isotherms were obtained. The Langmuir model was used to obtain the binding coefficients and the maximum binding capacity of the core-shell MNPs. The binding isotherms obtained showed that the CMA and QMA containing MNPs presented higher binding affinities and capacities. Despite this difference, all MNPs have higher binding affinities for PCB 126 than carbonaceous materials, like activated carbon and graphene oxide, the most widely used adsorption materials for water remediation today. And the binding affinities for all the Sty CMA MNPs and Sty QMA MNPs were similar to those observed for antibodies. The increase in ATRP reaction time increases the binding capacity of the MNPs given that as the polymer shell grows so does the available sites for π - π interaction to occur with the PCB molecules. The effect of increasing ATRP reaction time on the binding affinity and capacity of the MNPs for PCB 126 was further examined, and specifically, the data was analyzed for different normalization factors (total mass, polymer shell mass and surface area) to fit the Langmuir model. These results suggest the phenomenon occurring during the binding studies is not limited to a surface interaction between the nanoparticles and the PCB 126 molecules in solution. Finally, the importance of the polymeric shell composition was demonstrated by comparing the Langmuir

coefficients obtained in this work to previous work done by our group with similar materials. It was seen that the use of a hydrophobic, aromatic rich molecule like styrene within the polymeric shell provides more sites for π - π interactions to occur between the MNP surface and the PCB molecules, increasing the binding capacity almost 200 fold in some cases and increasing the binding affinity of the MNPs as well. Overall, we have developed magnetic core-shell nanoparticle systems with high affinities for PCBs in aqueous media with tunable shell thickness for optimal affinity, that can be magnetically decanted from solution with the use of a static magnetic field, and has the potential to be regenerated upon the exposure to an alternating magnetic field, for their use as nanoadsorbents in the environmental remediation of specific harmful contaminants.

CHAPTER 8. CONCLUSIONS

In this dissertation, the development of magnetic nanocomposite materials using plant derived acrylated polyphenols as crosslinker, i.e. curcumin multiacrylate (CMA) and quercetin multiacrylate (QMA), has been investigated for their use as adsorbents for organic contaminant in water and wastewater treatment. The binding capacity and affinity of these nanocomposite materials was evaluated using polychlorinated biphenyl (PCBs), as model organic pollutant, given their prevalence in environmental waters worldwide.

In **Chapter 3**, the development of core-shell magnetic nanoparticles through surface initiated atom transfer radical polymerization produced materials with high affinity for PCB 126, capable of outcompeting activated carbon in adsorption of this specific contaminant. The presence of the polyphenol functionalities, CMA or QMA, within the nanocomposite appeared to enhance the binding affinity for PCB 126. In **Chapter 4**, magnetic nanocomposite microparticles (MNMs) were developed with the same polymer compositions as the nanoparticles in Chapter 3. The incorporation of the π -electron rich sites from CMA and QMA proved to enhance the pollutant binding capacity for PCB 126. The presence of the iron oxide magnetic nanoparticles (IO MNPs) within the systems allow for magnetic decantation capabilities in solution and do not adversely affect the binding properties of the MNMs. The overall binding affinity of the MNMs for PCB 126 was higher than that of the core-shell systems developed in Chapter 3, suggesting a the micron-sized MNMs offered a unique advantage for their use in the environment: an easier manipulation and control of their fate in comparison to nanoparticles.

In **Chapter 5**, the development of an alternating magnetic field (AMF) modulated binding in magnetic nanocomposites as a low energy regeneration strategy in environmental remediation was proposed. An optimal regeneration strategy for adsorption materials used in environmental remediation completely desorbs the pollutant from the material, does not modify its initial properties of the adsorbent (chemical/ physical), allows for complete recovery of the contaminant, requires low energy consumption, has short regeneration times, does not generate harmful byproducts, and is easy to operate. Using the MNMs developed in Chapter 4, the exposure of 5 minutes to an AMF operating at 55 kA m⁻¹ and a frequency of 300 kHz to the spent MNMs (used in the binding of PCB 126), was shown to trigger the desorption of the bound PCB 126 in isooctane or 99:1 DI water to ethanol solvent. Upon exposure in isooctane, over 95% of the bound PCB 126 was released, allowing for the regeneration and reuse of the MNMs. The proposed AMF regeneration strategy allows for, almost, a complete desorption of the pollutant, complete and easy recovery of the adsorbent thanks to its ability to be magnetically separated, has a short regeneration time of only 5 minutes, does not generate harmful byproducts, and reduces operation costs by eliminating the need to heat the solution to high temperatures as is the case of traditional regeneration method used. The low energy regeneration strategy presented here can be readily extended to other contaminants and magnetic adsorbents, providing an efficient and high performance recycling technology with the potential to be used *in situ* or *ex situ*.

To demonstrate the applicability of the magnetic nanocomposites for the sorption of contaminant water treatment, the effect of environmental factors on the binding for PCB 126 was studied in **Chapter 6**. The effect of ionic strength, water hardness and solution

pH were evaluated. Both ionic strength and water hardness were shown to have minimal effects on the adsorption of the MNMs towards PCB 126 in the studied range. However, the solution pH did affect the binding of the MNMs, resulting in a decreased in binding for PCB 126 as the pH increased from 6.5 to 8.5. These results indicate that the developed MNMs can be used as magnetic adsorbents for polychlorinated biphenyls in groundwater and surface water remediation provided solution pH is taken into consideration and controlled.

In **Chapter 7**, a series of core-shell magnetic nanoparticles (MNPs) were developed via surface initiated atom transfer radical polymerization where the polymer shell consisted of styrene and the acrylated polyphenol moieties, CMA or QMA. The effect of reaction time on the binding of the core-shell MNPs was studied at two different initial acrylated polyphenol compositions. All the developed MNPs containing CMA or QMA exhibited an enhancement in binding affinity and capacity for PCB 126, and their binding affinities were higher than those of commonly used water remediation used carbonaceous materials, like activated carbon and graphene oxide, for PCB 126. The effect of increasing reaction time on the binding capacity of MNPs was not significant at the conditions studied. However, the binding affinity MNPs for PCB 126, which increased as the ATRP reaction time increased, suggesting binding affinity is dependent on the surface area of the core-shell MNPs, so as the polymer shell grows, so does the available sites for π - π interaction to occur. When initial acrylated polyphenol compositions were increased, a decrease in the binding affinity was observed at the same reaction time. This appears to indicate the existence of an optimal shell thickness at which the binding affinity is maximized, and once the shell thickness increases beyond that point, binding will be negatively affected. Finally,

by means of comparison to all previously developed core-shell MNP systems in Chapter 1, it was seen that the use of a hydrophobic, aromatic rich molecule like styrene within the polymeric shell provides more sites for π - π interactions to occur between the MNP surface and the PCB molecules, increasing the binding capacity almost 200 fold in some cases, and increasing the binding affinity of the MNPs as well.

Overall, we have developed magnetic nanocomposite systems for water remediation that can potentially revolutionize the environmental remediation approaches currently used for contaminated water sources. The polymer composition of the nanocomposite can be tuned to optimize binding capacity and affinity, and is enhanced by the incorporation of plant-derived acrylated polyphenols, CMA or QMA., obtaining higher affinities for PCB 126 than currently used remediation materials. These nanocomposites can be easily separated from the water source via magnetic decantation, offering an ease of application. Furthermore, the nanocomposites can be regenerated upon a short exposure to an alternating magnetic field for their further re-use, providing a green, reusable, and sustainable remediation technique that can be easily used *in situ* and *ex situ* with minimal or no disruptions to the environment. Given the binding affinity of the nanomaterials for PCB is based upon π - π interactions, these materials can be further explored as capture agents for other organic contaminants in the environment.

APPENDICES

APPENDIX 1. A NOVEL MAGNETIC CORE-SHELL NANOPARTICLES FOR THE REMOVAL OF POLYCHLORINATED BIPHENYLS FROM CONTAMINATED WATER SOURCES – SUPPLEMENTARY INFORMATION

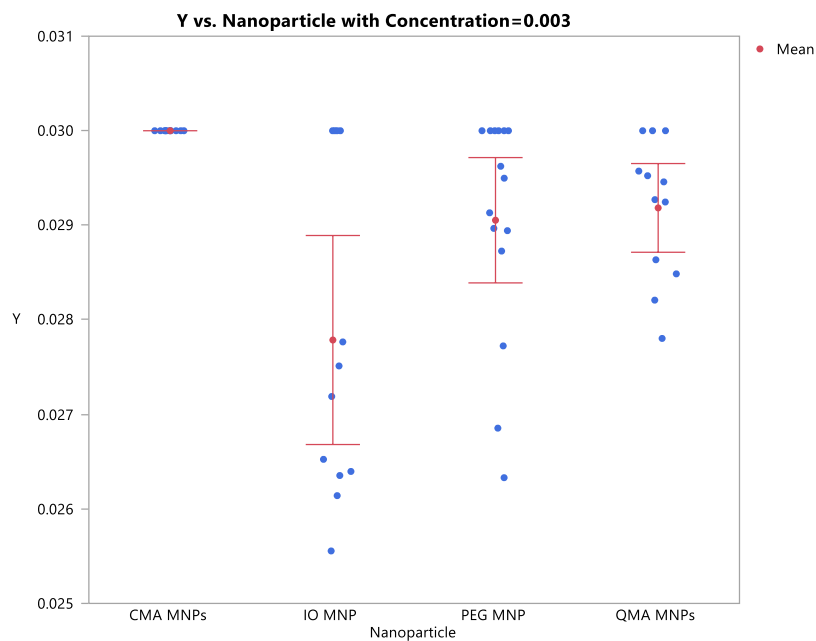


Figure A1-S1. One-way Analysis of Y (PCB bound/total mass (ug mg^{-1})) By Nanoparticle organized by system-initial PCB concentration = 0.003 ppm with p-values < 0.0002

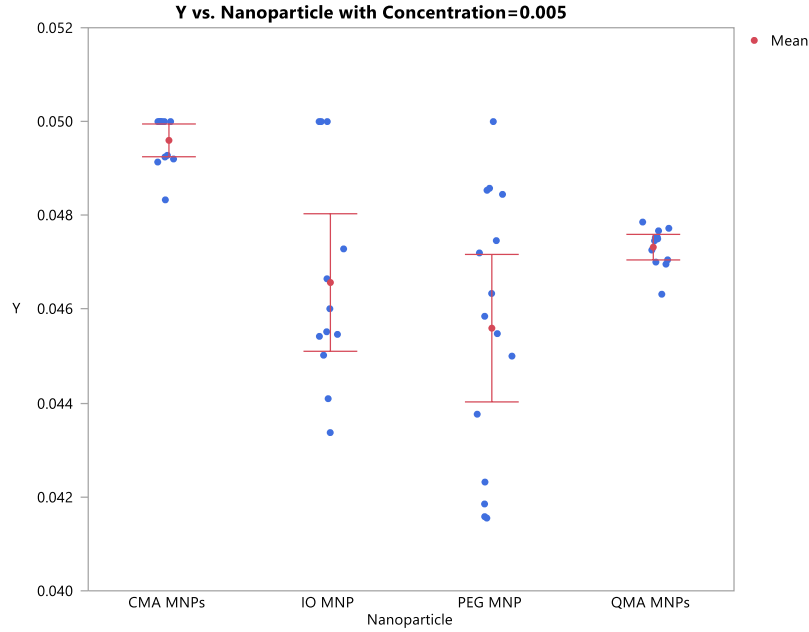


Figure A1-S2. One-way Analysis of Y (PCB bound/total mass (ug mg^{-1})) By Nanoparticle Organized by system-initial PCB concentration = 0.003 ppm with p-values < 0.0001

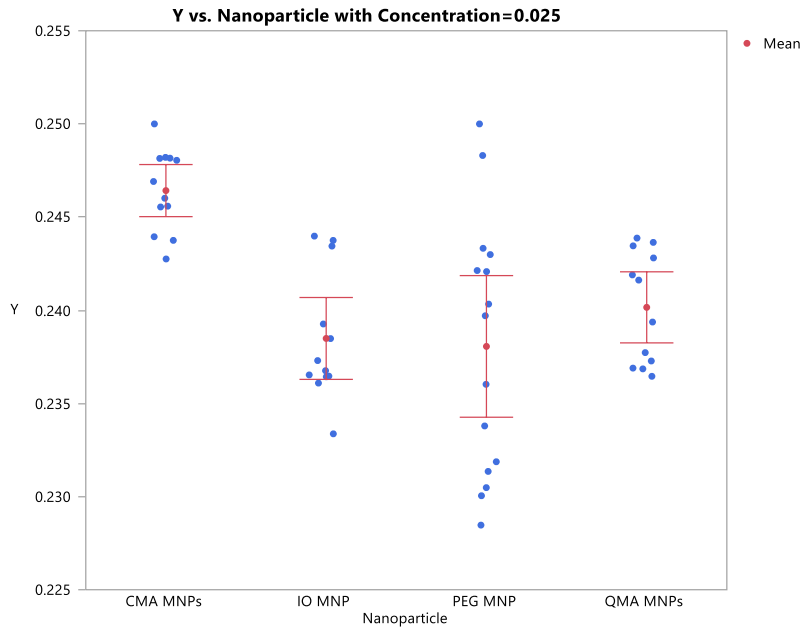


Figure A1-S3. One-way Analysis of Y=(PCB bound/total mass (ug mg^{-1})) By Nanoparticle Organized by system-initial PCB concentration = 0.01 ppm with p-values < 0.0001

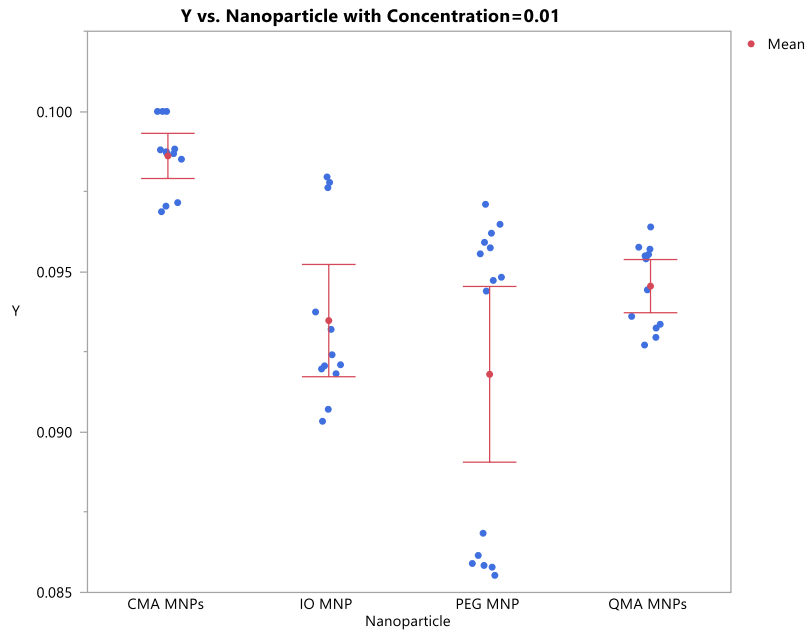


Figure A1-S4. One-way Analysis of Y (PCB bound/total mass (ug mg⁻¹)) By Nanoparticle Organized by system-initial PCB concentration = 0.025 ppm with p-values < 0.0001

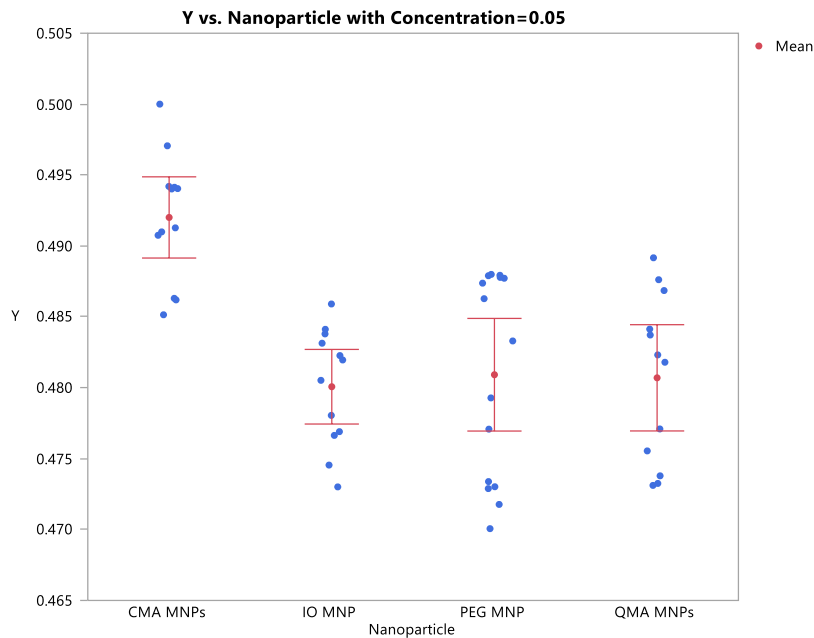


Figure A1-S5. One-way Analysis of Y (PCB bound/total mass (ug mg⁻¹)) By Nanoparticle Organized by system-initial PCB concentration = 0.05 ppm with p-values < 0.0001

APPENDIX 2. SYNTHESIS OF MAGNETIC NANOCOMPOSITE MATERIALS FOR BINDING OF CHLORINATED ORGANICS IN CONTAMINATED WATER SOURCES – SUPPLEMENTARY INFORMATION

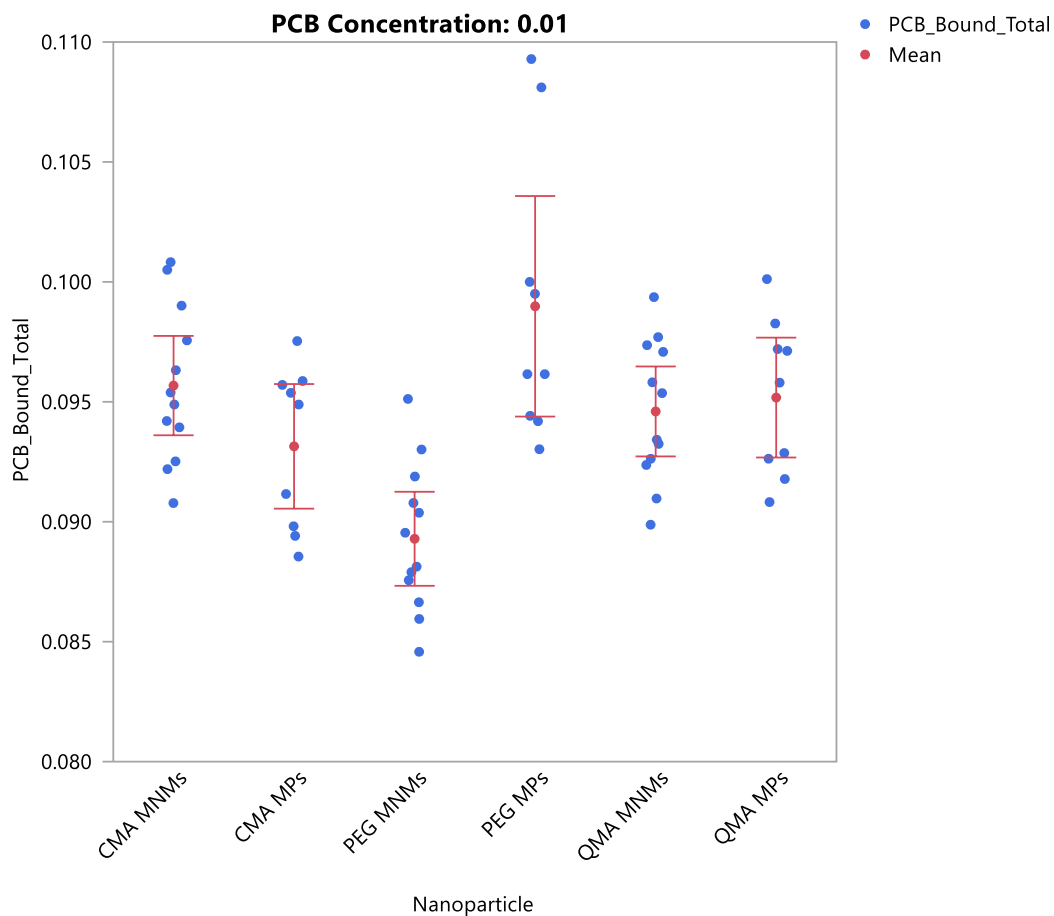


FIGURE A2-S1 One-way Analysis of Y (PCB bound/total mass (ug mg⁻¹) by microparticle system organized by system. Initial PCB concentration = 0.01 ppm

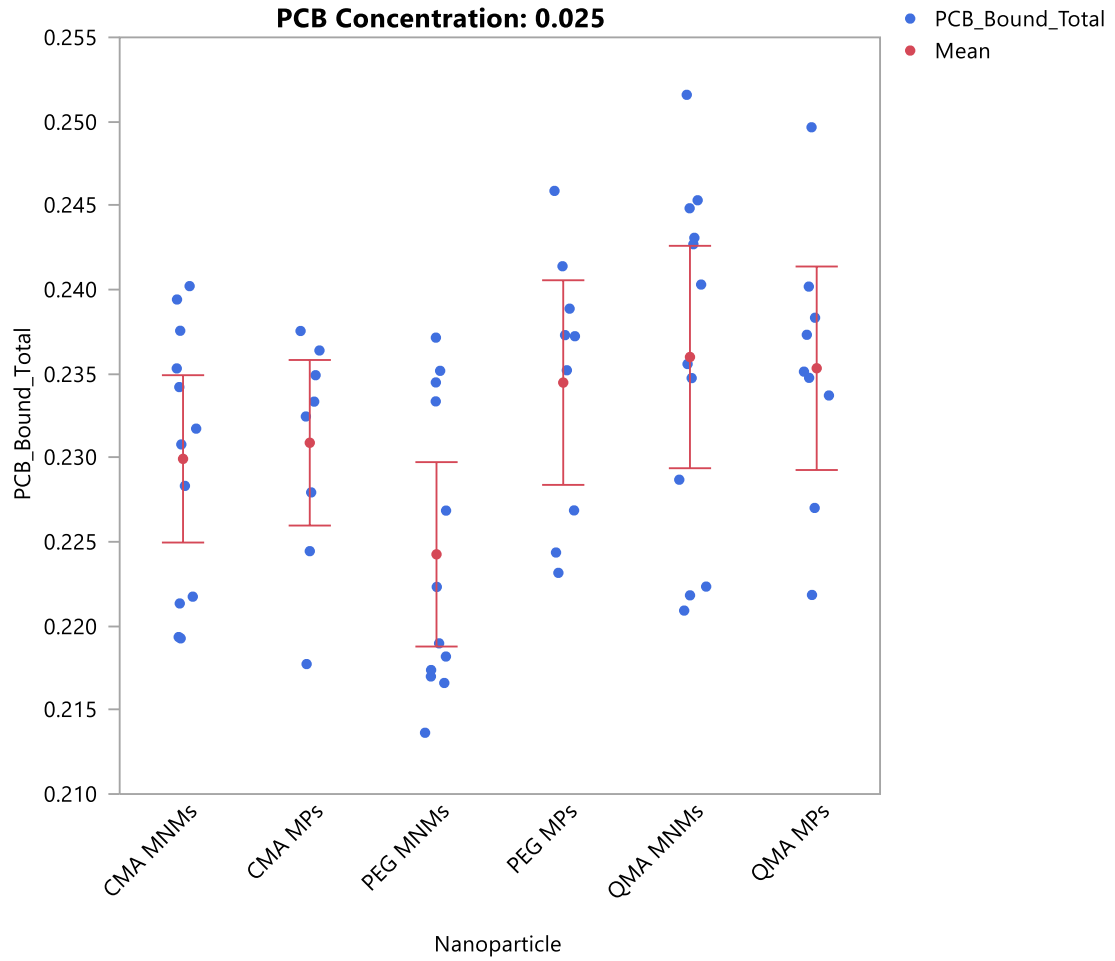


FIGURE A2-S2 One-way Analysis of Y (PCB bound/total mass (ug mg⁻¹) by microparticle system organized by system. Initial PCB concentration = 0.025 ppm

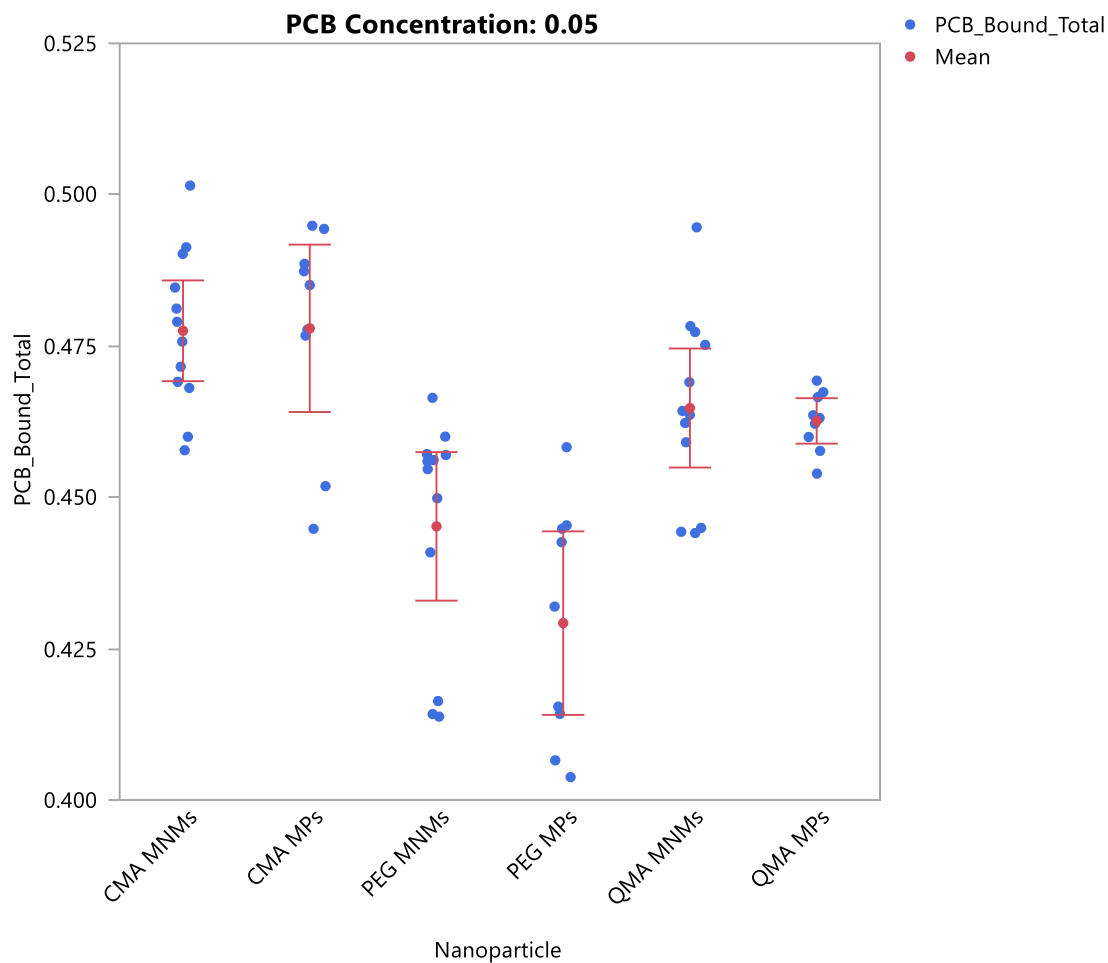


FIGURE A2-S3 One-way Analysis of Y (PCB bound/total mass ($\mu\text{g mg}^{-1}$) by microparticle system organized by system. Initial PCB concentration = 0.05 ppm

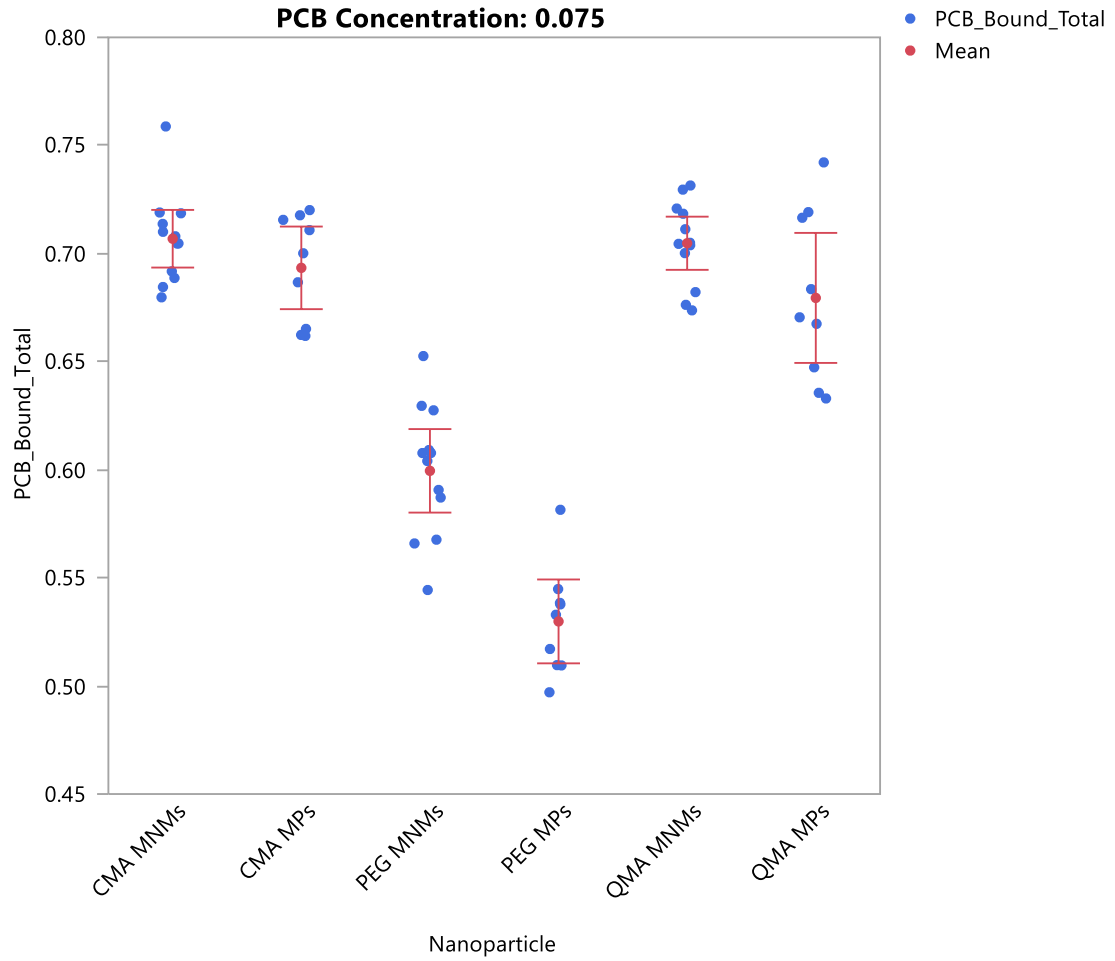


FIGURE A2-S4 One-way Analysis of Y (PCB bound/total mass ($\mu\text{g mg}^{-1}$) by nanoparticle system organized by system. Initial PCB concentration = 0.075 ppm

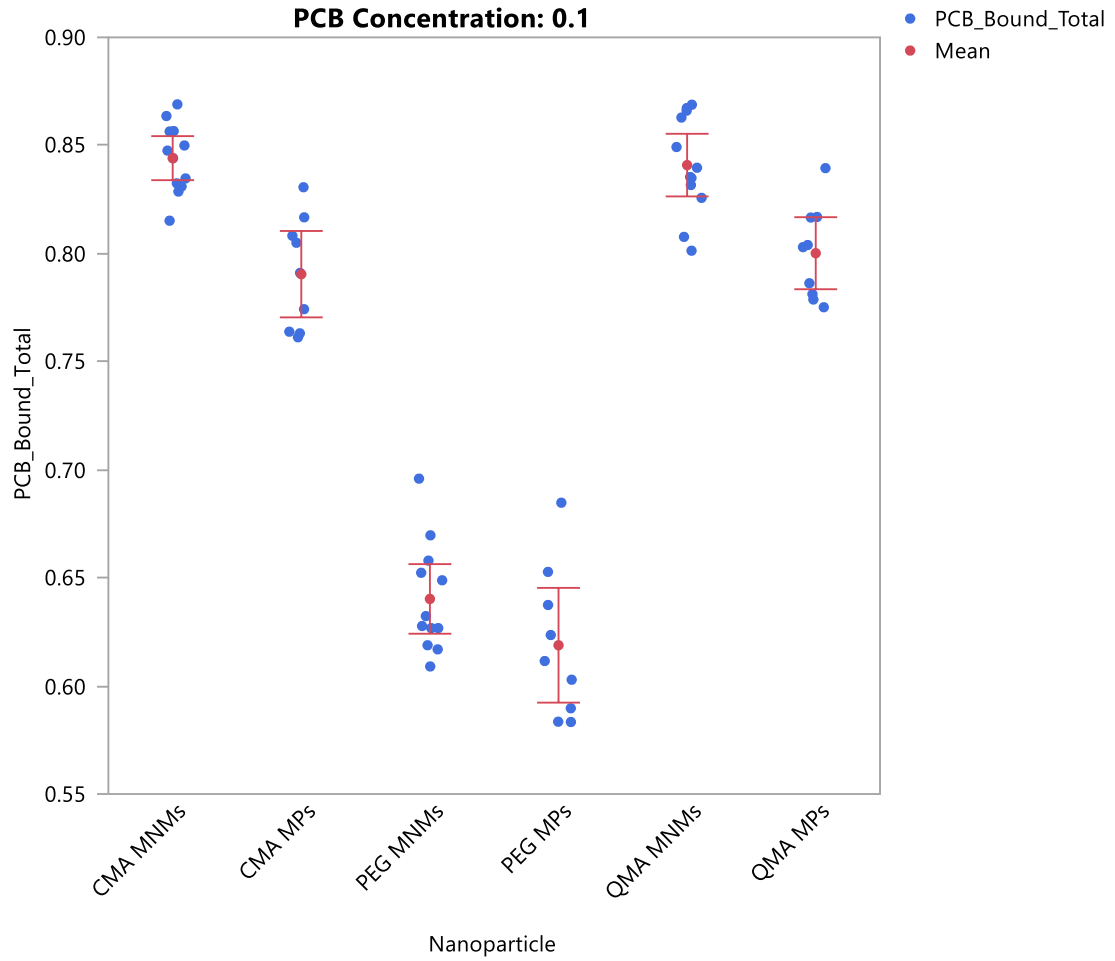


FIGURE A2-S5 One-way Analysis of Y (PCB bound/total mass ($\mu\text{g mg}^{-1}$) by nanoparticle system organized by system. Initial PCB concentration = 0.1 ppm

REFERENCES

- [1.] UNW-DPAC, UN Report: Water and industry in the green economy: Information brief, 2011.
- [2.] UNEP. *Natural solutions for water security. Water and Biodiversity*. International day for biological diversity – Convention on Biological Diversity. May 22, 2013
- [3.] UN. World Water Development Report. World Water Assessment Programme, 2016.
- [4.] K. Noguera-Oviedo, D. S. Aga, Lessons Learned from more than Two Decades of Research on Emerging Contaminants in the Environment *J. Hazard. Mater.* **2016**
- [5.] F. Derbyshire, M. Jagtoyen, R. Rao, A. Martin-Gullon, E. Grulke, in *Chemistry and Physics of Carbon*, Vol. 27 (Ed: L.R. Radovic), Mercel Dekker, New York, USA, **2001**, Ch. 1
- [6.] R. Jing, S. Fusi, B.V. Kjellerup, *Front. Environ. Sci.* **2018**, 6, 79
- [7.] R.C. Bansal, J.B. Donnet, F. Stoeckli. *Active Carbon*. Mercel Dekker, New York, USA **1988**
- [8.] FEECO International – A look at activated carbon thermal regeneration.
<https://feeco.com/a-look-at-activated-carbon-thermal-regeneration/> accessed 04/19
- [9.] Guerra, F.D., Attia, M.A., Whitehead, D.C. and Alexis, F. *Molecules*. **2018**, 23, 1760-1782
- [10.] World Health Organization. Progress on sanitation and drinking water. 2015 Update and MDG Assessment. Available at:
http://www.unicef.org/publications/index_82419.html
- [11.] T. Masciangioli, X.W. Zhang, *Environ. Sci. Technol.* **2003**, 37, 102A-108A
- [12.] X. Qu, J. Brame, Q. Li, P.J.J Alvarez, *Acc. Chem. Res.* **2013**, 46, 834-843
- [13.] Zhao Z, Lan J, Li G, Jiang G. Iron-based magnetic nanomaterials on wastewater treatment. In: Reisner, DE, Pradeep T, editors. *Aquananotechnology: Global prospects*. Baton Rouge: CRC Press, **2015**, 265-291
- [14.] Y. Guo, E. Du, *Energy Procedia*, **2012**, 17, 444-449
- [15.] A.S. Adeleye, J.R. Conway, K. Garner, Y. Huang, Y. Su, A.A. Keller, *Chem. Eng. J.* **2016**, 286, 640-662
- [16.] S. Thurm, S. Odenbach, *J. Magn. Magn. Mater.* **2002**, 252, 247-249
- [17.] R. Frimpong, J. Dou, M. Pechan, J.Z. Hilt. *J. Magn. Magn. Mater.* **2010**, 322, 326

- [18.] Q. Zhou, J. Li, M. Wang, D. Zhao. *Crit. Rev. Environ. Sci. Technol.* **2016**, *8*, 7833- 7826
- [19.] S. Thurm, S. Odenbach, J. Magn. *Magn. Mater.* 2002, *252*, 247-249
- [20.] R.E. Rosenweig, J. Magn. *Magn. Mater.* 2002, *252*, 370-374
- [21.] Y.K. Huang, A.A. Keller, *Water Res* **2015**, *80*, 159-168
- [22.] Y. Huang, A.A. Keller, *Sustainable Chem. Eng.* **2013**, *1*, 731-736
- [23.] S.C. Tang, I.M. Lo, *Water Res.* **2013**, *47*, 2613-2632
- [24.] J.S. Xu, Y.J. Zhu, *J. Colloid. Interface Sci.* **2012**, *385*, 58-65
- [25.] Z. Geng, Y. Lin , X. Yu, Q. Shen, L. Ma, Z. Li, N. Pan, X. Wang, *J. Mater Chem.* **2012**, *22*, 3527-3535
- [26.] P.S. Ajayan, L. Schadler, P.V. Braun, editors. *Nanocomposite Science and Technology*. Weinheim: Wiley-VCH, **2003**, 239pp
- [27.] S.T. Richardson, T.A. Ternes, *Anal. Chem.* **2014**, *86*, 2813-2848
- [28.] K.C. Jones, P. de Voogt,. *Environ. Pollut.* **1999**, *100*, 209-221
- [29.] V.D. Dang, D.W. Walter, C.M. Lee, *Am. J. Environ. Sci.* **2012**, *8*, 11-15
- [30.] N.B. Hopf, A.M. Ruder, P. Succop, *Sci. Tot. Environ.* **2009**, *407*, 6109-6119
- [31.] P.D. Jepson, et al. *Sci. Rep.* **2016**, *8*, 18573
- [32.] M.D. Mulder, A. Heil, P. Kukucka, J. Kuta, P. Pribylova, R. Prokes, G. Lammel, *Atm. Env.* **2015**, *121*, 66 -74
- [33.] T. Brazova, V. Hanzelova, D. Miklisova, *Parasitol. Res.* **2012**, *111*, 779-786
- [34.] I. Grabowska, *Polish J. Environ. Stud.* **2010**, *1*, 7-13
- [35.] J. Pumarega, M. Gasull, D.H. Lee, T. Lopez, M. Porta, *PLOS ONE*, **2016**, *11*,
- [36.] E. Yang, M. Pavuk, A. Sjodin, M. Lewin, R. Jones, J. Olson, L. Birnbaum, *Sci. Tot. Environ.* **2018**, *637-638*, 881-891
- [37.] H.I. Gomes, C. Dias-Ferreira, A.B. Ribeiro, *Sci. Total. Environ.* **2013**, *445-446*, 237-260
- [38.] E. Schwarts, K.M. Scow, , *Biodegradation*, **2001**, *12*, 201-207
- [39.] G.V. Lowry GV. Nanomaterials for groundwater remediation. In: Weisner MR, Bottero J, editors. *Environmental Nanotechnology*. New York: McGraw Hill Companies, **2007**, 297-336
- [40.] Y. Liu, H. Choi, D. Dionysiou, G.V.Lowry,.*Chem. Mater.* **2005**, *17*, 5315-5322

- [41.] C.R. Patmont, et al. *Integr. Environ. Asses. Manag.* **2015**, *11*, 195-207
- [42.] A. Balasubramani, H.S. Rifai, *Sci. Tot. Environ.* **2018**, *644*, 398-405 (27 AMF)
- [43.] V. S. Tran, H.H. Ngo, W, Guo, J. Zhang, S. Liang, C. Ton-That, X. Zhang, *Bioresource Technol.* **2015**, *182*, 353-363
- [44.] B. Beless, H. Rifi, D.F. Rodrigues, *Environ. Sci. Technol.* **2014**, *48*, 10372-10379
- [45.] M. Bystrzejewski, K. Pyrzyndka, A. Huczko, H. Lange, *Carbon*, **2009**, *47*, 1201-1206
- [46.] M.P. Ormad, N. Miguel, A. Claver, J.M. Matesanz, J.L. Ovelleiro, *Chemosphere*, **2008**, *71*, 97-106
- [47.] J.F. Liu, Z.S. Zhao, G.B. Jiang, *Environ. Sci. Technol.* **2008**, *42*, 6949-6954
- [48.] K.Y Foo, H. Hameed, *Desalin. Water Treat.* **2010**, *19*, 25-274
- [49.] Z. Jeirani, C.H. Niu, J. Soltan, *Rev. Chem. Eng.* **2017**, *33*, 491-522
- [50.] M.J. Rakowska, D. Kupryianchyk, M.P.J. Smit, A.A. Koelmans, J.T.C. Grotenhuis, H.H.M. Rijnaarts, *Water Res.* **2014**, *51*, 86-95
- [51.] F. Vince, A. Aoustin, P. Breant, F. Marechal, *Desalination*, **2008**, *220*, 37-45
- [52.] M. Miguet, V. Goetz, G. Plantard, Y. Jaeger, *Ind. Eng, Chem, Res.* **2016**, *55*, 7003-7011
- [53.] T. Masciangioli, W.X. Zhang. *Environ. Sci. Technol.* **2003**, *37*, 102A
- [54.] A. Pratt, *Front. Nanoscience.* **2014**, *6*, 259-307.
- [55.] M. Basnet, S. Ghoshal, N. Tufenkji, *Environ. Sci. Technol.* **2013**, *47*, 13355-13364
- [56.] N. Saleh, N. Sirk, Y. Liu, T. Phenrat, B. Dufour, K. Matyjaszewski, R. Tilton, G.V. Lowry, *Eng.* **2007**, *24*, 45-47
- [57.] K.K. Clark, A.A. Keller, *Water Res.* **2012**, *46*, 635-644
- [58.] F. Li, J. Lu, X. Kong, T. Hyeon, D. Ling, *Adv. Mater.* **2017**, *29*,
- [59.] N. Lee, D. Yoo, D. Ling, M. Cho, T. Hyeon, J. Cheon, *Chem. Rev.* **2015**, *115*, 10637-10689.
- [60.] H.L. Ding, Y.X. Zhang, S. Wang, J.M. Xu, S.C. Xu, G.H. Li, *Chem. Mater.* **2012**, *24*, 4572-4580
- [61.] A. Kertmen et al, *Langmuir*, **2017**, *33*, 10351-10365

- [62.] P. Wang, Q. Shi, Y. Shi, K.K. Clark, G.D. Stucky, A.A. Keller *J. Am. Chem. Soc.* **2009**, *131*, 182-188
- [63.] Y. Huang, A.N. Fulton, A.A. Keller, *Environ. Sci: Water. Res. Technol.* **2016**, *2*, 521-528
- [64.] Y. Huang, A.N. Fulton, A.A. Keller, *Sci. Tot. Environ.* **2016**, *571*, 1029-1036
- [65.] K.K. Clark, A.A. Keller, *Water Res.* **2012**, *46*, 635–644
- [66.] E.M. Martin Del Valle, Cyclodextrins and their uses: A review. *Process Biochem.* **2004**, *39*, 1033- 1046
- [67.] F. Fava, L. Bertin, S. Fedi, D. Zannoni, *Biotechnol. Bioeng.* **2003**, *81*, 381-390
- [68.] A. Alsaiee, B.J. Smith, L. Xiao, X. Ling, D.E. Helvling, W.R. Dichtel, *Nature* **2016**, *529*, 190-194
- [69.] J.Li, C. Chen, Y. Zaho, J.Hu, D. Shao, X. Wang, *Chem. Eng. J.* **2013**; *229*: 296 – 303
- [70.] D. Landy, L. Mallard, A. Ponchel, E. Monflier, S. Fourmentin *Environ. Chem. Let.* **2012**; *10*, 225-237
- [71.] M. Wang, P. Liu, Y. Wang, D. Zhou, C. Ma, D. Zhang, J. Zhan, *J. Colloid Interface Sci.* **2015**, *447*, 1-7
- [72.] R. Bhandari, P. Gupta, T.D. Dziubla, J.Z. Hilt, *Mater. Sci. Eng. C.* **2016**, *67*, 59-64
- [73.] R. Wilken, M.S. Veena, M.B. Wang, E.S. Srivatsan, *Mol. Cancer* **2011**, *10*, 12
- [74.] B.B. Aggarwal, S. Shishodia, *Biochem. Phamrmacol.* **2006**, *71*, 1397-1421
- [75.] I. Gharbi, S. Moret, O. Chaari, M. Issaoui, L.S. Conte, P. Lucci, M. Hammami, *Food Control*, **2017**, *75*, 160-177
- [76.] T.M. Gutierrez-Valencia, M.P. Garca de Llasera, *Food Chem.* **2017** *223* ,82
- [77.] A.J. Buczynska, B. Geypens, R. Van Grieken, K. De Wael, *Microchem. J.* **2015**, *119*, 83-92.
- [78.] Y.H. Fan, S.W. Zhang, S.B. Qin, X.S. Li, Y. Zhang. S.H. Qi, *Anal/ Bioanal. Chem.* **2017**, *409*, 3337-3346
- [79.] J.A.S. Costa, R.A. de Jesus, C.M.P. da Silva, L.P.C. Romao, *Powder Technol.* **2017**, *308*, 434-441
- [80.] P. Wang et al, *Chem. Eng., J.* **2016**, *306*, 208-288
- [81.] Z. Zhang, X. Hou, X. Zhang, H. Li, *Colloids Surf. A Physicochem. Eng. Asp.* **2017**, *520*, 39-45.

- [82.] S.B. Qin, Y.H. Fan, X.X. Mou, X.S. Li, S.H. Qi, *J. Chromatogr.* **2018**, *1568*, 29-37
- [83.] M. Sajid, *Trends Analyt. Chem.* **2018**, *98*, 114-127.
- [84.] Z. Huang, S. Liu, J. Xu, L. Yin, J. Zheng, N. Zhou, G. Ouyang, *Anal. Chim. Acta*, **2017**, *989*, 21-28.
- [85.] R. Barbey, L. Lavanant, D. Paripovic, N. schuwer, C. Sugnaux, S. Tugulu, H.A. Klok, *Chem. Rev.* **2009**, *109*, 5437-5527
- [86.] A. Amiri, M. Baghayeri, M. Kashmari, *Microchim. Acta.* **2016**, *183*, 149-156
- [87.] A.G Shilabin, A.A. Entezami, *Eur. Polym. J.* **2000**, *36*, 2005-2020
- [88.] M.A. Fard, A. Vosoogh, B. Barkdoll, B. Aminzadeh, *Colloid Surfaces.* **2017**, *531*, 189-187
- [89.] J. Fresnais, M. Yan, J. Courtois, T. Bostelmann, A. Bee, J-F. Berret, *J. Colloid Interface.* **2013**, *395*, 24-30
- [90.] Y.F. Shen, J. Tang, Z.H. Nie, Y.D. Wang, Y. Ren, L. Zuo, *Sep. Purif. Technol.* **2010**, *25*, 312
- [91.] C.T. Yavuz, J.T. Mayo, W. Yu, A. Prakash, J.C. Falkner, S. Yean, L. Cong, J.H. Shipley, A.M. Kan, M.R. Tomson, D. Natelson, V.L. Colvin, *Science*, **2006** *314*, 964-967
- [92.] L. Mohammed, H.G. Goma, G. Ragab, J. Zhu. *Particuology*, **2017**, *30*, 1-14
- [93.] X. Liu, Q. Hu, Z. Fang, X. Zhang, B. Zhang, *Langmuir.* **2009** *25*, 3-8
- [94.] N. Pandey, S.K. Shukla, N.B. Singh, *Nanocomposite*, **2017**, *3*,
- [95.] R. Li, L. Zhang, P. Wang, *Nanoscale*, **2015**, *7*, 17167
- [96.] M
- [97.] A. Giannakas, M. Pissanou, *J. Nanochem. Nanotechnol.* **2018**, *1*, 1
- [98.] O.K. Bishoge, L. Zhang, S.L. Suntu, H. Jin, A.A. Zewde, A. Qi, *J. Environ. Sci. Health A.* **2018**, *53*, 537-554
- [99.] W.S. Ngah, L.C. Teong, M.A.K.M Hanafiah, *Carbohydr. Polym.* **2011**, *83*, 1446-1456
- [100.] M.D. Ahmaruzzaman, *Adv. Colloids Interface Sci.* **2008**, *143*, 48-67
- [101.] C.G. wang, Q. Gao, S. Wang, Y.S. Gong, K.S. Xia, B. Han, M. Li, Y. Ling. *React. Funct. Polym.* **2016**, *100*, 97-106.
- [102.] S.T. Akar, E. San, T. Akar, *Carbohydr. Polym.* **2016**, *143*, 318-326

- [103.] L.M. Yang, L. Jiang, D. Hu, Q. Y. Yan, Z. Wang, S.S. Li, C. Chen, Q. Xen, *Carbohydr. Polym.* **2016**, *140*, 433-441
- [104.] M. Vakili, S.B. Deng, L. Shen, D.N. Shan, D.C. Liu, G. Yu, *Sep. Purif. Rev.* **2019**, *48*, 1-13
- [105.] L.A.D.S. Rodrigues, A. Figueiras, F. Veiga, R.M. de Freitas, L.C.C. Nunes, E.C. da Silva Filho, C.M. da Silva Leite, *Colloids Surf. B. Biointerfaces* **2013**, *103*, 642-651.
- [106.] L. Cottet, C.A.P. Almeida, N. Naidek, M.F. Viante, M.C. Lopes, N.A. Debacher, *Appl. Clay Sci.* **2014**, *95*, 25-31
- [107.] Z.B. Molu, K. Yurdakoc, *Microporous Mesoporous Mater.* **2010**, *127*, 50-60.
- [108.] F. Guo, S. Aryana, Y.H. Han, Y.P. Jiao, *Applied Sciences-Basel.* **2018**, *8*,
- [109.] H. Mabrouki, D.E. Akretche, *Desalin. Water Treat.* **2016**, *57*, 6033-6043.
- [110.] V. Rakic, N. Rajic, A. Dakovic, A. Auroux, *Microporous Mesoporous Mater.* **2013**, *166*, 185-194.
- [111.] C.J. Wang, Z. Li, W.T. Jiang, *Appl. Clay Sci.* **2011**, *53*, 723-728
- [112.] H. chiu, H. Xie, G. He, Y. Guan, Y. Zhang, *Appl. Clay Sci.* **2016**, *119*, 161-169.
- [113.] V. Arya, L. Phillip, *Microporous Mesoporous Mats.* **2016**, *232*, 273-280
- [114.] A.M. Redding, F.S. Cannon, S.A. Snyder, B.J. Vanderford *Water. Res.* **2009**, *43*, 3849-3861
- [115.] V. Arya, L. Phillip. S. M. Bhallamudi, *Ind. Eng. Chem. Res.* **2018**, *57*, 8978-8988
- [116.] A. Abdar, A.S. Yazdi, A. Amiri. N. Bagheri, *J. Sep. Sci.* **2016**, *39*, 2746-2753
- [117.] L.M. Sanchez, D.G. Actis. J.S. Gonzalez, P.M. Zelis, V. A. Alvarez, *J. Nanopart. Res.* **2019**, *21*, 64
- [118.] A. Hu, X. Yang, Q. Yang, Y. Liu, Q. Wang, G. Liao, D. Wang, *J. Mater. Sci.* **2019**, *54*, 2712-2728 (amf 23)
- [119.] Q. Liu, L.B. Zhong, Q.B. Zhao, C. Frear, Y.M. Zheng, *Appl. Matter. Interfaces.* **2015**, *7*, 14573-14583
- [120.] U.O. Aigbe, W.H. Ho, A. Maity, M. Khenfouch, V. Srinvasu. *J. Phys: Conf. Series.* **2018**
- [121.] Q. Li, Z. Zhan, S. Jin, B. Tan, *Chem. Eng. J.* **2017**, *326*, 109-116
- [122.] X. Huang, Q. Liu, S. Yao, G. Jiang, *Anal. Methods.* **2017**, *9*, 2768

- [123.] S.Hr, T. Zeng, S, Wang, H, Niu, Y. Cai, *Appl. Matter. Interfaces.* **2017**, 9, 2959-2965
- [124.] S. Mahpishanian, H. Sereshti, M. Ahmadvand, *J. Env. Sci.* **2017**, 55, 164-173
- [125.] X. Wan, Y. Zhan, Z. Long, G. Zeng, *Chem. Eng. J.* **2017**, 330, 491-504
- [126.] D. Li, J. Zhhu, M. Wang, W. Bi, X. Huang, D.D. Y. Chhong, *J. Chromatogr. A.* **2017**, 1491, 27-35
- [127.] Z. Li, X. Tang, K. Liu, J. Huang, Q. Peng, M. Ao, Z. Huang, *J. Env. Manage.* **2018**, 218, 363-373
- [128.] R. Xiao, X. Zhang, X. Zhang, J. Nu, M. Lu, X. Lu. Z. *CaTalanta*, **2017**, 166, 262-267
- [129.] W. Konicki, A. Helminiak, W. Arabczyk, E. Mijowska, *J. Colloid Interface Sci.* **2017**, 497, 155-164
- [130.] M.O. Akhrame, O.S. Fatoki, B.O. Opeolu *Polym. Bull.* **2019**, 76, 647-681
- [131.] UNEP. Natural solutions for water security. Water and Biodiversity. International day for biological diversity – Convention on Biological Diversity. May 22, 2013
- [132.] H. Mittal, S.B. Mishra. *Carbohydr Polym.* **2014**, 101, 1255
- [133.] P. Xu, G.M. Zeng, D.L. Huang, C.L. Feng, S. Hu, M.H. Zhao, C. Lai, Z. Wei, C. Huang, G.X. Xe, Z.F. Liu, *Sci. Total Environ.* **2012**, 424, 1-10
- [134.]
- [135.] V.D Dang, D.M. Walters, C.M Lee, *Am J Environ Sci.* **2012**, 8, 11
- [136.] N. Howell, M.P. Suarez, H.S. Rifai, L. Koenig, *Chemosphere.* **2008**, 70, 593-606
K.C. Jones and P. de Voogt. *Environ Pollut.* **1999**, 100, 209-221
- [137.] NCI. Table 2. Food sources of the total omega 6 fatty acids (18:2 + 20:4), listed in descending order by percentages of their contribution to intake, based on data from the national health and nutrition examination survey 2005–2006. NIH; 2013
[http://appliedresearch.cancer.gov/diet/foodsources/fatty_acids/table2.html].
- [138.] M.C. Petriello, B.J. Newsome, T.D. Dziubla, J.Z. Hilt, D. Bhattacharyya, B. Hennig B. *Sci Total Environ.* **2014**, 491-492, 11
- [139.] S.Y. Ham, Y.J. Kim, D.H. Lee, *Chemosphere.* **2008**, 106, 226
- [140.] O. Hutzinger, G.G. Choudrhy, B.G. Chittim, L.E. Johnston. *Environ. Health Perspect.* **1985**, 60, 3
- [141.] J. Zhu et al. *RSC Advances.* **2012**, 2, 4844
- [142.] S. Argawal et al. *J Environ Eng.* 2007, 133, 1075

- [143.] E. Hilal-Mert, H. Yildirim, A.T. Uzumcu, H. Kavas. *React. Funct. Polym.* **2013**, 73, 175
- [144.] G. Gollavelli, C. Chang, Y. Ling. *ACS Sustain. Chem. Eng.* **2013**, 1, 462
- [145.] L.A. Ali, W. Wan Ibrahim, A. Sulaiman, M. Kamboh, M. Sanagi, *Talanta.* **2016**, 148, 191
- [146.] M.S. Abdelwahab, E.M. Fathallah. *Chem. Eng. J.* **2013**, 223, 318
- [147.] X. Qu, P.J.J. huangrez, Q. Li. *Water Res.* **2013**, 47, 3931
- [148.] Q. Zhou, J. Li, M. Wang, D. Zhao. *Crit Rev Environ Sci Technol.* **2016**, 8, 7833-826
- [149.] Z. Geng, Y. Lin, X. Yu, Q. Shen, L. Ma, Z. Li, N. Pan, X. Wang. *J. Mater. Chem.* **2012**, 22, 3527
- [150.] C.R. Vestal, Z.J. Zhang. *J. Am. Chem. Soc.* **2002**, 124, 14312
- [151.] Y. Zhuo, S. Wang, B. Ding, Z. Yang. *Chem Eng J.* **2008**, 138, 578
- [152.] Y. Wang, X. Teng, J.S. Wang, H. Yang. *Nano Lett.* **2003**, 3, 789
- [153.] H. Mittal, S.B. Mishra. *Carbohydr. Polym.* **2014**, 101, 1255
- [154.] W.Y. Liu. *J. Biosci. Bioeng.* **2006**, 102, 1
- [155.] H. Choi, S. Argarwal, S.R. Al-Abed, *Environ. Sci. Technol.* **2009**, 43, 488
- [156.] S.A. Meenach, J.Z. Hilt, K.W. Anderson. *Acta Biomater.* **2010**, 6, 1039
- [157.] S. Kango. *Prog. Polym. Sci.* **2013**, 38, 1232
- [158.] J.L. Pellequer, S.W. Chen, Y.S. Keum, A.E. Karu, Q.X. Li, V.A. Roberts. *J. Molec. Recog.* **2005**, 18, 282.
- [159.] C. Lin, R. Chinnappan, K. Acharya, J.L. Pellequer, R. Jankowiak. *Biophys Chem.* **2011**, 154, 35
- [160.] H. Inui et al. *J. Agric. Food Chem.* **2012**, 60, 1605
- [161.] F. Gobas, X. Zhang. *Chemosphere.* **1992**, 25, 1961
- [162.] B. Sharma, K.H. Gardner, J. Melton, A. Hawkins, G. Tracey. *Environ. Eng. Sci.* **2009**, 26, 1371
- [163.] S. Palchoudhury, J.R. Lead. *Environ. Sci. Technol.* **2014**, 48, 14558
- [164.] V. Patil, T.D. Dziubla, D.S. Kalika. *Polymer.* **2015**, 75, 88
- [165.] V. Patil V, A.M. Gutierrez, M. Sunkara, A.J. Morris, J.Z. Hilt, D.S. Kalika, T.D. Dziubla. *J. Nat. Prod.* **2017**, 80, 1964

- [166.] P. Gupta, S. Authimoolam, J.Z. Hilt, T.D. Dziubla. *Acta Biomater.* **2015**, 27, 194
- [167.] R. Wydra, A. Kruse, Y. Bae, K.W. Anderson, J.Z. Hilt. *Mater. Sci. Eng. C.* **2013**, 33, 4660
- [168.] A.L. Andrade, D.M. Souza, M.C. Pereira, J.D. Fabris, R.Z. Domingues. *Quimica Nova.* **2012**, 33, 524
- [169.] I. Langmuir. *AIChE J.* **1916**, 38, 121
- [170.] G. Vaidyanathan, S. Sendhilkathan, R. Arulmurugan. *J. Magn. Magn. Mater.* **2007**, 313, 29
- [171.] L. Giraldo, A. Erto, J.C. Moreno-Pirajan. *Adsorption.* **2013**, 19, 465
- [172.] A. Hauser, R. Mathias, K.W. Anderson, J.Z. Hilt. *Mater. Chem. Phys.* **2015**, 160, 177
- [173.] L. Liu, R. Fokkink, A.A. Koelmans, *Environ. Toxicol. Chem.* **2015**, 35, 1650
- [174.] M.T.O. Jonker, A.A. Koelmans. *Environ. Sci. Technol.* **2002**, 26, 3725
- [175.] S. Kleineidam, C. Schüth, P. Grathwohl P. *Environ Sci Technol.* **2002**, 36, 304
- [176.] A.A. Koelmans, B. Meulman, T. Meijer, M.T.O. Jonker. *Environ. Sci. Technol.* **2009**, 43, 736
- [177.] T. Phatthanakittiphong, G. Tae Seo. *Nanomater.* **2016**, 6, 128
- [178.] S.S. Ingh, K.C. Barick, D. Bahadur, *Nanomater. Nanotechnol.* **2013**, 20, 1-19
- [179.] S. Kalia, S. Kango, A. Kumar, Y. Haldorai, B. Kumari, R. Kumar, *Colloid Polym. Sci.* **2014**. 292, 2025-2052
- [180.] J. Zhu, S. Wei, M. Chen, H. Gu, S.B. Rapole, S. Pallavkar, T.C. Ho, J. Hopper, Z. Guo, *Adv. Powder Technol.* **2013**, 24, 459-467
- [181.] A.A. Algadami, M.A. Khan, M. Otero, M.R. Siddiqui, B.H. Jeon, K.M. Batoo, *J. Cleaner Prod.* **2018**, 178, 293-304
- [182.] C.A. Sophia, E.C. Lima, *Ecotoxicol. Environ. Safety.* **2018**, 150, 1-17
- [183.] B. Chen, M.Y. Han, K. Pen, S.L. Zhou, W.D. Wei, S.Y. Liu, Z. Li, S. Li, G.Q. Chen, *Sci. Total Environ.* **2018**, 613-614, 931-943
- [184.] P.J.J. Alvarez, C.K. Chan, M. Elimelech, N.J. Halas, D. Villagran, *Nature Nanotechnol.* **2018**, 13, 634-341
- [185.] G. Ctstis, P. Schon, W. Bakker, G. Luthe, *Environ. Pollut. Res.* **2016**, 23, 4837-4843
- [186.] V.D. Dang, D.M. Walters, C.M. Lee, *Am. J Environ. Sci.* **2012**, 8, 11

- [187.] P. Tremolada, N. Guazzoni, R. Comolli, M. Parolli, S. Lazzaro, A. Binelli, A. *Environ. Sci. Technol.* **2015**, *22*, 19571-19583
- [188.] A. Perrard, C. Descorme, *Chemosphere*. 2016. *145*, 528-534
- [189.] O. Brien, M.N. Radha, K. A. Brown, M.R. Jones, C.A. Mirkin. *Angew Chem. Int. Ed.* **2014**, *53*, 9532-9538.
- [190.] B. Liu, W. Qi, L. Tian, S. Li, G. Miao, W. An, D. Liu, J. Lin, X. Zhang, W. Wu, *Nanoscale Res. Lett.* **2015**, *10*, 1172-1178
- [191.] F.F Bruno, A. Trotta, A. Fossey, S. Nagarajan, R. Nagarajan, L.A. Samuelson J. Kumar, *J Macromol. Sci. A*, **2010**, *47*, 1191-1196
- [192.] J. Ma, Y., Zhuang, F. Yu, *New J. Chem.* **2015**. *39*, 9299-9235
- [193.] I. Velzeboer, C.J.A.F. Kwadijk, A.A. Koelmans, *Environ. Sci. Technol.* **2014**, *48*, 4869-4876
- [194.] K. Yang, L. Zhu, B. Xing, *B. Environ. Sci. Technol.* **2006**, *40*, 1855–1861.
- [195.] J. Ma, Y. Zhuang, F. Yu, *New J. Chem.* **2015**, *39*, 9299-9235
- [196.] M. Kah, X. Zhang, M.T.O. Jonker, T. Hofmann, *Environ. Sci. Technol.* **2011**, *45*, 6011-6017
- [197.] M.I. Rakowska, D. Kupryianchyk, T. Grotenhuis, H.H.M. Runaarts, A.A.Koelmans, *Environ. Toxicol. Chem.* **2013**, *32*, 304-311
- [198.] Y.W. Chiu, Q.L. Li A.E. Karu, *Anal. Chem.* 2001. *73*, 5477-5484
- [199.] A.M. Gutierrez, R. Bhandari, J. Weng, A. Stromberg, T.D. Dziubla, J.Z. Hilt, *Mat. Chem. Phys.* 2019. *223*, 68-74
- [200.] N. Das, L.V.G. Basak, J.A. Salam, E.A. Abigail, *J. Microbiol. Biotechnol.* **2007**, *2*, 783–79
- [201.] P.K.T Liu, S.M. Feltch, N.J, Wagner, , *Ind. Eng. Chem. Res.* **1987**, *26*, 1540-1545
- [202.] D. Guo, Q. Shi, B. He. X. Yuan, , *J. Hazard. Mater.* **2011**, *186*, 1788-1793
- [203.] P.J. Lu, H.C. Lin, W.T. Yu, J.M. Chern, *J. Taiwan Institute Chem Engineers.* **2011**, *2*, 305-311
- [204.] L. Wang, N. Balasubramanian, *Chem Eng, J.* **2009**, *155*, 736-768
- [205.] K. Nath, M.S. Bhakhar, *Environ. Sci Pollut. Res.* **2011**, *4*, 534-546
- [206.] M. Breitbach, D. Bathen, H. Schmidt-Traub, H., *Ind. Eng. Chem. Res.* **2003**, *42*, 5635–5646

- [207.] M. Fayaz, P. Shariaty, J.D. Atkinson, Z. Hashisho, J.H. Phillips, J.E. Anderson, M. Nichols, *Environ. Sci. Technol.* **2015**, *49*, 4536-4542
- [208.] R. Pelech, E. Milchert, A. Wroblewska, *J. Colloid. Interf. Sci.* **2005**, *285*, 518–524.
- [209.] F. Cecen, O. Aktas, *Activated Carbon for Water and Wastewater Treatment: Integration of Adsorption and Biological Treatment*, Wiley-VCH: Weinheim, Germany, **201**
- [210.] S.W. Nahm, W.G. Shim, Y.K. Park, S.C. Kim, *Chem. Eng. J.* **2012**, *210*, 500-509
- [211.] S. Behrens, I. Appel, , *Cur. Opin. Biotechnol.* **2016**, *39*, 89-96
- [212.] (Work Submitted) A.M. Gutierrez, R. Bhandari, Y. Weng, A. Stromberg, T.D. Dziubla, J.Z. Hilt, Synthesis of magnetic nanocomposite microparticles for binding of chlorinated organics in contaminated water sources. *Journal*, **2019**
- [213.] .L. Rodovalho, G. Capistrano, J.A. Gomes, F.F. Sodre, J.A. Chaker, A.F.C. Campos, A.F. Bakuzis, M.H. Sousa *Chem. Eng. J.* **2016**, *302*, 725-732
- [214.] US EPA, Other federal statues and PCB regulations, <https://www3.epa.gov/region9/pcbs/otherstatutes.html>, accessed: 04, 2019
- [215.] L. Hahn, M.M. Lubtow, T. Lorson, F. Schmitt, A. Appelt-Menzel, R. Schobert, R. Luxenhofert, *Biomacomolec.* **2018**, *19*, 3119-3128
- [216.] N. Wang, X. Liang, Q. Li, Y. Liao, S. Shao, *RSC Adv.* **2015**, *5*, 15500-15506
- [217.] J. Dong, J.I. Zink, *ACS Nano.* **2014**, *8*, 5199-5207
- [218.] A. Riedinger, P. Guardia, A. Curcio, M. A. Garcia, R. Cingolani, L. Manna, T. Pellegrino *Nano Lett.* **2013**, *13*, 2399-2406
- [219.] A. Chiu-Lam, C. Rinaldi, , *Adv. Funct. Mater.* **2016**, *26*, 3933-3941
- [220.] R. Pinol, C.D.S. Brites, R. Bustamante, A. Martinez, N.J.O. Silva, J.L. Murillo, R. Cases, J. Carrey, C. Estepa, C. Sosa, F. Palacio, L.D. Carlos, A. Millan, *ACS Nano*, **2015**, *9*, 3134-3142
- [221.] Q. Huang, C.S. Hong, Aqueous solubility of non-ortho and mono-ortho PCBs at four temperatures. *Wat. Res.* **2002**, *36*, 3543-3552
- [222.] R.R. Schwarzenbach, T. E Egli, T. B. Hofstetter, U. von Grunten, B. Wehrli, *Annual Reviews further.* **2010**. *35*, 109-1036
- [223.] M. Fuerhacker, *Environ. Sci. Pollut. Res.* **2009**, *16*, S92-S97
- [224.] UNEP. Natural solutions for water security. Water and Biodiversity. International day for biological diversity – Convention on Biological Diversity. May 22, **2013**
- [225.] S. Ncube, L. Madikizela, E.Cukrowska, L. Cimuka, *Trends Anal. Chem.* **2018**, *99*, 101-116

- [226.] Y.H. Boon, N.N.M. Zain, S. Mohamad, H. Osman, M. Raoov, *Food Chem.* **2019**, 278, 322-332
- [227.] J. Yu, S. Zhu, L. Pang, P. Chen, G.T. Zhu, *J Chromatography A*, **2018**, 1540, 1-10
- [228.] M. Wang, P. Liu, Y. Wang, D. Zhou, C. Ma, D. Zhang, J. Zhan, *J. Colloid Interface Sci.* **2015**, 447, 1-7
- [229.] Q. Han, Z. Wang, J. Xia, X. Zhang, M. Dang, *Talanta*, **2012**, 101, 388-395
- [230.] Y.F. Li, T. Harner, L. Liu, Z. Zhang, N.Q. Ren, H. Jia, j. Ma, E. Sverko, *Environ. Sci. Technol.* **2010**, 44, 2784-2790
- [231.] US EPA, National Recommended Water Quality Criteria - Aquatic Life Criteria Table, <https://www.epa.gov/wqc/national-recommended-water-quality-criteria-aquatic-life-criteria-table>, accessed: 04/2019
- [232.] P. Nurerk, P. Kanatharana, O. Bunkoed, *Int. J. Environ. Anal. Chem.* **2017**, 97, 145-158
- [233.] S.C. Lung, Y. Yanagisawa, T.E. Ford, J.D. Spengler, *Chemosphere*, **2000**, 41, 1857-1864
- [234.] J. Ding, Q. Gao, D. Lao, Z. G. Shi, Y.Q. Feng, *J. Chomatogr. A*. **2010**, 1217, 7351-7358
- [235.] E.S. Kim, D.H. Lee, B.W. Yum, H.W. Chang, *J. Hazard. Mater.* **2005**, 119, 195-203
- [236.] 237 M.T.O. Jonker, S.A. Van der Heijden, M. Kotte, F. Smeden, *Environ. Sci. Technol.* **2015**, 49, 6791-6799
- [237.] 238 P.J. Reitsma, D. Adelman, R. Lohmann, *Environ. Sci. Technol.* **2013**, 47, 10429-10437
- [238.] J.O. Zoppe, N.V. Ataman, P. Mocny, J. Wang, J. Moraes, H.A. Klok, *Chem. Rev.* **2017**, 117, 1105-1318
- [239.] N. Ayres, *Polym. Chem.* **2010**, 1, 769-777
- [240.] D.X. Li, Y. Cui, K.W. Wang, Q. He Q, X.H. Yan, J.B. Li, *Adv. Funct. Mater.* **2007**, 17, 3134
- [241.] R. Chen, S. Maclaughlin, G. Botton, S. Zhu, *Polym.* **2009**, 50, 4293-4298
- [242.] M. Ejaz, V.A. Puli, R. Elupula, S. Adireddy, B.C. Riggs, D.B. Chrisey, S.M. Grayson, *J. Polym. Sci A*. **2015**, 53, 719-728
- [243.] E. Guisasola, A. Baeza, L. Asin, J.M. dela Fuente, M. Vallet-Regi, *Small Methods*, **2018**, 2,
- [244.] Y. Deng, A.F. Xu, Y.H. Yu, C. Fu, G.L. Liang, *Chembiochem*, **2019**, 20,
- [245.] M. Saeed, W.Z. Ren, A.G. Wu, *Biomater. Sci.* **2018**, 6, 708-725
- [246.] Y.Z. Dong, W.J. Han, H.J. Choi, *Polym.* **2018**, 10,

- [247.] M. Ejaz, V.S. Puli, R. Elupula, S. Adireddy, B.C. Riggs, D. B. Chrisey, S.M. Grayson, *J. Polym. Sci.* **2015**, *53*, 719-728
- [248.] V. Mahmoodi, T. Bastami, A. Ahmadpour, *Env. Sci, Pollut. Res.* **2018**, *25*, 8268-8285
- [249.] X. Shi, N. Li, D. Wu, N. Hu, J. Sun, X. Zhou, Y. Suo, G. Li, Y. Wu, *Analytical Methods.* **2018**, *10*, 5014-5025
- [250.] J. Huang, R. Deng, K. Huang, *Chem Eng. J.* **2011**, *141*, 951-957
- [251.] F. Shen, Y. J. Xu, Y. Wang, P.Y. Zhu, X.L. Dal, J. Cheng, Q. Zou, *J. Analysis Testing.* **2018**, *2*, 306-311
- [252.] G. Li, J. Fan, R. Jiang, Y. Gao, *Chem. Mater.* **2004**, *16*, 1835-1837
- [253.] A.D. Site. *J. Phys. Chem. Ref. Data*, **2000**, *30*, 2001
- [254.] J. He, Y. Wu, J. Wu, X. Mao, L. Fu, T. Qiang, J. Fang, C. Xiong, J. Xie, H. MA, *Macromol.* **2001**, *40*, 3090-3096
- [255.] X.A. Chen, Y.Z. Zhang, J.A. He, C.Y. Xiong, Y.H. Meng, G. Jin, H.W. Ma, *Sci. China Ser. B-Chem.* **2009**, *52*, 2307-2322
- [256.] J. Mandal, R.S. Varunprasaath, W. Yan, M. Divandari, N.D. Spencer, M. Dubner, *RSC Adv.* **2018**, 20048-20055
- [257.] (Work submitted) A.M. Gutierrez, T.D. Dziubla, J.Z. Hilt, Alternating Magnetic Field Modulated Binding in Magnetic Nanocomposites as a Low Energy Regeneration Strategy in Environmental Remediation, 2019
- [258.] I. Velzeboer, C.J.A.F. Kwadijk, A.A. Koelmans, *Environ. Sci. Technol.* **2014**, *48*, 4869-4876
- [259.] X. Zheng, H. Zheng, R. Zhao, Y. Sun, Q. Sun, S. Zhan, Y. Liu, *Mater.* **2018**, *11*, 1312
- [260.] P. Wu, H. Cai, H. Jin, Y. Tang, Y. *Sci Total Environ.* **2018**, *650*, 671-678
- [261.] M.A. Salam, R.C. Burk, *Water Air Soil Polut.* **2010**, *2010*, 101-111
- [262.] C. Kang, R. Crockett, N.D. Spencer, *Polym. Chem.* **2016**, *7*, 302-
- [263.] A. Ramakrishnan, R. Dhamorharana, J. Ruhe, *J. Poly. Sci.* **2006**, *44*, 1758-1769
- [264.] B. Sklarsova, P. Simko, P. Simon, B. Drobna, *J. Food Nutritional Res.* **2007**, *46*, 128-133

VITA

PERSONAL INFORMATION

Place of Birth: Cali, Valle del Cauca, Colombia

EDUCATION

Universidad de Los Andes, Bogotá D.C., Colombia, June 2012

B.S. Chemistry

Universidad de Los Andes, Bogotá D.C., Colombia, June 2011

B.S. Chemical Engineering

RESEARCH EXPERIENCE

NIEHS Superfund Research Program Trainee, August 2013-present

Graduate Research Assistant in Chemical Engineering, May 2012-August 2013

University of Kentucky

Advisors: Dr. J. Zach Hilt and Dr. Thomas Dziubla

Undergraduate Research Assistant, May 2011 -May 2012

Universidad de Los Andes

Advisor: Dr. Edgar Vargas

Undergraduate Research Assistant, May 2010 –May 2011

Universidad de Los Andes

Advisors: Dr. Andres Gonzalez and Sebastian Hernandez, MsC

AWARDS/HONORS

2018 CEECHE 2018 Trainee Travel Award – NIEHS

2018 Outstanding Graduate Student – Chemical and Materials Engineering, University of Kentucky

2017 Karen Wetterhahn Memorial Award Recipient – Superfund Research Program

2017 3rd Annual Materials and Chemical Engineering Graduate Student Association Fall Symposium First Place Poster Winner

2016 KC Donnelly Externship Award Supplement – Superfund Research Program

2016 CEECHE 2016 Trainee Travel Award – NIEHS

2014 Superfund Annual Meeting First Place Poster Winner

PUBLICATIONS

Angela M. Gutierrez, Rohit Bhandari, Jiaying Weng, Arnold Stromberg, Thomas D. Dziubla and James Z. Hilt. Novel magnetic core-shell nanoparticles for the removal of Polychlorinated Biphenyls from contaminated water sources – *Mat. Chem Phys.* 2019, 223: 68-74

Angela M. Gutierrez, Thomas D. Dziubla and J. Zach Hilt. Recent Advances on Iron Oxide Magnetic Nanoparticles as Sorbents of Organic Pollutants in Water and Wastewater Treatment. - *Rev Environ Health.* 2017, 32 (1-2): 111-117

Vinod S. Patil, Angela M. Gutierrez, Manjula Sunkara, Andrew J. Morris, J. Zach Hilt, Douglass S. Kalika, Thomas D. Dziubla. Curcumin acylation for biological and environmental applications. *J. Nat. Prod.*, 2017, 80 (7): 1964–1971

Angela M. Gutierrez, Rohit Bhandari, Jiaying Weng, Arnold Stromberg, Thomas D. Dziubla and James Z. Hilt. Magnetic nanocomposite microparticles for binding of chlorinated organics in contaminated water sources - Manuscript submitted

Angela M. Gutierrez, Thomas D. Dziubla and James Z. Hilt. Low energy regeneration strategy based on an alternating magnetic field for nanocomposites used in environmental remediation – Manuscript submitted

Angela M. Gutierrez, Thomas D. Dziubla and James Z. Hilt. Novel polyphenol magnetic core-shell nanoparticles with tunable coating thickness for PCB capture in environmental remediation – Manuscript in preparation

Rohit Bhandari, Angela M. Gutierrez, Thomas D. Dziubla and James Z. Hilt. Quercetin Functionalized Magnetic nanoparticles for Remediation of Polychlorinated Biphenyls - Manuscript submitted

PRESENTATIONS

A.M. Gutierrez, T.D. Dziubla, J.Z. Hilt. Reusable Adsorbents: Magnetic Nanocomposites for Contaminated Water Treatment. 2018 Superfund Annual Meeting, Sacramento, CA, November 29, 2018

A.M. Gutierrez, T.D. Dziubla, J.Z. Hilt. Development of Magnetic Nanocomposite Materials as Low Cost Reusable Adsorbents for Chlorinated Organics in Contaminated Water. Wetterhahn Award Invited talk at NIH, Durham, NC, October 7, 2018

A.M. Gutierrez, T.D. Dziubla, J.Z. Hilt. Development of Magnetic Nanocomposite Materials as Reusable Adsorbents for Chlorinated Organics in Contaminated Water. 2018 Central and Eastern European Conference on Health and the Environment (CEECH) Krakow, Poland, June 12, 2018

A.M. Gutierrez, D. Savage, S. Tang, R. Shah, I. Ahmed, M. Frazar, T.D. Dziubla, J.Z. Hilt. Polyphenolic Nanocomposite Materials for the Capture and Sensing of Chlorinated Organics in Contaminated Water Sources. Kentucky Water Resources Research Institute Symposium, Lexington, KY, March 19, 2018.

A.M. Gutierrez. Karen Wetterhahn Memorial Award. 2017 Superfund Annual Meeting, Philadelphia, PA, December 7, 2017

A.M. Gutierrez, T.D. Dziubla, J.Z. Hilt. Magnetic Nanocomposite Materials as Reusable adsorbents for Chlorinated Organics in Contaminated Water. American Institute of Chemical Engineers Annual Meeting, Minneapolis, MN, November 1, 2017

A.M. Gutierrez, T.D. Dziubla, J.Z. Hilt. Iron Oxide Magnetic Nanocomposites: Cost-effective Reusable Adsorbents as Water Remediation Technologies. Global Grand Challenges Summit 2017, July 19, 2017

A.M. Gutierrez, T.D. Dziubla, J.Z. Hilt. Magnetic Nanocomposite Materials as Capture Agents for Organic Pollutants in Water Treatment. American Chemical Society National Meeting, April 4, 2017

A.M. Gutierrez, R. Bhandari, S. Tang, I. Ahmed, B. Thompson, T. Dziubla, J.Z. Hilt. Polyphenolic Nanocomposite Materials for the Capture and Sensing of Chlorinated Organic Contaminants in Water Sources. Kentucky Water Resources Research Institute Symposium, Lexington, KY, March 20, 2017

A.M. Gutierrez, R. Bhandari, T.D. Dziubla, J.Z. Hilt. Novel Core-Shell Nanocomposite materials for on/off binding of organic pollutants contaminated water sources. 2016 Superfund Annual Meeting, Durham, NC, December 2016

A.M. Gutierrez, R. Bhandari, T.D. Dziubla, J.Z. Hilt. Novel Magnetic Nanocomposite Materials for the Rapid Removal of Polychlorinated Biphenyls from Contaminated Water Sources. American Institute of Chemical Engineers Annual Meeting, San Francisco, CA, November 13 - 18, 2016.

A.M. Gutierrez, R. Bhandari, T.D. Dziubla, J.Z. Hilt. Development of Novel Nanocomposite Materials for On/Off Binding of Organic Pollutants from Contaminated Water Sources. 2016 Central and Eastern European Conference on Health and the Environment (CEECH), Prague, Czech Republic, April 11, 2016

A.M. Gutierrez, R. Bhandari, S. Tang, I. Ahmed, T.D. Dziubla, J.Z. Hilt. Designing Polyphenolic Nanocomposite Materials for the Capture and Sensing of Polychlorinated Biphenyls in Contaminated Water Sources. Kentucky Water Resources Research Institute Symposium, Lexington, KY, January 29, 2016.

A.M. Gutierrez, R. Bhandari, T.D. Dziubla, J.Z. Hilt. Development of Magnetic Nanocomposite Materials for the Rapid Removal of PCBs form Contaminated Water Sources. Superfund Annual Meeting, San Juan, PR, November 19, 2015

A.M. Gutierrez, M. Petriello. TCE, PCBs, and Phthalates: Exposure, Mechanisms of Disease, and Clean-up Remedies. NIEHS-SRP Research Progress Webinar, Lexington, KY, August 24, 2015

A.M. Gutierrez, B.J. Newsome, T.D. Dziubla, J.Z. Hilt. Development of Polyphenolic Nanocomposite Materials for the Rapid Removal of Organic Pollutants from Contaminated Water Sources. KY EPSCoR Annual Conference, Lexington, KY, May 22, 2015

A.M. Gutierrez, B.J. Newsome, R. Bhandari, T.D. Dziubla, J.Z. Hilt. Development of Polyphenolic Nanocomposite Materials for Rapid Removal of Organic Pollutants from Contaminated Water Sources. Annual Meeting Superfund Research Program, November 12-14, 2014

A.M. Gutierrez, B.J. Newsome, T.D. Dziubla, J.Z. Hilt. Removal of Persistent Organic Pollutants from Contaminated Water Sources Utilizing Polyphenol-Functionalized Magnetic Nanocomposite Microparticles. Kentucky Innovation and Entrepreneurship Conference, September 5, 2014

A.M. Gutierrez, B.J. Newsome, T.D. Dziubla, J.Z. Hilt. Development of Iron Oxide Nanoparticle Composites for On/Off Binding of PCBs. Annual Meeting Superfund Research Program, Baton Rouge, LA, October 16, 2013

A.M. Gutierrez, B.J. Newsome, T.D. Dziubla, J.Z. Hilt. Magnetic Nanocomposite Microparticles for On/Off Binding of Persistent Organic Pollutants. AIChE National Conference, San Francisco, CA, November 6, 2013